

Lawrence Berkeley National Laboratory

Lawrence Berkeley National Laboratory

Title

THE STATE OF THE ART OF NUMERICAL MODELING OF THERMOHYDROLOGIC FLOW IN FRACTURED ROCK MASSES

Permalink

<https://escholarship.org/uc/item/2s99t6nn>

Author

Wang, J.S.Y.

Publication Date

1982-05-01



Lawrence Berkeley Laboratory

UNIVERSITY OF CALIFORNIA

RECEIVED
LAWRENCE
BERKELEY LABORATORY

EARTH SCIENCES DIVISION

FEB 9 1983

LIBRARY AND
DOCUMENTS SECTION

Submitted to Environmental Geology

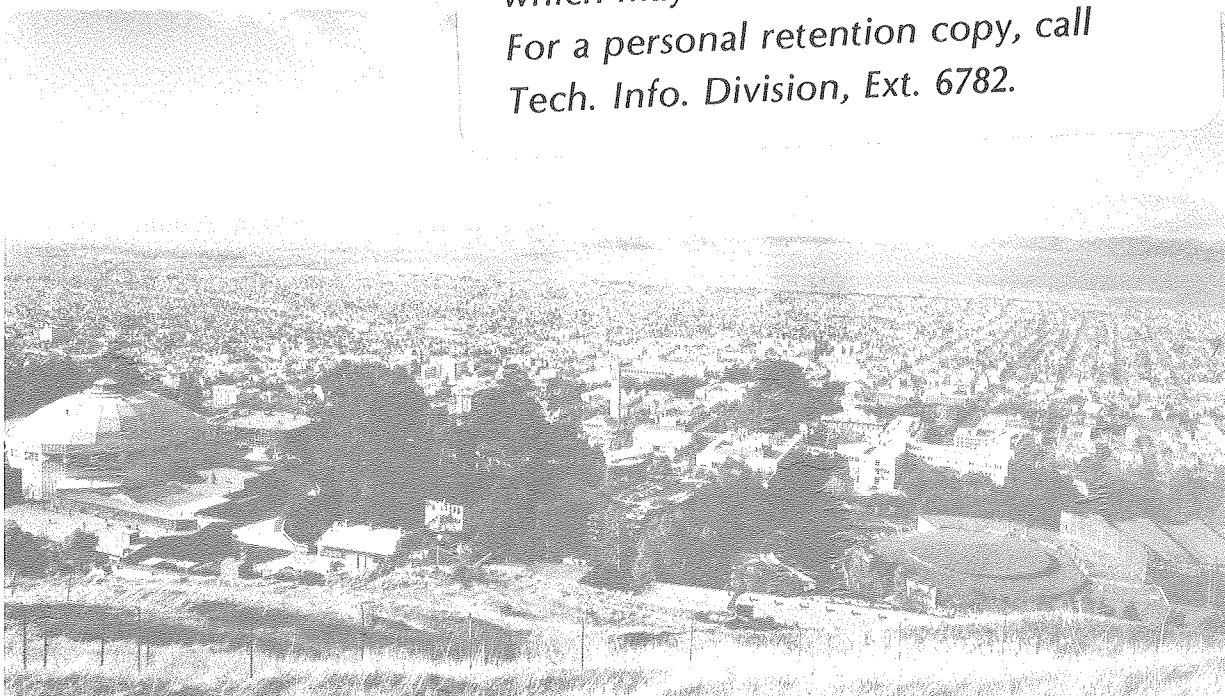
THE STATE OF THE ART OF NUMERICAL MODELING OF
THERMOHYDROLOGIC FLOW IN FRACTURED ROCK MASSES

J.S.Y. Wang, C.F. Tsang, and R.A. Sterbentz

May 1982

TWO-WEEK LOAN COPY

*This is a Library Circulating Copy
which may be borrowed for two weeks.
For a personal retention copy, call
Tech. Info. Division, Ext. 6782.*



LBL-10524
c.2

DISCLAIMER

This document was prepared as an account of work sponsored by the United States Government. While this document is believed to contain correct information, neither the United States Government nor any agency thereof, nor the Regents of the University of California, nor any of their employees, makes any warranty, express or implied, or assumes any legal responsibility for the accuracy, completeness, or usefulness of any information, apparatus, product, or process disclosed, or represents that its use would not infringe privately owned rights. Reference herein to any specific commercial product, process, or service by its trade name, trademark, manufacturer, or otherwise, does not necessarily constitute or imply its endorsement, recommendation, or favoring by the United States Government or any agency thereof, or the Regents of the University of California. The views and opinions of authors expressed herein do not necessarily state or reflect those of the United States Government or any agency thereof or the Regents of the University of California.

THE STATE OF THE ART OF NUMERICAL MODELING OF
THERMOHYDROLOGIC FLOW IN FRACTURED ROCK MASSES

J. S. Y. Wang, C. F. Tsang, and R. A. Sterbentz

Earth Sciences Division
Lawrence Berkeley Laboratory
University of California
Berkeley, California 94720

May 1982

This work was supported by the Assistant Secretary for Nuclear Energy, Office of Waste Isolation of the U. S. Department of Energy under Contract Number DE-AC03-76SF00098. Funding for this project is administered by the Office of Nuclear Waste Isolation at Battelle Memorial Institute.

ABSTRACT

The state of the art of numerical modeling of thermohydrologic flow in fractured rock masses is reviewed and a comparative study is made of several models which have been developed in nuclear waste isolation, geothermal energy, ground-water hydrology, petroleum engineering, and other geologic fields. The general review is followed by separate summaries of the main characteristics of the governing equations, numerical solutions, computer codes, validations, and applications for each model.

TABLE OF CONTENTS

LIST OF TABLES	vi
INTRODUCTION	1
COMPARATIVE REVIEW	6
Governing Equations	7
Numerical Solutions	24
Computer Codes	45
Validations	49
Applications	54
SUMMARIES OF INDIVIDUAL MODELS.	61
ROCMAS	62
TRUST-TERZAGI	74
CCC	87
Model of Duguid.	102
Model of O'Neill	114
GWTHERM	128
FINI	141
CFEST-FE3DGW	150
SWIFT.	159
Model of Coats	172
Model of Faust and Mercer.	185
MUSHRM	196
SHAFT79	209
ACKNOWLEDGEMENTS	220
NOMENCLATURE	221
ABBREVIATIONS	227
REFERENCES CITED	228

INTRODUCTION

This is a review of the state of the art of numerical modeling of thermohydrologic flow in fractured rock masses. The motivation for this study comes from the recent interest in the possibility of isolating nuclear waste materials in hard rock formations. During the last several years, a number of numerical models have been developed for generic studies of nuclear waste repositories. The capability of modeling subsurface fluid flow has also been extensively developed in ground-water hydrology, petroleum engineering, and other geologic fields. More recently, the interest in geothermal energy has contributed to the rapid advancement of this capability, especially in modeling nonisothermal flows. Although the focus of each field is different, some of the models in these fields can be adapted to the study of various thermohydrologic processes associated with waste repositories in hard rock formations. This study, sponsored by the Office of Nuclear Waste Isolation, U. S. Department of Energy, reviews a variety of these models.

Two features of this study are emphasized:

- (1) Modeling of thermohydrologic processes, and
- (2) Modeling of fractured rock masses.

The goal of the former is to understand the nonisothermal phenomena induced by the heat released by the nuclear wastes. The heat will raise the formation temperature and induce buoyancy flow through the rock mass surrounding a nuclear waste repository. The modeling of these thermohydrologic perturbations is important to the study of the potential hazard of radionuclides

being carried by the buoyant water to the biosphere. The temperature and pressure changes also affect the stress field in the rock and the mechanical stability of the repository structure.

The treatment of fractured rock masses--the second aspect of this review--tends to be either completely discrete, taking into account the detailed distribution of a few fractures, or completely random, using a continuum to represent the spatial average of fractures. An extension of the continuum approach is the double-porosity concept with two overlapping continua, one representing the fractures and another, the porous-medium blocks. The choice among the discrete, double-porosity, and porous-medium models depends not only on the characteristics of the fracture network, the size of the region, and the physical processes of interest but also on the availability of data and the limitation of the computational capability. For near-field simulation, it may be necessary to model the detailed fluid movement in order to understand the radionuclide transport, the thermal convection, and the rock displacement in the fracture network. For far-field phenomena, it may be sufficient to model the average behavior of fluid flow in the rock mass.

The present work is an attempt to bring together and to review the relevant models from different fields in order to evaluate the modeling capabilities for thermohydrologic flow in fractured rock masses. On the basis of a comprehensive literature survey and the communications with many model developers and with the Office of Nuclear Waste Isolation of the U. S. Department of Energy, several major models are selected for detailed review to bring out

their strengths, methods of approach, and other characteristics. These models are: ROCMAS, TRUST-TERZAGI, CCC, the model of Duguid, the model of O'Neill, GWTHERM, FINI, CFEST-FE3DGW, SWIFT, the model of Coats, the model of Faust and Mercer, MUSHRM, and SHAFT79. Table 1 lists their recent developers and their main characteristics. The selection is somewhat arbitrary and limited, but we hope that this review includes most of the main characteristics of other major models relevant to the study of thermohydrologic flow in fractured rock masses.

It is generally true that no one numerical model is able to solve all problems of thermohydrologic flow in fractured rock masses. Identification of the special features of each model may be important in selecting the most appropriate model for any given requirement. In the following section the characteristics of the models selected for study in this report are compared and discussed. Tables are given to compare and highlight the key features of interest.

After the general review, each model is summarized separately. The sections on each individual model are independent of the comparative study so that all information will be clearly identifiable and is easily accessible. Both the comparative review and the individual summary sections are written in similar format, with subsections on governing equations, numerical methods, computer codes, validations, and applications.

The comparative review provides general information about the different models, and the individual summaries identify the specific characteristics of each model. This report is intended to serve both as a practical review of

the state of the art of thermohydrologic and fracture flow modeling and as a source of information for use in future developments in this important field of study.

Many experts, including most of the developers of the models discussed herein attended a workshop held at Lawrence Berkeley Laboratory, February 19-20, 1980, on the subject of modeling fractured rock masses. The proceedings of the workshop contain the contributions from the modelers (Lawrence Berkeley Laboratory, 1980).

Table 1. Models Analyzed in the Present Study

Model	Current Development	Main Characteristics
ROCMAS	J. Noorishad, UCB	Stress-flow-(heat), fracture-porous, 2-D, FE. hydrology, geotechnical
TRUST TERZAGI	T. Narasimhan, LBL	Saturated-unsaturated flow-consolidation, 3-D, IFD. hydrology, soil mechanics
CCC	M. Lippmann, LBL	Flow-heat-consolidation, 3-D, IFD. geothermal, aquifer storage, waste isolation
Duguid	J. Duguid, ONWI	Flow, double-porosity, 2-D, FE. hydrology
O'Neill	K. O'Neill, CRRE A. Shapiro, Princeton	Flow-heat, double-porosity, 3-D, FE. geothermal
GWTherm	A. Runchal, ACR	Flow-heat-(transport), 2-D, IFD. waste isolation
FINI	A. Burgess, Acres	Flow-heat, 2-D, FE. waste isolation
CFEST FE3DGW	S. Gupta, BPNL	Flow-heat-solute, 3-D, FE. hydrology, waste isolation
SWIFT	S. Pahwa, Intera	Flow-heat-solute-(transport), 3-D, FD. waste isolation
Coats	K. Coats, Intercomp	Flow-heat, two-phase, 3-D, FD. geothermal, petroleum
Faust- Mercer	C. Faust, J. Mercer, Geotrans	Flow-heat, two-phase, 3-D, FD. geothermal
MUSHRM	J. Pritchett, S. Garg, S ³	Flow-heat-solute, two-phase, 3-D, FD. geothermal, geopressure
SHAFT79	K. Pruess, LBL	Flow-heat, two-phase, 3-D, IFD. geothermal, waste isolation

COMPARATIVE REVIEW

This section discusses the different approaches and approximations used in the models listed in Table 1. The characteristics of the models are reviewed under the following five headings:

- I. Governing Equations,
- II. Numerical Solutions,
- III. Computer Codes,
- IV. Validations, and
- V. Applications.

We have used tables to compare different choices of key elements adopted by these models. This section also discusses some of the general considerations in modeling thermohydrologic flow in fractured rock. More detailed description of the models can be found in the next section, which includes individual summaries of each model.

I. GOVERNING EQUATIONS

The state of ground water flowing through the fractures and pores is described by the velocity \bar{v} and any two thermodynamic quantities pertaining to the fluid--for instance, the pressure P and the temperature T . The fluid velocity \bar{v} within the fractures and pores is of particular interest in determining the convective transport and dispersion of radionuclides. In the continuum approximations used to model average behavior, the microscopic velocity \bar{v} within individual fractures or pores is related to the macroscopic velocity \bar{q} averaged over the rock mass by:

$$\bar{v} = \frac{\bar{q}}{\phi},$$

where ϕ is the porosity. For discrete modeling of fluid flow within a fracture, $\bar{v} \approx \bar{q}$, with $\phi \approx 1$. In most thermohydrologic models, the velocity is a derived quantity determined by the pressure and temperature distributions. The equations governing pressure and temperature are based on mass and energy conservation laws. The choice of pressure and temperature as variables describing the state of a fluid is arbitrary. All thermodynamic quantities are determined by the values of any two of them, together with the equation of state. Density ρ^W , internal energy U , enthalpy H , and others can also be used to determine the state of fluid flow and heat transfer.

This section discusses and compares the equations describing fluid velocity and the conservation laws of mass and energy used in the different models.

Fluid Velocity

The flux of fluid \bar{q} flowing relative to the solid rock is determined by the permeability of the formation \bar{k} , the viscosity of the fluid μ , and the driving forces of pressure gradient ∇P and gravitational body force $\rho \bar{g}$:

$$\bar{q} = - \frac{\bar{k}}{\mu} \cdot (\nabla P - \rho \bar{g}).$$

This is the familiar Darcy's law for the equation of motion. Darcy's law is an approximation of the general Navier-Stokes equation for momentum conservation.

Permeability \bar{k} is one of the most important hydraulic properties of the formation. In discrete modeling, the most frequently used approximation for fracture permeability is the parallel-plate model. The steady laminar flow between two parallel plates may be described by Darcy's equation with a discrete fracture permeability:

$$k^d = \frac{b^2}{12},$$

where b is the aperture of the parallel-plate flow path. The total flux through the cross section of aperture b and unit width is then proportional to b^3 (Witherspoon and others, 1980 and references therein). As a result of the b^3 nonlinear dependence of the flux, the fracture flow is sensitive to the displacement of the fracture surfaces induced by pressure changes in the fluid and stress changes in the rock blocks. The smooth parallel plate is an idealization of a real fracture. The surface roughness, asperity contact, and infill material may retard the flow and reduce the permeability. The texture

of the fracture surfaces also controls the mechanical behavior of a fracture. The fracture aperture varies nonlinearly with normal and shear stresses. Fracture permeability is one of the most difficult parameters to be measured (Brace 1980).

For large-scale modeling of a highly fractured rock mass, it is unrealistic to model all its fractures. In analogy to the porous medium, an equivalent permeability for the representation of the fractured rock mass may be defined over a large enough representative elementary volume. To date the equivalent permeability tensor can be constructed only for simple geometric models of fracture sets. For a set of parallel fractures with spacing Δ , the equivalent permeability is given by

$$k^f \approx \frac{b}{\Delta} k^d = \frac{b^3}{12\Delta},$$

and the corresponding porosity is b/Δ . In general, if sufficient data are available on the distributions of apertures, spacings, orientations, areal extent, and other fracture parameters, a statistical treatment will be necessary to derive the anisotropic permeability tensor. Although each individual fracture is highly permeable, the total permeability depends, among other factors, on the connectivity of the fracture network and may turn out to be small. The porosity ϕ is by definition the ratio of the void space to the total volume of a rock mass specimen. Only a small fraction of the void spaces in a fractured rock mass are continuous fracture flow paths that contribute to the permeability. Most of the other void spaces are disconnected fractures, isolated voids, and microcracks which are not paths for fluid flow (Norton and

Knapp 1977). The no-flow porosity may be important for the storage of fluid and for the diffusive transfer of radionuclides. It is, however, very difficult to distinguish quantitatively between the flow and no-flow porosity. The determination of the porosities is very important for the use of continuum models in the evaluation of the fluid velocity \bar{v} , which is related to the Darcy velocity \bar{q} by $\bar{v} = \bar{q}/\phi$. There may be a difference of several orders of magnitude in $\bar{v} = \bar{q}/\phi$ if the total porosity, instead of the flow porosity, is used.

In the double-porosity approximations, the equivalent continuum for the fractures and the equivalent continuum for the primary pores in the porous-medium blocks are treated as two overlapping systems. It is frequently assumed in double-porosity models that the equivalent fracture permeability \bar{k}^f is much larger than the porous medium permeability \bar{k}^m while the fracture porosity ϕ^f is much smaller than the porous medium porosity ϕ^m . In the thermodynamic description of a double-porosity medium, each point in space is characterized by two pressures, P^f , P^m , and/or two temperatures, T^f , T^m . The total pressure at a point is the sum of the two pressures: $P = P^f + P^m$ (Duguid and Lee 1977). The temperature at a point is related to the two temperatures by the weighted average: $T = (\phi^f T^f + \phi^m T^m)/(\phi^f + \phi^m)$ (O'Neill 1978).

Depending on the detail required for modeling, either the discrete fracture permeability k^d is used for small fracture grid blocks, or the equivalent continuum permeability k^f (or k^m) is used for large continuum grid blocks. The more detail required, the greater is the computational effort. The complexity of a model also depends on the couplings among the different processes through

the permeability functions. For the models reviewed, one of the following approximations for the treatment of permeability is used:

- (a) The permeability is independent of the variables (pressure, temperature, stress, etc.) and is treated as an input parameter for each grid block.
- (b) The permeability is a function of pressure and temperature, $k(P,T)$. The pressure change affects the effective stress $\sigma' = \sigma_N - P$ acting across the fracture surfaces. The normal stress σ_N is given and remains constant, so $\Delta\sigma' = -\Delta P$. An aperture-effective stress relationship $b(\sigma')$ and a permeability-aperture formula (for example, $k^d = b^2/12$) may be used to calculate the permeability as the pressure changes. The permeability-temperature dependence may also be important, to take into account the effects of thermal stress and thermally induced rock-fluid interactions.
- (c) The permeability is also a function of stress, $k(\bar{\sigma})$. In addition to the pressure and temperature field, the tensor stress field is modeled. The stress changes may be induced by hydraulic, mechanical, or thermal loading. The effective stress-displacement calculations and/or the thermomechanical calculations are used to determine the dependence of permeability on these variables.

The fluid velocity is inversely proportional to the dynamic viscosity μ .

The following are approximations for μ in the different models:

- (a) The viscosity is a constant. This is the case for isothermal saturated flow. The constant viscosity μ_0 is frequently combined with the permea-

bility as one lumped parameter, the hydraulic conductivity:

$$K_F = \frac{k\rho_o^w g}{\mu_o}.$$

- (b) The viscosity is a function of temperature $\mu(T)$. Most of the nonisothermal saturated flow models use formulas or tables to account for this dependence.
- (c) Under two-phase conditions, the effects of viscosity is modified by the relative permeabilities, which are mainly functions of fluid saturation S . In two-phase flow, the total flux has the liquid component l and the vapor component v . Each component is then proportional to k^α/μ^α , $\alpha = l, v$. The relative permeabilities, $k_r^\alpha(S^\alpha) < 1$, account for the reduction of the flux and μ^α is defined as the viscosity for each component.

The fluid flow is proportional to the driving force or gradient. The following are approximations used in the models:

- (a) The variation in the gravitational force $\rho^w g$ is neglected. This is a good approximation for slightly compressible flow when the liquid density variation with pressure is small. For some of the saturated-flow models, the hydrostatic pressure is subtracted from the fluid pressure and the driving force is expressed in terms of the incremental pressure P' or the hydraulic head h :

$$P' = P(\bar{r}, t) - P_o(z) = P - \int_z^o \rho^w(z') g dz' \approx P + \rho_o^w g z = P - \rho_o^w g D,$$

and

$$h = \int_0^P \frac{dP'}{\rho^W(P')g} + z = h_p + z \approx \frac{P}{\rho_0^W g} + z.$$

h_p is the pressure head component of h .

- (b) The Boussinesq approximation is used for the gravitational force imbalance (buoyancy) between hot and cold water. The buoyancy force is

$$(\rho^W - \rho_0^W)\bar{g} = -\beta_T^W(T - T_0)\bar{g},$$

where the thermal expansivity β_T^W is assumed to be constant. The density variation with temperature is considered only in the buoyancy force and is neglected in other terms of the governing equations.

- (c) The driving forces are the pressure gradient and the gravitational body force, $\nabla P - \rho^W \bar{g}$, for nonisothermal, saturated flow.
- (d) For two-phase flow, the density of liquid and the density of vapor are different. The driving force for each phase is $\nabla P - \rho^{\alpha} \bar{g}$, $\alpha = l, v$. Both phases have equal pressure.
- (e) The driving force for each phase is $\nabla P^{\alpha} - \rho^{\alpha} \bar{g}$, $\alpha = l, v$. The pressure difference between the phases, or the capillary pressure $P_c(S^V) = P^V - P^l$, is taken into account.
- (f) The inertial force is included. Darcy's equation represents the balance of the viscous dragging force $-\mu \bar{q}/k$ with the pressure gradient ∇P and

the gravitational body force $\rho^w \bar{g}$ but neglects the inertial force or acceleration $\rho^w \partial \bar{v} / \partial t$. The latter force is important for regions where the flow velocity is highly varying, for example, within large fractures near a wellbore. At high velocity, transition from laminar flow to turbulent flow may also occur. The pressure loss in a turbulent region will reduce the effective driving force.

Table 2 compares the approximations for the permeability of the formation, the viscosity of the fluid, and the driving force used in the models for determining the fluid velocity.

Table 2. Fluid Velocity:

$$\bar{q} = -\frac{\bar{k}}{\mu} \cdot (\text{driving force per unit volume}) = -\bar{K}_F \cdot (\text{hydraulic gradient})$$

Model	Permeability	Viscosity	Driving Force or Gradient
ROCMAS	$k^d(\sigma')$, k^m (c)	$1/\mu_o$ (a)	∇P (a)
TERZAGI	$\bar{k}(\sigma')$ (b)	$1/\mu_o$ (a)	$\rho^w g \nabla(z+h_p)$ (a)
CCC	$\bar{k}(\sigma', T)$ (b)	$1/\mu(T)$ (b)	$\nabla P - \rho^w \bar{g}$ (c)
Duguid	\bar{k}^f , k^m (a)	$1/\mu_o$ (a)	$\rho^w (\partial \bar{q} / \partial t) + \nabla P^i$, $i=f, m$ (a) (f)
O'Neill	\bar{k}^i (a)	$1/\mu(T)$ (b)	∇P^i , $i = f, m$ (a)
GWTherm	\bar{K}_F (a)	$\mu_o / \mu(T)$ (b)	$\nabla h + (\rho^w / \rho_o^w - 1) \hat{z}$ (b)
FINI	\bar{K}_F (a)	$\mu_o / \mu(T)$ (b)	$\nabla h - \beta_T^w (T - T_o) \hat{z}$ (b)
CFEST	\bar{K}_F (a)	$\mu_o / \mu(T)$ (b)	∇h (c)
SWIFT	\bar{k} (a)	$1/\mu(T, C)$ (b)	$\nabla P - \rho^w \bar{g}$ (c)
COATS	\bar{k} (a)	$k_r^\alpha(S) / \mu^\alpha(T)$ (c)	$\nabla P^\alpha - \rho^\alpha \bar{g}$, $\alpha = l, v$ (e)
Faust-Mercer	\bar{k} (a)	$k_r^\alpha(S) / \mu^\alpha(T)$ (c)	$\nabla P - \rho^\alpha \bar{g}$, $\alpha = l, v$ (d)
MUSHRM	$\bar{k}(P_c - P, T)$ (a)	$k_r^\alpha(S) / \mu^\alpha(T)$ (c)	$\nabla P - \rho^\alpha \bar{g}$, $\alpha = l, v$ (d)
SHAFT79	\bar{k} (a)	$(k_r / \mu)^\alpha(\rho, U)$ (c)	$\nabla P - \rho^\alpha \bar{g}$, $\alpha = l, v$ (d)

Fluid Flow Equation

The governing equation for the fluid flow is based on the conservation of fluid mass, or equivalently, the balance of the rate of change, the flux, and the prescribed source/sink of fluid mass:

$$\frac{\partial(\phi \rho^W)}{\partial t} + \nabla \cdot (\rho^W \bar{q}) = Q_F.$$

This equation of continuity, combined with Darcy's equation for \bar{q} , determines the pressure field. It is applicable either to a fracture with $\phi \approx 1$ or to a porous medium with $\phi \ll 1$. The variation of the porosity of the formation and the variation of the density of the fluid determine the transient term $\partial(\phi \rho^W)/\partial t$.

In the models reviewed, one of the following approximations for the porosity change $\Delta\phi$ is used.

- (a) $\Delta\phi = 0$ for constant porosity.
- (b) $\Delta\phi$ is linear in pressure change, $\Delta\phi = \beta_P^P \Delta P$ ($= \beta_h^P \Delta h_p$). The compressibility of pores β_P^P (or β_h^P) is assumed to be constant.
- (c) $\Delta\phi$ is nonlinear in pressure change. The porosity or the void ratio is a nonlinear function of the effective stress, $\sigma' = \sigma_N - P$, but the normal stress σ_N is given and remains constant.
- (d) $\Delta\phi$ is coupled to the stress-strain changes. The pressure change affects the stress field of the rock blocks, causing a strain, which in turn affects the porosity.

The density of the fluid ρ^W will also change in response to pressure and temperature changes. The approximations for the density change $\Delta\rho^W$ are:

- (a) $\Delta\rho^W = 0$ for incompressible flow with constant density.
- (b) $\Delta\rho^W$ is linear in pressure change, $\Delta\rho^W = \beta_P^W \rho^W \Delta P$, for slightly compressible, isothermal flow. The compressibility of water β_P^W is assumed to be constant.
- (c) ρ^W is slightly compressible with pressure increase and expandable with temperature increase, $\Delta\rho^W = \beta_P^W \rho^W \Delta P - \beta_T^W \rho^W \Delta T$. The fluid compressibility - β_P^W and the thermal expansivity β_T^W are assumed to be constants for nonisothermal, saturated flow. For a fluid with dissolved substances, ρ^W can also change with concentration C .
- (d) ρ is a nonlinear function of pressure and temperature.
- (e) For a liquid-vapor mixture, the density is $\rho = S^l \rho^l + S^v \rho^v$, with the saturations related by $S^l + S^v = 1$. Steam tables or nonlinear formulas are required to evaluate the sensitive changes of density. On the phase diagram, the nonlinearity of the fluid properties is most evident in the vicinity of the saturation line at which the variables change slope. Under two-phase conditions, the temperature is determined by the pressure, $T = T_S(P)$, and the saturation can be treated as a variable instead of the temperature. In some two-phase models, the density itself is treated as a primary variable.

The approximations for $\Delta\phi$ and $\Delta\rho^W$ in the different models are compared in Table 3. For some saturated flow models, the transient term $\partial(\phi\rho^W)/\partial t$ in the fluid flow equation is expressed in terms of constant total compressibility of the formation or the coefficient of specific storage S_s :

$$\frac{\partial(\phi\rho^W)}{\partial t} = \rho^W \frac{\partial\phi}{\partial t} + \phi \frac{\partial\rho^W}{\partial t} = \rho^W \beta_P \frac{\partial P}{\partial t} + \phi \rho^W \beta_P \frac{\partial P}{\partial t} = \frac{S_s}{g} \frac{\partial P}{\partial t} = \rho^W S_s \frac{\partial h}{\partial t}$$

Table 3. Fluid Flow Equation: $\frac{\partial}{\partial t} (\phi \rho^w) + \nabla \cdot (\rho^w \mathbf{q}) = Q_F$.

Model	Porosity Change	Density Change
ROCMAS	$\phi(\sigma')$ (d)	$\Delta \rho^w = \beta_P^w \rho^w \Delta P$ (b)
TERZAGI	$\Delta \phi = (1 - \phi) a_v \Delta P$ (c)	$\Delta \rho^w = \beta_P^w \rho^w \Delta P$ (b)
CCC	$a_v = - \partial e / \partial \sigma', \sigma' = \sigma_N - P$	$\rho^w(P, T)$ formula (d)
Duguid	$\Delta \phi^i = \phi^i \phi^j \beta_P^w \Delta P^j - (1 - \phi^i) \phi^i \beta_P^w \Delta P^i$ (a)	$\Delta \rho^w = \beta_P^w \rho^w \Delta P^i, i, j = f, m$ (b)
O'Neill	$\Delta \phi = \beta_P^P \Delta P$ (b)	$\Delta \rho^w = \beta_P^w \rho^w \Delta P - \beta_T^w \rho^w \Delta T$ (c)
GWTherm		$\Delta(\phi \rho^w) = \rho^w S_S \Delta h$ (b)
FINI		$\Delta(\phi \rho^w) = \rho^w S_S \Delta h$ (b)
CFEST	$\Delta \phi = \beta_h^P \Delta h_P$ (b)	$\Delta \rho^w = \beta_h^w \rho^w \Delta h_P - \beta_T^w \rho^w \Delta T + a_C \Delta C$ (c)
SWIFT	$\Delta \phi = \beta_P^P \Delta P$ (b)	$\Delta \rho^w = \beta_P^w \rho^w \Delta P - \beta_T^w \rho^w \Delta T + a_C \Delta C$ (c)
COATS	$\Delta \phi = \beta_P^P \Delta P$ (b)	$\rho(P, S)$ table, $\rho^\alpha(P, T)$ formula (e)
Faust-Mercer	$\Delta \phi = \beta_P^P \Delta P$ (b)	$\rho(P, H)$ formula (e)
MUSHRM	$\phi(P_C - P, T)$ (b)	ρ, U packages (e)
SHAFT79	$\Delta \phi = \beta_P^P \Delta P$ (b)	ρ, U table (e)

Heat Transfer Equation

The governing equation for the heat transfer through the formation is based on the conservation of energy:

$$\frac{\partial(\rho^m U)}{\partial t} + \nabla \cdot (\rho^w q_H) - \nabla \cdot \bar{K}_H \cdot \nabla T = Q_H.$$

The conservation of energy is expressed in terms of the rate of change of internal energy U of the fluid-rock mixture, the convective flux of enthalpy H of the fluid, the diffusive flux (conduction and/or dispersion) driven by the temperature gradient, and the heat source/sink Q_H . For single-phase models, the thermodynamic functions U and H are usually expressed in terms of temperature and/or pressure. Under two-phase conditions, steam tables or formulas are required to evaluate the nonlinear changes of U and H , together with the density ρ and other fluid properties. Some of the two-phase models use U or H as a primary variable.

For the transient internal energy accumulation term, $\partial(\rho^m U)/\partial t$, the different expressions used in the models are:

(a) $C_H^m \frac{\partial T}{\partial t}$, with a constant bulk heat capacity C_H^m ($= \rho^m c^m$) for the fluid-rock mixture.

(b) $[\phi \rho^w c^w + (1-\phi) \rho^r c^r] \frac{\partial T}{\partial t}$, where $\rho^w c^w$ is the heat capacity of fluid and $\rho^r c^r$ is the heat capacity of the rock.

(c) $\frac{\partial}{\partial t} [\phi \rho U + (1-\phi) \rho^r c^r T] = \frac{\partial}{\partial t} [\phi S^l \rho^l U^l + \phi S^v \rho^v U^v + (1-\phi) \rho^r c^r T]$ for two-phase flow.

$$(d) \quad \frac{\partial}{\partial t} [\phi \rho H + (1-\phi) \rho^x c^x T] - \frac{\partial}{\partial t} (\phi P) \approx \frac{\partial}{\partial t} [\phi S^l \rho^l H^l + \phi S^v \rho^v H^v + (1-\phi) \rho^x c^x T]$$

for two-phase flow. The enthalpy H is related to the internal energy U by the definition $H = U + P/\rho$. The pressure term due to compressible work is usually neglected in the two-phase energy equation.

The convective flux term can be expressed as:

- (a) $C_H^w \bar{q} \cdot \nabla T$ or $\rho^w c^w \bar{q} \cdot \nabla T$, where C_H^w or $\rho^w c^w$ is the heat capacity of the fluid. The heat is carried by the fluid with velocity \bar{q} .
- (b) $\nabla \cdot (\rho^w \bar{q} H)$ for saturated flow.
- (c) $\nabla \cdot (\rho^l \bar{q}^l H^l + \rho^v \bar{q}^v H^v)$ for two-phase flow.
- (d) $\nabla \cdot (\rho^l \bar{q}^l U^l + \rho^v \bar{q}^v U^v)$ for two-phase flow. The pressure work has been neglected.

Two approximations are used to describe the diffusive flux:

- (a) $\nabla \cdot K_T \nabla T$ for isotropic conduction with a scalar thermal conductivity K_T .
- (b) $\nabla \cdot \bar{\bar{K}}_T \cdot \nabla T$ for anisotropic conduction with a tensorial thermal conductivity $\bar{\bar{K}}_T$.
- (c) $\nabla \cdot (\bar{\bar{K}}_T + \bar{\bar{K}}_{TD}) \cdot \nabla T$ for both conduction and dispersion through the formation. The thermal dispersion depends on the fluctuations of microscopic velocities. The dispersive contribution can be regarded as an enhancement to heat conduction in the presence of fluid movement. Usually a linear relationship is assumed between the components of the dispersivity $\bar{\bar{K}}_{TD}$ and the components of the microscopic velocity $\bar{v} = \bar{q}/\phi$.

Table 4 summarizes the expressions of the heat transfer equation in different models.

Table 4. Heat Transfer Equation: $\frac{\partial(\rho^m U)}{\partial t} + \nabla \cdot (\rho^w q_H) - \nabla \cdot \bar{K}_H \cdot \nabla T = Q_H$

Model	Heat Accumulation	Convection	Diffusion
ROCMAS	$C_H^m \frac{\partial T}{\partial t}$ (a)		$-\nabla \cdot \bar{K}_T \cdot \nabla T$ (a)
CCC	$[\phi \rho^w c^w + (1-\phi) \rho^r c^r] \frac{\partial T}{\partial t}$ (b)	$\rho^w c^w q \cdot \nabla T$ (a)	$-\nabla \cdot \bar{K}_T \cdot \nabla T$ (b)
O'Neill	$[\phi^i \rho^w c^w + (1-\phi^i) \rho^r c^r] \frac{\partial T^i}{\partial t}$ (b)	$\rho^w c^w q^i \cdot \nabla T^i$ (a)	$-\nabla \cdot (\bar{K}_T^i + \bar{K}_{TD}^i) \cdot \nabla T^i$ (c)
GWATHERM	$C_H^m \frac{\partial T}{\partial t}$ (a)	$\nabla \cdot C_H^w q^w T$ (a)	$-\nabla \cdot \bar{K}_T \cdot \nabla T$ (a)
FINI	$C_H^m \frac{\partial T}{\partial t}$ (a)	$C_H^w q \cdot \nabla T$ (a)	$-\nabla \cdot \bar{K}_T \cdot \nabla T$ (b)
CFEST	$[\phi \rho^w c^w + (1-\phi) \rho^r c^r] \frac{\partial T}{\partial t}$ (b)	$\rho^w c^w q \cdot \nabla T$ (a)	$-\nabla \cdot \bar{K}_T \cdot \nabla T$ (b)
SWIFT	$\frac{\partial}{\partial t} [\phi \rho^w U + (1-\phi) \rho^r c^r T]$ (b)	$\nabla \cdot (\rho^w q_H)$ (b)	$-\nabla \cdot (\bar{K}_T + \bar{K}_{TD}) \cdot \nabla T$ (c)
Coats	$\frac{\partial}{\partial t} [\phi S^l \rho^l U^l + \phi S^v \rho^v U^v + (1-\phi) \rho^r c^r T]$ (c)	$\nabla \cdot (\rho^l q_H^l + \rho^v q_H^v)$ (c)	$-\nabla \cdot \bar{K}_T \cdot \nabla T$ (a)
Faust-Mercer	$\frac{\partial}{\partial t} [\phi \rho^H + (1-\phi) \rho^r c^r T]$ (d)	$\nabla \cdot (\rho^l q_H^l + \rho^v q_H^v)$ (c)	$-\nabla \cdot \bar{K}_T \cdot \nabla T$ (a)
MUSHRM	$\frac{\partial}{\partial t} [\phi \rho^U + (1-\phi) \rho^r c^r T]$ (c)	$\nabla \cdot (\rho^l q_U^l + \rho^v q_U^v)$ (d)	$-\nabla \cdot \bar{K}_T \cdot \nabla T$ (a)
SHAFT79	$\frac{\partial}{\partial t} [\phi \rho^U + (1-\phi) \rho^r c^r T]$ (c)	$\nabla \cdot (\rho^l q_H^l + \rho^v q_H^v)$ (c)	$-\nabla \cdot \bar{K}_T \cdot \nabla T$ (a)

Coupling of Fluid Flow and Heat Transfer

The fluid flow equation and the heat transfer equation are coupled through the fluid velocity \bar{q} in the flux terms and through the temperature and pressure dependences of the fluid properties (ρ^w , μ) and formation properties (k , ϕ). In most models using Darcy's approximation, the flow velocity equation is substituted into the fluid flow equation and the heat transfer equation. The elimination of \bar{q} simplifies the set of governing equations for thermohydrologic flow to two equations for the pressure and temperature fields. Once these fields are determined, the Darcy velocity \bar{q} or the microscopic fluid velocity \bar{v} is calculated from the pressure gradient, bouyancy force, viscosity, and permeability.

For low-permeability formations, the flow-induced convective transfer and the thermal dispersion are less important than the conductive transfer through the rock. In this case, the temperature field is independent of the fluid flow, and the temperature equation with heat conduction only can be decoupled from the pressure equation. However, the fluid flow field depends on the temperature field. The heat generated by the wastes affects the fluid flow directly through changes of fluid properties and indirectly through changes in rock stresses which may alter the permeability and porosity of a formation. The complete determination of the fluid flow field requires thermal-hydrologic-mechanical calculations. For fractured rock masses with very deformable fractures, the couplings may be strong. With the fluid flow field determined, the radionuclide transport can be modeled.

II. NUMERICAL SOLUTIONS

Numerical methods are generally required to solve complex equations and coupled processes in heterogeneous and anisotropic formations under various initial and boundary conditions. In most numerical models, the governing equations are approximated by algebraic equations relating unknown variables at discrete nodal points and at different time intervals. The governing equations for thermohydrologic flows have diffusive terms $\nabla \cdot (\rho^w k / \mu) \cdot \nabla P$ and $\nabla \cdot \bar{K}_H \cdot \nabla T$; a convective term $\rho^w c^w q \cdot \nabla T$; and storage-capacity terms $S_g (\partial P / \partial t)$ and $C_H (\partial T / \partial t)$. The accuracy and efficiency of a model depend on the numerical approximations for evaluating the spatial gradient ∇ and the time derivative $\partial / \partial t$ and on the solution scheme of the algebraic equations.

This section discusses the general features of numerical methods and summarizes the space discretization, time stepping, and equation solver of different models.

Spatial Approximations

The finite-difference, the integrated finite-difference, and the finite-element methods are frequently used to approximate the spatial terms in the governing equations. The distinctions among the different methods are in the numerical approximation of the gradient operator ∇ , in the evaluation of variable-dependent coefficients, and in the spatial discretization of the region. For the modeling of complex fractured formations, it is important to have the capability of handling a large number of nodes with a nonuniform, irregular distribution in multidimensional space.

(a) Finite-Difference Method

In most of the finite-difference models, the distribution of nodes is regular, with either uniform or nonuniform spacings along orthogonal coordinate systems (x-y-z, r- θ -z, ...). Surrounding each nodal point there is a region bounded by interfaces normal to the coordinate axes; this region is called a nodal block, cell, or element. Between two nodes indexed by i, i+1 in the x-direction, the interface i+1/2 can intersect the x-axis either midway between i, i+1, or at other off-center locations.

For the evaluation of a spatial gradient, the partial differential of a variable is directly expressed in terms of the difference between two neighboring nodal values. For example, the x-component of the fluid flux term $\nabla \cdot (\rho^w \bar{q}) = -\nabla \cdot (\rho^w k / \mu) \cdot \nabla P$ is approximated at node i by

$$\frac{(\rho^w q_x)_{i+1/2} - (\rho^w q_x)_{i-1/2}}{x_{i+1/2} - x_{i-1/2}},$$

and the $\partial P / \partial x$ in $\rho^w q_x$ at the interface $i \pm 1/2$ is further approximated by

$$\frac{P_{i \pm 1} - P_i}{x_{i \pm 1} - x_i}.$$

With these two steps, the nodal value P_i is algebraically related to its two neighboring values for a one-dimensional problem or six neighbors in a three-dimensional problem. The coefficients at the interfaces $i \pm 1/2$ can be evaluated as the arithmetic mean, for example:

$$\left(\frac{\rho^w}{\mu}\right)_{i \pm 1/2} = \frac{\left(\frac{\rho^w}{\mu}\right)_{i \pm 1} + \left(\frac{\rho^w}{\mu}\right)_i}{2},$$

or as the harmonic mean, for example:

$$\left(\frac{1}{k}\right)_{i\pm 1/2} = \frac{\left(\frac{\Delta x}{k}\right)_{i\pm 1} + \left(\frac{\Delta x}{k}\right)_i}{\Delta x_{i\pm 1} + \Delta x_i},$$

where $\Delta x_i = |x_{i+1/2} - x_i|$, $\Delta x_{i+1} = |x_{i+1/2} - x_{i+1}|$. These finite-difference approximations can be generalized for an irregular grid. For example, the factor 1/2 in the arithmetic mean can be replaced by other fractional weighting factors; the Δx_i in the harmonic mean can be replaced by the normal distance from the node to the interface between the neighboring nodes if the neighboring nodes are not along the coordinates in an irregular grid system.

For the first-order convective term $\rho^w c^w \bar{q} \cdot \nabla T$ in the heat transfer equation, the central difference in space, or central weighting,

$$\frac{T_{i+1/2} - T_{i-1/2}}{x_{i+1/2} - x_{i-1/2}}$$

with $T_{i\pm 1/2} = 0.5(T_{i\pm 1} + T_i)$ can be used for $\partial T / \partial x$. With this central weighting scheme, the space truncation approximation of the convective term is correct to the second order. However, there is a tendency for the solutions with central weighting to oscillate artificially at high flow velocity. The convective flux associated with the flow velocity \bar{q} carries heat downstream; a nodal point between an upstream and a downstream node will have temperature closer to the upstream value. The central weighting scheme does not take into account this convective effect. In the upstream weighting scheme, the interface temperature is set equal to the upstream value, that is, $T_{i+1/2} = T_{i+1}$ if fluid flows from $i+1$ to i . In other words, a backward difference, $T_{i+1} - T_i$, is used for the convective term at node i . The upstream weighting is also

frequently used in the evaluation of the relative permeability k_r^α and the enthalpy H^α in two-phase, vapor-liquid fluid flow models. The upstream weighting eliminates the oscillation but introduces a space-discretization error which is virtually equivalent to physical diffusion. The error of numerical diffusion in the upstream weighting scheme and the error of numerical oscillation in the central weighting scheme may be compensated and minimized by using the partial upstream weighting $T_{i+1/2} = a T_{i+1} + (1 - a)T_i$ with $0.5 \leq a \leq 1$, or the discontinuous weighting with central weighting at low flow velocity and upstream weighting at high flow velocity, or other weighting schemes.

The conductive term $\nabla \cdot \bar{\bar{K}}_T \cdot \nabla T$ in the heat transfer equation, like the $\nabla \cdot (\rho \bar{w} k / \mu) \cdot \nabla P$ in the fluid flow equation, is a second-order diffusive term. If the dispersivity $\bar{\bar{K}}_{TD}$ is added to the thermal conductivity $\bar{\bar{K}}_T$, the temperature equation is coupled to the fluid flow not only in the convective flux but also through the sensitive dependence of $\bar{\bar{K}}_{TD}$ on fluid velocity. As the velocity changes direction and magnitude, the effective conductivity-dispersivity $\bar{\bar{K}}_{TD} + \bar{\bar{K}}_T$ changes. These changes complicate the algebraic treatment of the diffusive term but may stabilize the numerical oscillation or decrease the relative importance of the numerical diffusion.

(b) Integrated Finite-Difference Method

The integrated finite-difference method is a generalization of the finite-difference method. In the integrated finite-difference method, the region to be modeled is partitioned into arbitrarily shaped polyhedrons. The numerical equations are formulated from the integral form of the governing equations, or equivalently, from the conservation laws over each finite volume block. The

formulation emphasizes the direct representation of the conservation laws in relating the rates of change of mass and energy in each block to the fluid and heat fluxes over the interfaces bounding that block (Edwards 1972; Narasimhan and Witherspoon 1976). To evaluate the rates of change and the fluxes over the boundary surfaces of a volume element, the block volume, surface areas, and normal distances from the node to the faces of the polyhedron are required and can be treated as input data specified by the modelers. These additional input requirements allow the flexibility in the mesh design for irregular grid systems. For a regular mesh in orthogonal coordinates, the integrated finite-difference method is essentially equivalent to the finite-difference method. Both methods use the simple finite differencing, or linear interpolation between neighboring nodal values, in the evaluation of spatial gradients normal to the interfaces.

(c) Finite-Element Method

Similar to the integrated finite-difference method, the finite-element method also has the flexibility of specifying the distribution of nodes and using an irregular mesh to divide the region into elements. However, the spatial relationship between the nodes and the volume elements are different in the two methods. In the finite-element method, an element is the region bounded by curves connecting the nodes. Therefore a node is on the boundary of an element instead of within a block as its centroid. Different element shapes can be defined. For example, a two-dimensional linear triangular element is a triangle with three nodal vertices, a quadrilateral element has four corner nodes, and a three-dimensional orthorhombic element has eight corner nodes (Zienkiewicz 1977; Pinder and Gray 1977). Within a model, different

types of elements can be used. The fractures can be treated with special long, thin elements while the porous medium blocks can be treated with large triangular or quadrilateral elements.

The value of a variable within an element is interpolated in terms of the values of the variable at the corner nodes. Simple polynomials (linear, quadratic, or cubic) are frequently used as linear independent basis functions for the interpolation. For linear interpolation, the values at the corner nodes are sufficient to define the basis functions for the interpolation. For quadratic or cubic interpolations, the basis functions are specified with either the values at additional side nodes or the values of the partial derivatives of the variable at the corner nodes. For example, the three-dimensional hermite interpolation functions are a set of four cubic polynomials defined by the value and its three partial derivatives at each corner node.

The finite-element numerical equations are usually formulated with either the Galerkin scheme or the variational approach. In the Galerkin finite-element scheme, a trial solution with basis function interpolation is substituted into the differential equations. The space-differential operators operate on the basis functions. The residue of the trial solutions is integrated over the element weighted by the basis functions. The integration is usually carried out using two- or three-point Gaussian integration for each dimension. If the trial solution is expanded in terms of a complete set of an infinite number of linearly independent functions in the elements, the trial solution is exact and the residue would vanish. In the Galerkin weighted residual method, the number of basis functions is finite and the residue is forced to be zero by

requiring the orthogonality of the residue to the same set of basis functions used in the expansion of the trial solution. For the convective terms, the problems of numerical oscillation and numerical diffusion also exist in the finite-element method. Upstream basis functions can be used.

An equivalent expression of the governing partial differential equations can be given in terms of variation of functionals. A functional is an integral over space with the integrand bilinear in the variable basis functions. Upon variational operation on a functional, the corresponding differential equations emerge. The variational approach for fluid flow is based on the same minimum energy principle or Lagrangian formulation as that used to study the equilibrium states in mechanics or stress analysis. In the variational approach to the finite-element method, the trial solutions, as expansions in basis functions, are substituted into the functional integrals. The differential operators in the functional integrals operate on the basis functions in a manner similar to that in the weighted residual procedure of the Galerkin formulation.

With the use of the Gaussian algorithm for element integration, the coefficients, such as $\rho^W k/\mu$ in the pressure equation and $\rho^W c^W q$ in the temperature convection term, are evaluated at the Gaussian points within an element. This is different from the finite-difference method with the coefficients calculated at the interfaces between blocks. The finite-element method, with the use of the basis function interpolation over more than two points, can evaluate gradients in both normal and tangential directions and handle tensorial quantities more easily.

(d) Spatial Approximations in Models

Table 5 summarizes the dimension, the space discretization method, the basic block or element shape, the evaluation of the coefficient, and the upstream weighting of different models.

Table 5. Spatial Approximations

Model	Method	Shapes	Coefficient evaluation	Upstream weighting
ROCMAS	2D, FE	quadrilateral (two-node for fracture flow)		
TERZAGI	3D, IFD	polyhedron	Harmonic mean for k, ρ^W	
CCC	3D, IFD	polyhedron	Harmonic mean for $k, \rho^W/\mu, K_T$	$0.5 \leq a \leq 1$
Duguid	2D, FE	quadrilateral	2x2 Gaussian quadrature	
O'Neill	3D, FE	orthorhombic hermite basis	2x2x2 Gaussian quadrature 3x3x3 for $\rho^W k/\mu$	
GW THERM	2D, FD	rectangular (x-z, r-z)	Arithmetic mean	$a = 0.5,$ low q ; $a = 1.,$ high q
FINI	2D, FE	triangular, quadratic basis (6-node gap for fracture)	4 or 7 integration points	
CFEST	3D, FE	quadrilateral	$2^3, 3^3,$ or 5^3 Gaussian	
SWIFT	3D, FD	orthorhombic	Arithmetic mean for $\rho^W/\mu, \rho^W \bar{g}$	$a = 0.5$ or $a = 1$
Coats	3D, FD	orthorhombic	Harmonic mean for k arithmetic mean for $\rho/\mu, \rho \bar{g}$	$a = 1$ for k_T, H
Faust-Mercer	3D, FD	orthorhombic	Harmonic mean for k, K_T arithmetic mean for ρ, μ, T^1	$a = 1$ for k_T, H
MUSHRM	3D, FD	orthorhombic		$a = 1$ for convection
SHAFT79	3D, IFD	polyhedron	Harmonic mean for k, K_T arithmetic mean for ρ (optional for $k_T/\mu, H$)	$0.5 \leq a \leq 1$ for $k_T/\mu, H$

Temporal Approximations

First-order finite difference in time is frequently used to approximate the time derivative $\partial/\partial t$ for the transient rates of change in the governing equations. According to the conservation laws or the governing equations, the rates of change of mass and energy are balanced by the fluid and heat fluxes and the source/sink terms. Before the discussion on the implicit transient treatment, nonlinear coefficient evaluation, and coupling equation solution, it is of interest to note that the temporal approximations are closely related to the spatial methods used in a model.

In the integrated finite-difference and finite-difference methods, the value of the variable at a given node represents the average of the values within the block enclosed by the surrounding interfaces on which the fluxes are evaluated. The balance between the rate of accumulation within the block and the net flux across the interfaces is explicitly preserved in the numerical equations. In the finite-element method, each element is shared by the nodes on the boundary, and each node is surrounded by several elements. Although the transient term can be handled easily in the weighted residual formulation, the mathematical relationship between the rate of accumulation associated with a block and the fluxes evaluated at the Gaussian points in the surrounding elements is an indirect representation of the conservation law. In the diagonal or lumped-capacity approach, the time derivative in the governing equation is determined independently of the orthogonalization process.

(a) Implicit Equations

With either the finite-difference or the finite-element method, the analysis of the transient equation results in a system of equations of the matrix form:

$$[A] \left\{ \frac{df}{dt} \right\} + [B] \{f\} + \{R\} = 0,$$

where the column $\{f\}$ contains the nodal values of pressure, temperature, or other thermodynamic variables. The coefficient matrix $[A]$ contains the coefficients of the fluid storage S_g or the heat capacity C_H associated with the time derivative $\{df/dt\}$, $[B]$ contains the spatial approximations (finite difference or finite element) of the fluxes, and $\{R\}$ contains the known information such as source/sink or boundary conditions.

The first-order temporal finite difference from time t to $t+\Delta t$ is:

$$\left\{ \frac{df}{dt} \right\} \approx \frac{\{f\}_{t+\Delta t} - \{f\}_t}{\Delta t}.$$

To solve the unknown $\{f\}_{t+\Delta t}$ from the known solution $\{f\}_t$, the other terms in the governing equations can be interpolated between $t+\Delta t$ and t . With linear interpolation, the matrix equation becomes

$$\frac{[A]}{\Delta t} (\{f\}_{t+\Delta t} - \{f\}_t) + [B] (\lambda \{f\}_{t+\Delta t} + (1 - \lambda) \{f\}_t) + \lambda \{R\}_{t+\Delta t} + (1 - \lambda) \{R\}_t = 0.$$

For the forward-differencing explicit scheme with interpolation factor $\lambda = 0$, the $\{f\}_{t+\Delta t}$ can be easily determined by multiplying the matrix equation with $\Delta t [A]^{-1}$. The explicit scheme generally requires a minimum of computational effort. However, it is only conditionally stable. Usually the implicit schemes with the interpolation factor $0.5 < \lambda < 1$ are stable. The central

differencing Crank-Nicholson scheme ($\lambda = 0.5$) is accurate in Δt to the second order. The backward differencing implicit scheme ($\lambda = 1.0$) is usually unconditionally stable and is correct in time to the first order.

(b) Nonlinear Coefficients

In the above discussion about the implicit schemes, we have not taken into consideration the dependence of the coefficient matrices [A] and [B] on time. In general, the fluid storage S_g or the heat capacity C_H in [A] and the hydraulic conductivity $\rho^w \bar{k} / \mu$, the diffusive coefficients $\bar{K}_T + \bar{K}_{TD}$, or the convective flux $\rho^w \bar{q}$ in [B], depend on the time-dependent variables. These time-dependencies of the coefficients cannot be neglected for the thermohydrologic flows which have a sensitive dependence of fluid properties ρ^w and μ on variables P and T. The formation properties, especially the permeability k^d of discrete fractures, can also be sensitive functions of P and T. Empirical $k^d(P, T)$ relationships or hydromechanical and thermomechanical calculations may be required to model the large changes of permeability and aperture of fractures with thermohydrologic flows.

In the semi-implicit scheme, the known values of the variables at time t are used in the calculations of the coefficients. In a fully implicit scheme, the coefficient matrices [A] and [B] are evaluated at $t + \Delta t$. In the latter case, the matrix equation is no longer linear in $\{f\}_{t + \Delta t}$, and iterative procedures are needed to handle these nonlinearities. The Newton-Raphson procedure, or predictor-corrector method, is frequently used. The Newton-Raphson procedure involves approximating the nonlinear equations with a first-order

Taylor series expansion about an assumed solution. If for each grid block the nonlinear set of equations is expressed in vector form as:

$$\bar{V}(\bar{x}) = 0,$$

where \bar{x} is the vector of unknown variables at each grid block, the linearized set of equations is:

$$\bar{V}(\bar{x}^k) + \sum_i \left[\frac{\partial \bar{V}(\bar{x})}{\partial x_i} \right]^k (x_i^{k+1} - x_i^k) = 0,$$

where i sums over the number of unknown variables per equation at each grid block. (For example: the number is $14 = 2(1 + 6)$ for a (P,T) two-variable model with a three-dimensional rectangular grid having each grid block connected to 6 neighbors). The partial derivatives of the nonlinear coefficients are calculated at the values of the variables at the old k -th iteration, and the changes in the variables $(x_i^{k+1} - x_i^k)$ are solved by the linearized equation. The iteration proceeds until it converges to a specified criterion. The Newton-Raphson iteration is frequently used in two-phase, steam-water models to handle nonlinear thermodynamic variables near the saturation line. In the structure analysis of nonlinearly deformable fractures, the variable stiffness method and the load transfer method are modifications of the Newton-Raphson scheme (Goodman 1976).

(c) Coupling Solution Schemes

The coupled equations of pressure and temperature can be solved either sequentially or simultaneously. The sequential method solves the equations separately and treats the variables as unknowns only when their respective equations are being solved. The fluid flow equation for pressure is solved

first using the most current estimate of the temperature field in the evaluation of the density and viscosity of fluid. Then the heat transfer equation for temperature is solved using the new pressure gradients in the evaluation of the Darcy flux. The steps are repeated until successive iterations yield compatible results. A model using this sequential approach is usually more easily constructed from simpler models solving uncoupled equations. On the other hand, many cycles may be required if the couplings are strong. The coupled variables can also be solved simultaneously, which involves larger matrices.

(d) Temporal Approximations in Models

Table 6 summarizes the implicit interpolation factor, the treatment of nonlinear coefficients, and the solution scheme for coupled equations used in the different models.

Table 6. Time Difference

Model	Interpolation factor	Nonlinear coefficients	Solution Scheme
ROCMAS	predictor-corrector scheme	$\bar{\sigma}$, \bar{u} stiffness perturbation	P, \bar{u} simultaneously
TERZAGI	$\lambda = 0, 0.5, 1$ (0.57 - 1)	M_c , k from projection	
CCC	$\lambda = 0, 0.5, 1$ (0.57 - 1)	Iteration	P, T simultaneously
Duguid	$\lambda = 0.5, 1$		P^i, q^{-i} simultaneously
O'Neill	$\lambda = 0.5, 1$	Iteration	P, T^i sequence & iteration
GWTherm	$\lambda = 1.$		P, T sequence
FINI	$\lambda = 2/3$ (diffusion term)		Iteration
CFEST	$\lambda = 1.$	Iteration	P, T, C sequence & iteration
SWIFT	$\lambda = 0.5, 1.$	H, μ iteration	P, T, C sequence & iteration
Coats	$\lambda = 1.$	Newton-Raphson	P, S or P, T simultaneously
Faust-Mercer	$\lambda = 1.$	Newton-Raphson	P, H simultaneously
MUSHRM	$\lambda = 1.$	Newton-Raphson	ρ , U simultaneously
SHAFT79	$\lambda = 1.$	Newton-Raphson	ρ , U simultaneously

Matrix Solvers

After temporal finite difference, spatial discretization, and linearization of the coefficients in the governing equations, the partial differential equations are transformed into a system of simultaneous linear algebraic equations or a matrix equation of the form

$$[M] \{f\} = \{F\}.$$

The size of the matrix depends on the number of nodes, the number of variables and the solution schemes. For example, in a region with m nodes for solving simultaneously the two thermodynamic variables P and T , the matrix is $2m \times 2m$ in size. The solution for the $2m$ unknown nodal values at time $t+\Delta t$ in $\{f\}$ can be obtained through the use of direct elimination methods or the use of iterative methods.

(a) Direct Elimination Methods

Many of the direct methods are variations of the Gaussian elimination procedure. In this procedure, one unknown is eliminated from one equation at a time. The procedure works in a systematic way so that a general matrix equation is reduced to a triangular system. In the lower-triangular system, the first equation has one unknown, the second equation has two unknowns, etc. The triangular system can be solved step by step, the first unknown being determined by the first equation and then the second unknown being determined by the second equation upon substitution of the first solution. This forward substitution proceeds until all the unknowns are determined. Similarly, the upper-triangular system can be solved by backward substitution.

The L-U decomposition is one method of Gaussian elimination. With the matrix $[M]$ decomposed into a lower- and an upper-triangular matrix, $[M] = [L][U]$, the matrix equation $[M]\{f\} = \{F\}$ is equivalent to two triangular systems:

$$[L]\{g\} = \{F\} \quad \text{and} \quad [U]\{f\} = \{g\}.$$

If $[L]$ and $[U]$ are known, the matrix equation can be solved by forward and backward substitution. With a given $n \times n$ matrix $[M]$, the matrices $[L]$ and $[U]$ are not unique. There are n^2 elements in $[M]$ and $0.5n(n+1)$ unknown elements in $[L]$ and the same number in $[U]$. Therefore, there are $n(n+1) - n^2 = n$ elements which can be set to any value. In the Doolittle method, the diagonal elements of $[L]$ are set to unity. With the n diagonal elements fixed, other elements in $[L]$ and $[U]$ can be determined algebraically. Alternatively in the Crout method, the diagonal elements of $[U]$ are set to unity instead. The Crout and the Doolittle method are two popular direct-elimination solution schemes.

The efficiency of a direct matrix solver depends strongly on the structure of a matrix. For the tridiagonal banded matrix frequently encountered in the application of numerical methods, the number of algebraic operations is approximately $5n$, which is much smaller than the $n^3/3$ required for Gaussian elimination of a general $n \times n$ matrix (Dahlquist and Bjorck 1974). In the alternating-direction-implicit (ADI) finite-difference method for a regular grid in two- or three-dimensional space, the partial differentials along different directions are solved and updated sequentially for fractional ($1/2$ or $1/3$) time steps. Each nodal unknown for a quasi-one-dimensional fractional step is connected to only two neighboring unknowns, so that the matrix has nonzero elements only on the diagonal and two nearest off-diagonals.

The matrix equation can then be easily solved by the tridiagonal or Thomas' algorithm.

In most two- or three-dimensional methods, the matrix is sparse, with the number of nonzero off-diagonal matrix elements in each row or column depending on the number of neighbors of the corresponding node. The positions of the off-diagonal matrix elements relative to the diagonal element depend on the ordering of the nodes. Different ordering or numbering schemes can be made either to optimize the banding of matrix elements or to express parts of the matrix in diagonal or triangular form and minimize the computational effort. Another procedure required to ensure numerical stability and to minimize round-off errors is the pivoting operation, which interchanges one row with another row or one column with another column in the matrix. It is necessary to perform the pivoting operation if zero or nearly zero elements are used during the Gaussian elimination procedure.

(b) Iterative Methods

If the matrix is sparse and large, iterative methods may offer certain advantages over direct methods. An iterative method starts from a first approximation, which is successively improved until a sufficiently accurate solution is obtained. Some examples of iterative methods are briefly described here to demonstrate the procedure involved (Dahlquist and Bjorck 1974).

If one diagonally splits a matrix $[M]$ into lower- and upper-triangular systems, $[M] = [D] + [L] + [U]$. The matrix equation $[M]\{f\} = \{F\}$ can be rewritten as:

$$([D] + [L])\{f\} = -[U]\{f\} + \{F\}.$$

An approximate solution from the k -th iteration step to the $(k+1)$ -th step is

$$\{f\}^{k+1} = ([D] + [L])^{-1}(-[U]\{f\}^k + \{F\}).$$

This is the matrix form of Gauss-Seidel's method. The inverse of the lower triangular $([D] + [L])$ can be handled by forward substitution.

If the residual from k -th to $(k+1)$ -th iteration is denoted by

$\{r\}^k = \{f\}^{k+1} - \{f\}^k$, the generalized iterative method $\{f\}^{k+1} = \{f\}^k + w\{r\}^k$ is the successive overrelaxation (SOR) method. In matrix form, the new solution is:

$$\{f\}^{k+1} = ([D] + w[L])^{-1}(((1 - w)[D] - w[U])\{f\}^k + w\{F\}).$$

The relaxation factor w should be chosen so that the rate of convergence is optimized. Eigenvalue analyses are frequently used for determining the best relaxation factor. For real, symmetric, and positive-definite matrices, $0 < w < 2$. Other relaxation or acceleration schemes can be constructed in a manner similar to that used for the successive overrelaxation method.

The advantages of direct methods and iterative methods can be combined in the block iterative methods. In the block iterative methods, the coefficient matrix is partitioned into blocks and all elements of a block are operated on during one iterative step. Within each block, a direct solution scheme is used. The alternating-direction-implicit procedure is an example of the block iterative method. Each block is tridiagonal and can be easily solved. In general, the block iterative method is superior to the corresponding point iterative method.

(c) Matrix Solvers in Models

Table 7 summarizes the main characteristics of the matrix solver for each model. In many cases, the major portion of the computational effort is on the solution of the matrix equation. The nature of the problem, the size of the grid system, and the limitation of the computer storage determine the choice of the matrix solver and the efficiency of a model. With the rapid development of general-purpose matrix solving packages and the improvement of computing and storage capacity, more models are switching from iterative methods to direct-solution methods. Direct solvers usually require larger core storage but minimize convergent tests.

Table 7. Matrix Solvers

Model	Matrix Solution Characteristics
ROCMAS	Crout L-U decomposition
TERZAGI	Evans' accelerated iterative scheme
CCC	Block ordering with permutation matrices and L-U decomposition
Duguid	Crout or Doolittle L-U decomposition
O'Neill	Envelope storage and sparse matrix decomposition
GWATHERM	Tridiagonal algorithm
FINI	Symmetric decomposition
CFEST	Nonzero element compressed matrix storage and elimination
SWIFT	Two-line SOR or alternating diagonal ordering and elimination
Coats	Alternating diagonal ordering and elimination
Faust-Mercer	3-D: slice SOR; 2-D: alternating diagonal ordering
MUSHRM	Tridiagonal algorithm
SHAFT79	Block ordering with permutation matrices and L-U decomposition

III. COMPUTER CODES

After formulation of the governing equations and the selection of the numerical methods, the implementation of the computer code is a major effort in the development of a model. A general purpose code should be easy to use by both the developers and other users. This section discusses some of the practical aspects of using a code. Although detailed knowledge of the governing equations and the numerical methods are helpful in using a code, a user may be more interested in its capabilities and the input-output of the code. The following nine subjects characterize a code from a user's viewpoint.

Documentation

The user's manual, the code listing, the computer systems used, and the background of code development are of general interest. Table 8 summarizes the source information of the codes.

Spatial Grid

The basic shape of blocks or elements were discussed in the previous section (Table 5). Versatility in grid mesh design for modeling is especially important for fracture simulations which require complex discretization of the spatial domain.

Material Properties

In preparing to use a code, it is essential to know the required input of material properties and the modeling capabilities to treat heterogeneity, anisotropy, pressure-, temperature-, and stress-dependence. The capabilities of different models were summarized earlier; see Table 2 for permeability;

Table 8. Computer Codes

Model	Code Listing	User's Manual	Computer Systems	References
ROCMAS	yes	yes	CDC	Noorishad and Ayatollahi (1980)
TERZAGI	yes	yes	CDC, IBM	Narasimhan and Witherspoon (1977, 1978), Narasimhan (1980a,b)
CCC	yes	yes	CDC, IBM	Lippmann and others (1977b) Mangold and others (1979) Bodvarsson and others (1979)
Duguid	yes		CDC, IBM	Duguid (1973) Duguid and Abel (1974) Duguid and Lee (1977)
O'Neill	yes	yes	IBM	O'Neill (1977, 1978)
GWTherm	Dames and Moore	yes	CDC	Dames and Moore (1978) Runchal and others (1979)
FINI	Acres	yes	GE	Burgess (1977), Skiba (1977) Skiba and others (1977) Ratigan and others (1977)
CFEST FE3DGW	yes (FE3DGW)	yes (FE3DGW)	CDC, PDP, Burroughs	Gupta and Tanji (1976, 1977) Gupta and others (1975, 1980)
SWIFT	yes	yes	CDC, IBM	Dillon and others (1978) U.S. Geological Survey (1976)
Coats	Intercomp			Coats (1977) Coats and others (1974, 1977)
Faust- Mercer	yes (2D)	yes (2D)		Faust and Mercer (1979a,b, 1977a,b)
MUSHRM	S ³			Pritchett (1975, 1978) Garg and Pritchett (1977)
SHAFT79	yes	yes	CDC	Pruess and others (1979a,b,c) Pruess and Schroeder (1979, 1980)

Table 3 for porosity and rock medium compressibility; and Table 4 for heat capacity, thermal conductivity, and dispersivity.

Fluid Properties

The evaluations of the fluid properties determine the thermodynamic range of applicability of a nonisothermal model. The dependence of density and viscosity on temperature and pressure can be calculated either from a given formula or interpolated from tabulated values, as shown in Tables 2 and 3.

Sources and Sinks

The fluid source and sink terms simulate the injection and production at wells which are used to measure the in-situ material properties of the fractured rock formation. The localized, time-dependent heat sources from the radioactive decay of the waste in a repository will induce temperature increases, stress changes, and buoyancy flows which are important for the repository evaluations.

Initial Conditions

The initial conditions determine the solutions at later times. In simulations over long time spans, it is frequently necessary to stop at intermediate times to check the solutions and then continue the calculations. A convenient restart procedure is desirable.

Boundary Conditions

The flexibility of treating various boundary conditions by the program is important for complex problems.

Time Stepping and Solution Control

The time steps can be specified by the user or controlled by the program according to specified criteria. It is important in the use of a code to know the procedures used in the program for checking the convergence of solutions. Convergence tests and error estimations should be included in the program. For the simulation of fluid flow around a repository, high accuracy in the pressure solutions is required to calculate the pressure gradients and the fluid velocities to be used in radionuclide transport calculations.

Output

The printer and graphic output are important for the analysis and presentation of the results of modeling.

IV. VALIDATIONS

Testing of a code is important in checking the mathematical validity, the numerical stability, and the versatility of the model. The numerical results can be validated either against analytic solutions and other known numerical results to test the accuracy of the code or against laboratory data and field experiments to determine the applicability of the model. This section briefly describes some frequently used analytic solutions and discusses certain other validation procedures.

Analytic Solutions

For simple one- and two-dimensional equations with constant coefficients and well-defined initial and boundary conditions, either the pressure equation or the temperature equation may be solved in terms of elementary analytic functions or special functions. In some cases, the solution exists in the form of a simple integral which can be easily evaluated numerically. Some examples of transient analytic or semianalytic solutions are listed below.

1. Theis Solution

For radial systems, the simplest pressure transient solution is the well-known Theis solution or exponential integral solution, with the long-term pressure drop approximately proportional to the logarithm of time (Theis, 1935). The Theis solution applies to a fully penetrating line source well in a laterally unbounded homogeneous aquifer, or equivalently a horizontal fracture. The Theis solution has been generalized to cases with variable flow rates, finite wellbore with storage and skin effects, finite aquifers, leaky aquifers, partial penetration, multi-layer systems, etc (see review by Weeks 1977).

2. Double-porosity solutions

For a double-porosity system, the formation fluid from the blocks supplies the flow in the fractures. The transient pressure drop has two logarithmic portions, showing the delayed pressure responses due to the porous-medium after the early response due to fracture flow (Barenblatt and others 1961, Warren and Root 1963, Streltsova-Adams 1978a,b).

3. Two-phase Radial Flow

For two-phase flow, the radial propagation of a flashing front due to mass production can be described by modified exponential integral solutions (Garg 1978).

4. Instantaneous and Continuous Sources

In addition to the Theis solution for a line source, the solutions for other source shapes can be easily derived using the Green's function technique. Other examples of are the point source, the planar source, the disk source, the finite line source, the finite cylindrical source, etc. (Carslaw and Jaeger 1959).

5. Single Fracture Solutions

For a single horizontal or vertical fracture imbedded in a porous medium formation, solutions using superposition of point sources or Green's function technique have been developed in the petroleum literature (Cinco-Ley and Samaniego 1978; Gringarten and Ramey 1974; Raghavan 1977).

6. Linear Convective-dispersive Solutions

A popular solution for testing the temperature (or concentration) equation with a convective term is the horizontal linear injection solution (Ogata and Banks 1961). A generalized solution with heat loss due to vertical conduction to overburden and underburden (Avdonin 1964) has also been used for validation. The propagation and spreading of the temperature front is regarded as a standard test for problems of numerical oscillation and numerical diffusion for various upstream weighting schemes.

Numerical Solutions and Laboratory Experiments

Self-consistency and accuracy of a model can be checked numerically. For a given problem, the dependence of the numerical results on different grid spacings and time steps is one approach used to check the convergence and consistency of a numerical code. The comparison of a new code with another code for the same problem with the same grid and time steps is also a frequently used procedure. This is especially the case when the earlier modeling results agree with an experiment. Laboratory experiments with well-defined initial and boundary conditions are very valuable for model validations.

History Matching

Besides being verified against analytic solutions, numerical solutions, and laboratory experiments, a model should attempt to match the history of field data over a long period of time. Even in a field with many wells, the subsurface conditions are so complicated that the input parameters characterizing the reservoir are usually very difficult to estimate. Nevertheless,

reasonable success in matching long-term data and in predicting the future are important factors to be considered in reviewing a model. The success of history matching and prediction depends not only on the soundness of the code but also on the knowledge and experience of the modelers on the geological and physical processes to be modeled.

Table 9 summarizes the field validations or history-matching studies performed by the different models.

Table 9. Field Validations and Model Applications

Models	Field Validations	Applications
ROCMAS		Dam foundations; Well testing, deformable fractures
TERZAGI	Pixley, consolidation	East Mesa, resource estimation; Well testing, pulse packer; Subsidence
CCC	Auburn, aquifer storage	Cerro Prieto, reinjection; Generic studies: aquifer storage, geothermal, repository; Well testing
Duguid		Leaky aquifers
O'Neill		Hot water injection
GW THERM		Generic study: repository; Hanford repository
FINI		KBS, repository; AECL, repository
CFEST		Sutter Basin, groundwater; Long Island, groundwater; Repositories in salt, granite
SWIFT		WIPP, salt repository; NRC, geosphere transport
Coats		Two-phase flow in fractures; Convection
Faust-Mercer	Wairakei, geothermal	Steam near canister
MUSHRM	Wairakei, geothermal	Gulf Coast, geopressure; Salton Sea, precipitation
SHAFT79	Serrazzano, geothermal	Krafla, geothermal; Reservoir depletion; Sandia, repository.

V. APPLICATIONS

Numerical simulations are useful not only for the better understanding of physical processes and for sensitivity studies, but also for the design of experiments and for the development of testing procedures to determine necessary model input parameters. As more test results are obtained to improve the knowledge of a system, more realistic models can be developed. For waste isolation in hard rock formations, model applications of interest include well testing analysis, mined cavern design, in-situ testing design and interpretations, regional rock formation responses to perturbation and long-term simulations over geological time scales. Specific applications of the models are indicated in Table 9. In the following, general areas of application of the models are discussed. The focus will be mainly on fracture-related problems and thermally-induced phenomena.

Well Testing Analysis

In geological exploration and site evaluation, well tests are very important for the study of hydrologic properties of the formation. Well tests can be steady or transient, use a single well or multiple wells, use a packed interval for detailed studies or a well left open for integrated studies, and use production, injection, or pressure pulses to induce the pressure changes.

For a shallow well intercepting a horizontal fracture in a hard-rock formation, the simplest analysis to determine the fracture permeability from the flow rate and pressure drop is to use the steady-radial pressure solution. Although the assumption of steady flow and the requirement of a constant flow

rate are difficult to maintain for low-permeability fractures at greater depths, many field test data are first analyzed with this procedure. This analysis is applicable for either production or injection tests. One of the interesting anomalies observed in shallow-fracture systems is that fluid can be injected more easily than it is produced. This suggests the possibility that high fluid pressure opens the fracture and increases the permeability (Gale 1977).

Pressure transient tests can be used to determine both the permeability and the storage capacity of the formation. Most of the pressure transient solutions for porous media and simple-fracture systems are based on extensions of the Theis solution. In well testing analysis, the measured pressure-time curves are compared to calculated solutions of different parameters, initial and boundary conditions, and geometries. One of the difficulties in well test analysis is that pressure-time curves in different cases are very similar in shape; and the inverse problem, determining the parameters, has no unique solution (Earlougher 1977). For multiple-fracture systems, the same difficulty is expected to occur in the determination of fracture parameters.

In petroleum engineering where interest lies in improving production by hydraulic fracturing, the focus of fracture well testing is to determine the extent and orientation of single, large fractures induced in fluid-producing formations and to estimate enhanced productivity due to flow through the fractures. In geothermal engineering, many reservoirs are known to be naturally fractured. Man-made fractures are also of interest for hot-dry-rock geothermal studies. However, in waste isolation studies, it may be more difficult to

perform and analyze conventional well tests. For example, the formation may be too tight to conduct a constant-flow rate test within a reasonable period of time. The propagation of pressure perturbations through the complicated fracture network may be highly anisotropic and difficult to detect. The anomalies in the well testing data will stimulate additional numerical modeling efforts to understand the in-situ multiple-fracture systems.

Mined Cavern Tests

Nuclear waste repositories are likely to be mined tunnels separated by wide pillars in a suitable rock formation. Prior to the construction of a repository, field experiments in underground mined caverns either newly excavated or extended from an old mine can provide valuable data for the characterization of the rock formation. Currently, in the United States, the granite and tuff formations in Nevada Test Site and the basalt formation in Hanford Reservation are being tested. Belgium, Canada, France, Sweden, United Kingdom, and West Germany are also studying various rock formations for waste isolation. The influences of fractures on the heat transfer and fluid flow in underground field experiments are illustrated by the granite experiment in Stripa, Sweden.

The test drifts in Stripa, Sweden, are approximately 340 m below the surface in granite adjacent to an abandoned iron mine. Three heater experiments were carried out. Two "full-scale" experiments simulated the short-term near-field heating effects of an individual nuclear waste canister at two different thermal power levels, 5 kW and 3.6 kW. The third experiment used an array of eight scaled-down heaters with decaying power to study the thermal interaction between adjacent canisters. The rock mass adjacent to the heaters

was monitored extensively by using thermocouples to measure temperature rises, extensometers, and deformation gauges to measure rock displacements (Witherspoon and others 1979a). Analysis of the temperature data indicates that the temperature field data agree with the theoretical prediction, assuming heat conduction is the only mode of heat transfer (Chan and others 1978). However the thermally induced displacements are substantially smaller than the prediction based on elastic responses of rock mass. One possible explanation of this discrepancy is the presence of fractures which deform differently than the intact rock.

Although groundwater convection may not be important for heat transfer, the presence of water was noted in some of the heater holes. The test site is believed to be below the groundwater table and seepage into the drift was noted. The seepage of groundwater has been used in a macropermeability experiment (Witherspoon and others 1979b). The inflow to a 33 m-long x 5 m-diameter drift was measured by evaporating the seepage into the ventilation air while measuring the change in water vapor content. In order to measure this change in water vapor content, the drift was sealed off and the wet and dry temperatures of the inlet and exhaust were taken. During the experiment, air in the drift was kept at a constant temperature. The pressure distribution within the rock formation was measured in 15 boreholes, 30 to 40 m long, drilled into the surrounding rock in different directions. For each borehole, six packers were installed at approximately 5 m intervals. There were a total of 90 packed zones sampling approximately 10^6 m^3 of rock mass in three-dimensional space. The pressure distribution and the flow rate can be used

to determine the hydrologic properties of the rock mass around the drift. Preliminary quasi-steady analyses indicate that the existence of a low permeability zone surrounding the drift may be due to the closure of fractures under the tangential compressive stress component. Beyond the low permeability zone, the average hydraulic conductivity is estimated to be about 10^{-12} m/sec. The details of the pressure distributions are being analyzed. This macropermeability experiment is one approach to determining how a fractured-rock mass can be modeled as a continuum. Numerical modeling of these experiments should be useful for repository studies.

Repository Simulations

Generic models and conceptual designs are being made for various repository configurations in different rock formations. Numerical simulations will be the primary method of assessing the repository impact over spatial dimensions of thousands of meters and over time spans of thousands of years. Several models considered in this study have used stratified porous media or simple discrete fracture systems to represent the fractured rock formations (Dames and Moore 1978; Burgess and others 1979; Gupta and others 1980; Wang and Tsang 1980).

The velocity of groundwater flow is the quantity of interest for thermo-hydrologic repository simulations. Typically, calculations start with the determination of the temperature rise surrounding the repository and follow with an evaluation of the buoyancy pressure gradient resulting from the density change of hot fluid. Permeability and porosity, together with the total pressure gradient from the superposition of the buoyancy component and the

ambient component, determine the flow velocity. Additional calculations can be made for the movement or track of water particles from the repository to the ground surface.

As more data on rock formations are available, more detailed models will be constructed to simulate the flow field and radionuclide transport. There is also a need for numerical models that take into account the stochastic distributions of the rock parameters. We expect that the repository studies will lead to a better understanding of the behavior of fractured rock masses.

Geothermal Studies

Recent interest in the use of geothermal energy has contributed to the rapid advancement in numerical modeling of nonisothermal flows, especially the changes from liquid to two-phase, steam-water mixture. Although two-phase phenomena are likely to be limited in a repository environment, the simulations of geothermal reservoirs for pressure and temperature changes are of interest to repository studies of comparable formation sizes. We will briefly discuss one example--the geothermal field at Wairakei, New Zealand--to illustrate the use of a porous-media model for the simulation of the production of steam from an initially liquid-dominated, fractured reservoir over a twenty-year period.

Although the fluid is believed to be produced from a highly fractured zone in the vicinity of the interface between the reservoir and the bed rock, the reservoir as a whole (over 300 m thick) was modeled as a porous medium layer. The pressure decline over the whole field since the start of fluid

production has been successively modeled by the history-matching procedure (Pritchett and others 1980; Mercer and Faust 1979). However, the "best" parameters used in the match do not agree with the values determined from core samples in the laboratory. The core sample porosity is higher and the permeability is much lower than those inferred by the model. The discrepancy can be attributed to the presence of fracture systems which control the fluid flow field.

The fractures may also control the subsidence observed in this geothermal field. The maximum subsidence has been observed outside the main production area. The rate of subsidence is not proportional to the pressure decline. These observations cannot be explained by a simple pore-collapse model. The subsidence is believed to be induced by a seismic slippage of a fault which acts as a hydrologic boundary.

Similar success in modeling the pressure distribution in porous-media has been achieved for the fractured two-phase reservoir in Serrazzano, Italy (Pruess and others 1980). Currently the Cerro Prieto field in Mexico is being studied (Lippmann and Goyal 1979). These geothermal field studies should be useful for a better understanding of the thermohydrologic flow in fractured rock masses.

SUMMARIES OF INDIVIDUAL MODELS

This section summarizes details of the individual models under the same five headings used in the previous section, Comparative Review:

- I. Governing equations
- II. Numerical solutions
- III. Computer codes
- IV. Validations, and
- V. Applications.

We have attempted to make the notation consistent for all models. These summaries will be useful for a more detailed comparison among models and for identifying the strengths of each model. They will also be helpful in providing a concise introduction to potential users.

ROCMAS

ROCMAS (ROCK MASS) is a finite-element program for coupled flow and stress in deformable, saturated, fractured rock media. The two-dimensional code combines the capability of isothermal transient pressure analysis and stress-strain analysis in formations with discrete fractures and porous blocks. The option of thermally induced stress analysis has been implemented. Coupling of the pressure field and the mechanical deformation is founded on the extension of Biot's consolidation theory for porous elastic medium to nonlinear fracture behavior. The current version of the model is described in Noorishad and others (1980). Summaries of early developments and related information are found in Ayatollahi (1978) and Ayatollahi and others (1980). The early version of this code is known as PORFRC.

I. GOVERNING EQUATIONS

In this model, the fluid movement and the solid deformation are coupled. Each point in space, either inside a discrete fracture or within a rock block, has a pressure variable P and a solid displacement vector \bar{u} . The coupling between P and \bar{u} can be described in the following loop. As the pressure changes, the effective stress acting on the rock solid changes accordingly and affects the displacement or strain of the solid. The displacement of solid changes the permeability of the flow path and results in changes in the pressure field. The mathematical form of the coupling between the fluid flow and rock displacement can be written down as a set of three equations for the pressure-strain, strain-stress, and stress-load balance relations.

Pressure-Strain Equation

The pressure-strain equation describing the fluid flow is:

$$\frac{1}{M^i} \frac{\partial P}{\partial t} - \alpha^i \frac{\partial \epsilon}{\partial t} = \nabla \cdot \frac{k^i}{\mu} \nabla P,$$

where M^i and α^i ($i = d$ for discrete fractures and $i = m$ for porous-medium blocks) are material properties (Biot constants) representing the responses of fluid mass content to changes in pressure and changes in volumetric strain ϵ . The coupling between the pressure and the displacement is mainly through the sensitive dependence of the permeability on the fracture aperture b , and through the transient derivative $\partial \epsilon / \partial t$. The discrete fracture permeability $k^d = b^2 / 12$ for parallel-plate laminar flow is used in this model. In general, the volumetric strain ϵ is determined by the pressure and the stress field. In most uncoupled models, the derivative $\partial \epsilon / \partial t$ is approximated in terms of the pressure derivative $\partial P / \partial t$, and the fluid flow equation is reduced to a simple transient pressure equation with the storage coefficient in front of $\partial P / \partial t$ determined by the porosity of the formation and the compressibilities of the fluid and void structures.

Stress-Strain Relation

In more general cases with coupling, the volumetric strain $\epsilon = \epsilon_{xx} + \epsilon_{zz}$ depends on the effective stress field. The fluid pressure counteracts the rock stress normal to the fluid-solid interfaces. The effective stress-strain relation can be formally written in the form of Hook's law (Biot 1941, 1955, 1956, 1961):

$$\bar{\sigma} - \alpha^i \bar{P} = C^i : \bar{\epsilon}.$$

For isotropic elastic porous rock media, the components of the tensor \bar{C}^m can be expressed in terms of two elastic constants--for example, Young's modulus and Poisson's ratio. For anisotropic, inelastic deformable fractures, the stress-strain relation is very nonlinear. In this model, a nonlinear normal stress-normal displacement relation and a nonlinear shear stress-shear displacement relation are used (Goodman and others 1968). The normal and shear stiffness (change of stress per unit change of displacement) as functions of stresses characterize the fracture behavior. The displacement \bar{u} is simply related to the strain $\bar{\epsilon}$ by the component definition

$$\epsilon_{ij} = 0.5 \left(\frac{\partial u_i}{\partial x_j} + \frac{\partial u_j}{\partial x_i} \right).$$

Load Balance

The third equation for the unknowns P , $\bar{\sigma}$ and $\bar{\epsilon}$ is Newton's first law of static equilibrium applied to an infinitesimal volume element of the fluid-filled medium

$$\nabla \cdot \bar{\sigma} + \rho^i \bar{f} = 0,$$

where ρ^i is the bulk mass density and \bar{f} is the body force. One body force or volumetric force is the gravity \bar{g} . Both the gravity effects on the fluid and rock can be taken into account. Gravitational drainage of fluid can be modeled.

Thermal Stress

The thermally induced stress, as well as the static stress can be included as part of the total applied stress $\bar{\sigma}$. The temperature field used in the

thermal stress analysis is calculated by a heat conduction subroutine in the program. With this option, partial thermal-mechanical-hydrologic coupling is included in this code.

II. NUMERICAL SOLUTIONS

Variational Finite-Element Method

The finite-element method is used to discretize the space domain. The two-dimensional space is decomposed into finite-element quadrilateral domains with four-corner nodes. Each node has the values of three variables: the pressure P and the two components of solid displacement \bar{u} . Isoparametric bilinear polynomial basis functions are used to interpolate from the nodal values to the space within an element representing the porous rock medium. For a fracture, it is assumed that the aperture is small and fluid flow is along the fracture surfaces. The pressure difference between adjacent nodes across the aperture is negligible, and a one-dimensional element can be used for interpolating between two end point pressures (Wilson and Witherspoon 1974). For the fracture displacements, it is convenient to take the same spatial (global) coordinates for each pair of points across the small aperture for the four-corner element. However, the relative movements of the surfaces in the direction vertical to the fracture plane and along the fracture are important for the structure analysis. The fracture element in terms of these relative displacements is used (Goodman and others 1968).

For N nodes in a modeled domain, the matrix equations relating the $3N$ nodal variables are obtained by a variational formulation. The method starts

with the adaptation of a variational principle. The variational functional, written for general initial and boundary conditions, includes all the terms of the static structural-analysis variational, the terms of the transient fluid flow analysis, and a coupling term for the two functionals.

Taking variation of the discretized functional with respect to field \bar{u} and P results in the following pair of matrix equations

$$[K]\{\bar{u}\} + [C]\{P\} = \{F\}$$

$$[C]^T\{\bar{u}\} + ([E] + 1 * [H])\{P\} = 1 * [Q]$$

where the matrix $[K]$ contains the coefficients of the stiffness of stress-displacement of both inelastic fractures and elastic medium, $[C]$ the Biot coupling coefficients, $[E]$ the fluid storage coefficients, $[H]$ the fluid hydraulic conductivities, and $[Q]$ the fluid boundary fluxes. The column vector $\{\bar{u}\}$ contains the $2N$ nodal values of \bar{u} for the m porous nodes and $N-m$ fracture nodes, $\{P\}$ the N values of P , and $\{F\}$ the body force and boundary loads.

Predictor-Corrector Time Stepping

The notation $1*$ in the matrix equation represents the time integration from 0 to t . To step from t to $t+\Delta t$, this model uses a predictor-corrector scheme. The solution is first predicted at $t+\theta\Delta t$ with $2 \geq \theta \geq 1$.

$$1 * P_{\theta} = A(t+\theta\Delta t) = \int_0^{t+\theta\Delta t} P(\tau)d\tau = A(t) + \frac{1}{2} \theta\Delta t(P_t + P_{t+\theta\Delta t}),$$

and then it is corrected by linear interpolation:

$$1 * P_1 = A(t+\Delta t) = A(t) + \frac{1}{2}\Delta t(P_t + P_{t+\theta\Delta t}).$$

The unknown at $t+\Delta t$ is given by

$$P_{t+\Delta t} = P_t + \frac{1}{\theta}(P_{t+\theta\Delta t} + P_t) .$$

It is noted that $\theta = 1$ is the central differencing Crank-Nicholson scheme. The coefficient $\theta > 1$ is used to damp out the numerical oscillation while slightly slowing down the convergent rate (Taylor 1974).

Stiffness Perturbation Scheme

The nonlinear behavior of fracture stress-displacement is dealt with by the stiffness perturbation technique (Goodman and others 1968) during each time step. The stiffness matrix depends on the displacements when the displacements are out of the linear range. Iterations proceed until the stiffness matrix stabilizes within convergent criteria.

Matrix Solver

Within one iteration the matrix equation of $\{\bar{u}\}$ and $\{P\}$ is solved by a direct procedure. The matrix is decomposed into lower- and upper-triangular matrices by the Crout method. This reduces the matrix equation to two triangular systems which can be solved by backward and forward substitution procedures.

III. COMPUTER CODES

Documentation

The code is written in FORTRAN IV and is currently being used on the CDC 7600 at Lawrence Berkeley Laboratory. The user's manual with code listing are available for the stress-flow version (Noorishad and Ayatollahi 1980). Setup of the data follows the organization of other finite-element programs at the University of California, Berkeley. Familiar options of stress and strain analysis codes and fluid flow codes are included in this code. One version of the program is adopted for thermally induced stress calculations.

Spatial Grid

The two-dimensional grid consists of four-corner quadrilateral elements for the porous rock medium and two-node elements for the discrete fractures. The fractures may extend from one boundary to another, intersect each other, or be isolated in the porous rock medium. An axisymmetric grid is also used.

Material Properties

The constant permeability of the porous-rock medium and the initial aperture of the fracture are input parameters. For coupled calculations, the pressure- and stress-induced changes in displacement will be used to update the aperture and the fracture permeability.

The parameters M^i in the fluid flow equation for the porous-rock medium and fracture can be estimated in general from the porosity and the compressibility of fluid as $1/\psi\beta_p^i$. The coupling constants α^i are dimensionless.

$\alpha^i = 0$ decouples the pressure calculation from the stress-strain analysis. For material with highly incompressible solid grains, $\alpha \approx 1$.

The mechanical properties required are Young's modulus and Poisson's ratio for the elastic porous rock medium and the initial normal stiffness, tangential stiffness, cohesion, and angle of friction for the fracture.

Fluid Properties

The fluid density and viscosity are input parameters.

Sources and Sinks

For thermally induced stress calculation, the heat source is handled in the separate heat conduction subroutine.

Initial Conditions

Distribution of stresses, pressure, and displacement can be specified for the initial time or for the restarting time.

Boundary Conditions

Pressure and flux boundary conditions can be specified for the fluid flow. Static load, thermal load, and displacement boundary conditions can be specified for the stress-strain analysis.

Time Steps and Solution Control

The time step can be increased logarithmically. A convergent criterion is specified on the stiffness difference in the iteration-perturbation procedure to handle the nonlinear fracture behavior.

Output

At the end of each time step, the pressure, displacement and/or temperature on the nodal points and the flow flux and the stress components on the element can be printed. Graphic output of the mesh with the plot of the principal components of stress and displacement are generated in the program.

IV VALIDATIONS

The code has been developed from an early iterative finite-element program with steady-state flow and static force-displacement analysis in a jointed formation with impermeable rock (Noorishad 1971; Noorishad and others 1971). Most of the recent efforts to validate this code are focused on the transient fluid flow behavior in fractures embedded in porous-rock media. The recently developed thermally induced stress option has also been tested by comparison with numerical solutions using SAP IV. Validation of the capability to handle coupling between transient fluid flow and stress-strain analysis is limited because of the lack of analytic solutions and other numerical results. The documented tests (Ayatollahi 1978; Ayatollahi and others 1980) on the transient fluid flow in porous media and in fractures are listed below.

(a) Continuous Finite-Radius Well Source: The early-time transient pressure responses of an axisymmetric flow to a producing well are compared with the analytic solution of Mueller and Witherspoon (1965).

(b) Finite Axisymmetric Aquifer: The late-time pressure responses with no flow as well as constant outer boundaries are compared with the analytic solutions.

(c) Vertical Fractures: The pressure responses for a single vertical fracture and two perpendicular vertical fractures intersecting a well at the center of a rectangular porous medium are compared with the analytic solutions of Raghavan and others (1978).

(d) Vertical Fracture Near a Well: The pressure responses for an observation well in a system with a fracture not intersecting, but aligned with a producing and an observation well, are compared with the analytic solution of Cinco-Ley and others (1978).

(e) Horizontal Fracture: The pressure responses for a horizontal fracture located at the center of an aquifer and intersecting a well in an axisymmetric region are compared with the analytic solution of Gringarten and Ramey (1974).

V. APPLICATIONS

The importance of the coupling between the fluid flow and the mechanical deformation in fractures has been analyzed by the iterative steady-state version of this code. The flow through a jointed dam foundation has been simulated (Noorishad and others 1971). It is noted that a deformable fracture system has lower flow through the foundation and higher uplift pressure than a rigid network of fractures. The code has also been used in the analyses of laboratory experiments of large rock samples with tension fractures and of field tests in shallow fractured formations (Gale 1975). It is well known that high pressure at a wellbore can open up the fractures and will result in a high injection rate, while low pressure at a wellbore during withdrawal can close the fracture and decrease the hydraulic conductivity of flow.

The recently developed transient code has not yet been applied extensively to field situations. The thermally induced option is developed for application in near-heater or canister field experiments in fractured rock formations, for example the granite experiments in Stripa, Sweden.

VI. SUMMARY

This model is for the study of coupled fluid flow and stress in deformable fractured rock masses. The effective mass theory of Biot is used to relate the pressure changes with the displacements of the rock matrix. The deformation of the fracture surfaces in turn affects the fracture flow through the sensitive dependence of permeability on aperture.

The code combines techniques of fluid flow modeling and stress-strain analysis. The two-dimensional finite element code incorporates the flow element of Wilson and Witherspoon (1974) for the fracture flow, the joint element of Goodman and others (1968) for the representation of mechanical behavior of the fracture. A stiffness-perturbation scheme for handling nonlinear fracture behavior and a predictor-corrector scheme for damping out numerical oscillation are used in the program.

The model is based on a general theory which is of fundamental interest and practical importance. The code has the capability of handling a range of complex problems in fluid flow, induced rock mass deformations, and soil consolidation. The inclusion of the thermal stress option is relevant for waste disposal problems. Further developments to couple the fluid flow with heat transfer or to incorporate dynamic stress analysis can increase the range of applicability. More extensive application of the code is called for. Documentation of validations on stress analysis will be of interest.

TRUST-TERZAGI

TRUST (Transient flow in Unsaturated and Strained porous medium) is an integrated finite-difference program for saturated-unsaturated, three-dimensional isothermal flow in deformable media. TERZAGI is the saturated flow version. The deformation of the medium is calculated using the one-dimensional consolidation theory of Terzaghi. Soil consolidation and fracture well testing have been studied. TRUST-TERZAGI is described in Narasimhan (1975, 1980a,b), Narasimhan and Witherspoon (1976, 1977, 1978), Narasimhan and others (1978), and Narasimhan and Palen (1979).

I. GOVERNING EQUATIONS

In this model, the governing equation for isothermal fluid flow in a deformable medium is described by an integral equation of the form

$$M_c \frac{Dh_p}{Dt} = \int_A \rho^w \frac{k\rho^w g}{\mu} \nabla(z + h_p) \cdot d\bar{A} + \int_V Q_F dv.$$

The Darcy velocity is:

$$\bar{q} = - \frac{k\rho^w g}{\mu} \nabla(z + h_p).$$

The quantity h_p represents the average pressure head $P/\rho_o^w g$ over the volume element V bounded by the surface A , and D/Dt denotes a material derivative in the deforming medium. The volume V contains the constant rock solid volume V^r and the variable pore volume V^p . The fluid flow equation is in general non-linear, since the fluid mass capacity M_c , the fluid density ρ^w , the permeability k , and the fluid mass source/sink Q_F can be dependent on h_p or t .

Fluid Mass Capacity

The fluid mass capacity, M_c , represents the change of fluid mass content $S\phi\rho^w V$ with unit change of pressure head. The fluid mass capacity is determined by the compressibility of the fluid β_p^w , the deformability of the pores a_v , and the desaturation of the water in the pores dS/dh_p :

$$M_c = V^r \rho^w \left(S e \rho_o^w \beta_p^w g + S \rho_o^w g \lambda' a_v + e \frac{dS}{dh_p} \right).$$

For saturated rock, $S = 1$ and $\lambda' = 1$, the fluid mass capacity M_c can be expressed in terms of the more familiar coefficient of specific storage S_s as $M_c = V \rho^w S_s$, with $S_s = \rho^w g [\phi \beta_p^w + (1 - \phi) a_v]$. S_s is usually treated as a constant for each material. For unsaturated flow, the dependence of the saturation S on the pressure head is a multivalued hysteresis relationship which can be handled by the model.

Deformation

The coefficient a_v in the fluid mass capacity M_c is determined by the dependence of the void ratio, $e = V^p/V^r = \phi/(1 - \phi)$, on the effective stress σ' : $a_v = -de/d\sigma'$. In Terzaghi's one-dimensional consolidation theory, the effective stress σ' is related to the normal stress σ_N by $\sigma_N - P$ for the saturated region and $\sigma_N - \lambda P$, $0 \leq \lambda \leq 1$, for the unsaturated region. In the calculation of vertical subsidence, the normal overburden stress σ_N is given, and the vertical displacement due to pore pressure change is evaluated by an e versus σ' relationship.

When the rock (soil) is loaded to levels never attained before, the void ratio decreases very nonlinearly as the effective stress increases for most material. The plot of e versus $\log \sigma'$ is usually a reasonable straight line with slope C_c (compression index) for virgin loading and with slope C_s (swelling index) for unloading or rebounding. In terms of C_c , the coefficient of compressibility $a_v = -de/d\sigma' = C_c/2.303\sigma'$. In this model, the consolidation behavior can be modeled by specifying C_c (or C_s). If one is not interested in modeling the inelastic consolidation, then a_v can be specified to be a constant.

Depending on the e versus σ' relationship chosen, the model can account for the effects of either elastic or inelastic normal deformations of the fractures or pores for cases involving constant external loads and change of internal loads due to pore pressure change.

The change of void ratio e may also affect the permeability k profoundly. In the numerical model, one could use convenient experimental relationships or simply tabulate k as a function of effective stress or void ratio. One relationship used in the model is:

$$k = k_o \exp \left[\frac{2.303(e - e_o)}{C_k} \right],$$

where k_o and e_o are arbitrary reference values of the permeability and void ratio, respectively, and C_k is the slope of the best-fitted straight line for the relationship of e versus $\log k$.

II. NUMERICAL SOLUTIONS

Spatial Gradients

The model uses the integrated finite-difference method to discretize the flow regime and to handle the spatial gradients. In the integrated finite-difference method, the volume elements can be arbitrarily shaped polyhedrons. The spatial gradient between nodes (centroids of V) m and n is approximated by $(h_{P,m} - h_{P,n}) / (d_{n,m} + d_{m,n})$, where $d_{n,m}$ is the normal distance from node n to the interface between n and m . The quantities k and ρ on the interface between m and n are evaluated as harmonic means to preserve continuity of flux at the interface. Thus

$$k_{m,n} = k_m k_n \frac{d_{m,n} + d_{n,m}}{k_m d_{n,m} + k_n d_{m,n}},$$

and $\rho_{m,n}^w$ is similarly calculated. The harmonic mean of k is correct when k changes stepwise at the interface.

Integrated Finite Difference Equation

First-order finite difference in time is used. In terms of the interface conductance,

$$U_{n,m} = \rho_{n,m} \frac{k_{n,m} \rho_{n,m} g}{\mu} \frac{A_{n,m}}{(d_{n,m} + d_{m,n})},$$

the implicit finite-difference equation corresponding to the governing integral equation is:

$$M_{c,n} \frac{\Delta h_{P,n}}{\Delta t} = \sum_m U_{n,m} \left[(z_m + h_{P,m}^t + \lambda \Delta h_{P,m}) - (z_n + h_{P,n}^t + \lambda \Delta h_{P,m}) \right] + (Q_F V)_n.$$

The difference equation relates the mass accumulation in element n with the mass fluxes across the interfaces from the neighboring elements m . This equation is valid for an arbitrary element n connected to an arbitrary number of elements m .

Explicit-Implicit Scheme

For explicit differencing procedures with the interpolation factor $\lambda = 0$, the solution of the finite-difference equation is unstable if Δt exceeds the critical value

$$\Delta t_n^c = \frac{M_{c,n}}{\sum_m U_{n,m}} .$$

In the mixed explicit-implicit scheme, the node blocks will be reclassified as implicit nodes only when needed to assure stability. The implicit interpolation factor is made to vary between 0.57 and 1.0. A solution in time may be obtained by this optimized mixed explicit-implicit procedure or by choosing a backward-differencing implicit scheme, a central-differencing Crank-Nicholson scheme, or a forward-differencing explicit scheme.

Iterative Procedure

The implicit difference equation is solved by an iterative scheme (Evans and others 1954; Edwards 1972). To proceed from the k -th step to the $(k+1)$ -th step in the finite-difference equation, set

$$\Delta h_{p,n}, \text{ left-hand side} = \Delta h_{p,n}^{k+1}$$

$$\Delta h_{p,n}, \text{ right-hand side} = (1 + s)\Delta h_{p,n}^{k+1} - s\Delta h_{p,n}^k$$

$$\Delta h_{P,m}, \text{ right-hand side} = \Delta h_{P,m}^k$$

until convergence criteria are satisfied. The acceleration factor $s = 0.2$ is used. Recently a direct solver option has been incorporated into TERZAGI. The implicit equations can now be solved either iteratively or directly.

For cases in which the fluid mass capacity and the permeability are functions of h_p , M_c and k are evaluated at an estimated average value of $h_{p,n}$ before carrying out the calculations of $\Delta h_{p,n}$ for that time step. The estimated $\Delta h_{p,n}$ is obtained from $\Delta h_{p,n}$ calculated for the last time step and the ratio of maximum rates of change during the proceeding two time steps. This estimation and other safeguards against possible sources of instability are discussed in Edwards (1972).

Integral Formulations

The main advantage of the integrated finite-difference method is the straightforward formulation of the numerical equations from the integral form of the governing equation over arbitrarily shaped blocks. The chief limitation of the method is that the finite-difference gradient approximation is inadequate in evaluating tangential gradients along the interfaces and in handling tensorial properties such as the stress fields which generally rotate with time. The model is currently being extended to handle three-dimensional deformation using integral formulation. Except for the procedure used in evaluating the gradients, the integrated finite-difference method and the modified Galerkin finite-element method (with diagonal capacity matrix) are conceptually very similar (Narasimhan and Witherspoon 1976). Both these

approaches derive their ability to handle complex geometries from the integral nature of the formulation.

III. COMPUTER CODES

Documentation

The codes are written in FORTRAN IV and have been adapted to a number of computer systems at Lawrence Berkeley Laboratory, Lawrence Livermore Laboratory, Battelle Pacific Northwest Laboratory, Atomic Energy of Canada Limited, Science Applications, Inc., University of Arizona, and the University of Waterloo. The user's manual has been prepared (Narasimhan 1980a). The code listings of TERZAGI and TRUST are available from T. N. Narasimhan at Lawrence Berkeley Laboratory. The input is organized into data blocks.

Spatial Grid

In this model there is no restriction upon choice of basic block shape or numbering of nodes. The geometric configurations of the nodal elements can be arbitrary and may be one-, two-, or three-dimensional, with rectangular, cylindrical, axial, or spherical symmetry. The volumetric properties of the blocks and the geometric properties of connections between nodes are required input data. For complex problems, the design of a mesh will require the most effort when using this program. Auxiliary computer programs for mesh and input data generation are available for a number of grid systems, including the case with cylindrical or elliptical rings near a well, gradually changing to rectangular blocks in the far field. This mesh is relevant for the simulation of horizontal or inclined fractures intersecting the well with cylindrical or elliptical

cross section and intersecting other planar fractures within the rock mass with linear intersections.

Material Properties

Each grid block can be assigned a different material with a different permeability and a different fluid storage coefficient. For each material, the permeability k can be (i) a constant, (ii) a function of effective stress σ' with tabulated values, or (iii) a function of void ratio by specifying the slope of the e versus $\log k$ curve. The model can handle anisotropic permeability by orienting grid blocks parallel to the principal axes of anisotropy.

The fluid storage capacity of each material can be (i) specified by a constant specific storage S_g , (ii) determined by the coefficient of compressibility a_v , or (iii) varied with effective stress by specifying the slope C_c and C_s of the e versus $\log \sigma'$ loading and unloading curves. The initial void ratio e_0 and initial stress σ' are input parameters for (ii) and (iii). The specific weight and the depth of the grid block are used to calculate the overburden stress.

Fluid Properties

The water density, viscosity, and compressibility are input parameters. The water compressibility and the formation compressibility are used to calculate the fluid storage capacity.

Sources and Sinks

The volumetric fluid generation rate may vary with spatial position, time, or the pressure head.

Initial Conditions

The pressure head, volumetric generation rate, preconsolidation stress, and boundary conductance may be specified for each grid block for the initial time or for the restarting time.

Boundary Conditions

Prescribed pressure head as well as prescribed flux boundaries can be simulated. The external source or sink, coupled to the system by means of boundary conductance, may vary with time. The model can handle finite diameter wells (wellbore storage effects) and fractures as part of the flow region. For saturated-unsaturated flow, it will handle a seepage boundary.

Time Steps and Solution Control

The mass balance is calculated by the program. The maximum or minimum allowed time step can be specified. The size of time step can also be controlled by specifying the desired maximum change in pressure head in each time step. The criteria that may be specified for ending a problem are: the attainment of steady state; upper limits on the problem time or the computer time; the number of time steps; and upper and lower limits on the value of pressure head.

Output

The value of pressure head and its time derivative at a selected node and the pressure heads and fluxes of all the grid blocks can be output at regular time intervals or cycles. Separate graphic programs can be used to process the output data.

IV. VALIDATIONS

The codes have been validated with analytic solutions, other numerical solutions, laboratory tests, and field data. The following is a list of solved problems.

Analytic Solutions

- (a) Continuous Line Source: The Theis problem is solved with 9 nodes in radial coordinates.
- (b) Continuous Point Source: This problem is solved by using grid blocks which grade gradually from spherical near the point source to cubic-shaped at the outer boundary.
- (c) Steady Radial Flow: The flow rate from an outer cylindrical radius to the wellbore is calculated.

Fracture Flow

- (a) Vertical Fracture: The well testing type curves of finite-conductivity vertical fractures are compared with the semianalytic solutions of Cinco-Ley and others (1978) in Narasimhan and Palen (1979).
- (b) Horizontal Fracture: The pressure decay curves of pulse packer tests are calculated both numerically and semianalytically in Wang and others (1977).

Soil Consolidation

- (a) Compaction: A simulation of clay columns with depth-dependent permeability is compared with the numerical result of Schiffman and Gibson (1964).

- (b) Subsidence: The simulation of field data in a multilayer system is compared with the numerical result of Helm (1975).

Unsaturated Flow

- (a) Moisture: A calculated moisture content profile is compared with the analytic solution of Philip (1969).
- (b) Infiltration: The simulation of rain infiltration into dry soil is compared with the numerical solution of Rubin and Steinhardt (1963).

V. APPLICATIONS

This model has been applied to soil mechanics, hydrogeology, geothermal, and well testing. The following is a brief summary.

Fracture Well Testing

- (a) Rough Fracture Flow: The laboratory testing of partially closed fracture flow has been analyzed by this model (Iwai 1976). The presence of contact area reduces the flow.
- (b) Finite Conductivity Vertical Fracture: The fluid flow from a surrounding reservoir to a well intercepting a single vertical fracture has been analyzed. The fracture deformability, finite fracture conductivity, fracture geometry, and wellbore storage and damage, all affect the transient pressure response to fluid production.
- (c) Pulse Packer Test: The model has been used in the development of pulse packer testing for fractures.
- (d) Hydraulic Fracturing: The model has been adapted to handle a propagating fracture (Narasimhan and Palen 1979).

Geothermal

- (a) Resource Evaluation: The capability of producing fluid from the East Mesa geothermal reservoir has been studied.
- (b) Subsidence: A simulation of the subsidence in Wairakei geothermal reservoir is currently under way.
- (c) Injection: Several pressure calculations have been performed.

Deformable Soil

- (a) Consolidation: Saturated flows have been studied in consolidation of a heterogeneous, doubly draining clay column, in simulation of field consolidation due to periodic water-level changes observed at Pixley, California and in consolidation of a column of clay slurry.
- (b) Infiltration: Unsaturated flows have been studied in infiltration into a moderately saturated soil, in infiltration into a column of extremely dry soil, and in axisymmetric flow into a soil-water sampler.
- (c) Drainage: Saturated-unsaturated flows have been studied in drainage from a one-dimensional soil column, in drainage from a sand box, and in consolidation around an excavation in soft clay.
- (d) Soil Liquification: Pore pressure generation and dissipation have been modeled in a three-dimensional system.

VI SUMMARY

This model is for the study of fluid flow in deformable saturated and unsaturated formations. The governing equation is written in integral form, and the numerical equation is formulated directly from mass conservation consideration. The significance of the dependence of mass storage capacity upon elastic and inelastic deformation is emphasized.

Familiarity with the mesh set-up procedure allows this integrated finite-difference code to handle complex geometries and various modeling conditions. The mixed explicit-implicit scheme and other program controls allow efficient calculations of transient flows.

The results of modeling consolidation in deformable soil indicate the importance of the dependence of fluid flow on deformation. The applications to well testing of simple fracture systems probe the numerical approach for handling discrete fractures.

Further development of an auxiliary program for generating a mesh grid of complex fracture networks will be of interest. The modeling experience in soil consolidation can be extended to modeling inelastic fracture deformation.

CCC

CCC (Conduction - Convection - Consolidation) is an integrated finite-difference program which solves three-dimensional heat and mass flow equations in saturated media and computes one-dimensional deformations using the consolidation theory of Terzaghi. The model has been applied to problems in geothermal reservoir engineering, aquifer thermal energy storage, well testing in porous and fractured media, radioactive waste isolation, and other fields. Details of the model are given by Lippmann and others (1977b), Mangold and others (1979, 1980), and Bodvarsson and others (1979).

I. GOVERNING EQUATIONS

The governing equations employed in the model are the mass and energy balance laws. The mass flow equation can be written in integral form as:

$$\frac{D}{Dt} \int_V \frac{S_s}{g} \rho dV = - \int_A \rho^w \bar{q} \cdot d\bar{A} + \int_V Q_F dV.$$

This equation applies to any element of volume V and surface area A containing solid rocks in V^r and/or liquid water in V^p . The storage coefficient S_s describes the storage capacity of the element. It can be expressed in terms of the total compressibility β_P^m and the porosity ϕ : $S_s = \phi \rho^w g \beta_P^m$.

The energy equation can similarly be written in integral form as:

$$\frac{D}{Dt} \int_V \rho^m c^m T dV = \int_A K_T \nabla T \cdot d\bar{A} - \int_A \rho^w c^w \delta T \bar{q} \cdot d\bar{A} + \int_V Q_H dV,$$

where $\rho^m c^m$ represents the integrated heat capacity of the volume element, i.e., $\rho^m c^m = \phi \rho^w c^w + (1-\phi) \rho^r c^r$

On the right-hand side of the energy equation, the first term represents heat conduction as expressed by Fourier's law, K_T being the thermal conductivity of the rock-fluid mixture. The remaining terms are the convective term and the source term. In the convective term, δT denotes the interface temperature, i.e., the temperature of the fluid entering the volume element. In the energy equation, local thermal equilibrium between the fluid and the rock is assumed. The energy changes due to fluid compressibility, acceleration, and viscous dissipation have also been neglected.

The mass flow equation and the energy equation are coupled through the pressure- and the temperature-dependent parameters as well as through the convective term. In the model, Darcy's law has been used to describe the fluid flux through fractures and porous media:

$$\bar{q} = - \frac{k}{\mu} (\nabla P - \rho^w \bar{g}),$$

where k is the absolute permeability, μ is the dynamic viscosity of the fluid, and \bar{g} is the acceleration due to gravity. The energy and mass flow equations are nonlinear with pressure/temperature-dependent parameters ρ^w , k , μ , K_T , and c . Furthermore, the parameters ϕ , S_g , and k are stress dependent.

Deformation

The model employs the one-dimensional theory of Terzaghi to calculate the deformation of the medium. The basic concept in the theory is the relationship between the effective stress σ' and the pore pressure P . For saturated

media, this effective stress can be written as $\sigma' = \sigma_N - P$, where σ_N denotes the normal stress. The effective stress can easily be calculated from this equation at any time, given that the normal stress σ_N is known and remains constant.

The consolidation behavior of each material is described by the "e - log σ' curves", where e is the void ratio: $e = V^D/V^X = \phi/(1 - \phi)$. In practice, consolidation tests are used to obtain these curves for each material. A typical consolidation curve consists of a so-called virgin curve and a series of parallel swelling-recompression curves. When the rock is loaded to levels never before attained, the deformation is represented by the virgin curve, but for swelling or load levels below the preconsolidation stress, the deformation is represented by the swelling-recompression curves. (The model neglects hysteresis between swelling and recompression curves.) In the model, the "e - log σ' curves" are generally approximated by straight lines, one of slope C_c (compression index) for virgin loading, and others of slope C_s (swelling index) for unloading or low-level reloading.

The stress-dependent parameters in the governing equations, ϕ , S_s , and k , can easily be calculated, given the consolidation curves for each material. The porosity is computed using the equation $\phi = e/(1 + e)$, and the specific storage S_s can be calculated using the expression $S_s = \rho^W g [\phi \beta_p^W + (1 - \phi) a_v]$. The coefficient of compressibility a_v can be expressed as $a_v = -de/d\sigma' = C_c/(2.303 \sigma')$.

In calculating the permeability k , the following empirical relation is used:

$$k = k_0 \exp \left[\frac{2.303 (e - e_0)}{C_k} \right],$$

where k_0 and e_0 are arbitrary reference values of the permeability and void ratio, respectively. For a given material, C_k is the slope of the best-fitted line of void ratio e versus $\log k$.

II. NUMERICAL SOLUTIONS

Integrated Finite-Difference Method

The model uses the integrated finite-difference method to discretize the flow regime and to handle the spatial gradients. The flow regime is divided into arbitrarily shaped polyhedrons constructed by drawing perpendicular bisectors to lines connecting nodal points. This permits easy evaluation of the surface integrals in the governing equations (Edwards 1972; Narasimhan 1975; and Sorey 1975).

In numerical notation the governing equations can be written as follows:

Mass balance:

$$\frac{(S V)_n}{g} \frac{\Delta P_n}{\Delta t} = \sum_m \left(\frac{\rho^w kA}{\mu} \right)_{n,m} \left(\frac{P_m - P_n}{d_{n,m} + d_{m,n}} - \rho_{n,m}^w \bar{g} \right) + (Q_F V)_n.$$

Energy balance:

$$\begin{aligned} (\rho^m c^m V)_n \frac{\Delta T_n}{\Delta t} = \sum_m \left[\frac{(KA)_{n,m}}{d_{n,m} + d_{m,n}} (T_m - T_n) \right. \\ \left. + \left(\frac{\rho^w w kA}{\mu} \right)_{n,m} (T_{n,m}) \left(\frac{P_m - P_n}{d_{n,m} + d_{m,n}} - \rho_{n,m}^w \bar{g} \right) \right] + (Q_H V)_n. \end{aligned}$$

These equations are valid for an arbitrary node n connected to an arbitrary number of nodes m . The nodal point distances to the interface for node n and node m are represented by $d_{n,m}$ and $d_{m,n}$.

Upstream Weighting

To evaluate the interface temperature $T_{n,m}$, the model employs an upstream weighting criterion

$$T_{n,m} = aT_n + (1 - a)T_m.$$

In this equation, a , the upstream weighting factor, is restricted in value to the range of 0.5 - 1.0 for unconditional stability.

Implicit Formulation

In the model, the equations are solved implicitly to allow for larger time steps to be taken. The implicit formulation is incorporated by means of the following expressions:

$$T_n = T_n^O + \lambda \Delta T_n,$$

$$T_m = T_m^O + \lambda \Delta T_m,$$

$$P_n = P_n^O + \lambda \Delta P_n,$$

$$P_m = P_m^O + \lambda \Delta P_m.$$

The weighting factor λ is generally allowed to vary between 0.5 and 1.0 for unconditionally stable solutions, but it may also be specified as a constant. If λ is specified to be 0 during the simulation, the solution scheme is fully explicit (forward differencing), and the time step cannot be greater than a critical stable value (see Narasimhan 1975). If $\lambda = 0.5$, the Crank-Nicholson (central-differencing) scheme results. For $\lambda = 1.0$, a fully implicit (backward differencing) scheme is employed.

Spatial Gradients

The spatial gradients between nodes are estimated by a linear approximation,

$$\bar{\nabla}P = \frac{P_m - P_n}{d_{n,m} + d_{m,n}}.$$

The permeability and thermal conductivity of the matrix and the density of the fluid at the interfaces are evaluated using the harmonic means to preserve continuity of flux at the interface, as for example,

$$k_{m,n} = k_m k_n \frac{d_{m,n} + d_{n,m}}{k_m d_{n,m} + k_n d_{m,n}}.$$

Direct Solver

With implicit formulation, gradient approximation, and coefficient evaluation, the governing equations can be written in the forms:

$$C_{n,n} \Delta P_n - C_{n,m} \Delta P_m = b_n,$$

$$K_{i,i} \Delta T_n - K_{i,j} \Delta T_n + K_{i,n} \Delta P_n - K_{i,m} \Delta P_m = B_i.$$

These two equations can be combined into a single matrix equation

$[A]\{X\} = \{b\}$ for simultaneous solution, where the matrix $[A]$ consists of the coefficients $C_{n,m}$, ... and $K_{i,i}$, These are in general a function of the temperature and pressure, and therefore result in a set of nonlinear equations. The vector $\{X\}$ contains the unknowns ΔP and ΔT , and the vector $\{b\}$ represents the known explicit quantities.

The solution of the nonlinear set of equations is obtained using an efficient direct solver (Duff 1977) and an iteration scheme for the nonlinear coefficients. Basically, the solver uses LU decomposition and a Gaussian elimination procedure to solve a set of linear equations.

The matrix of coefficients (the [A] matrix) is preordered using permutation matrices such that the resultant matrix is in lower-triangular block form. Gaussian elimination is then performed within each diagonal block in order to obtain factorization into the lower triangular and the upper triangular. Finally, the factorization is used to solve the matrix equations. In this solution package (Duff 1977), no restriction is placed upon the characteristics of the matrix of coefficients. The matrices need not be symmetrical or of a specified degree of sparsity.

The nonlinear coefficients are presently handled using an iteration scheme. Future development of the code includes incorporating the Newton-Raphson scheme for efficient and accurate determination of the nonlinear coefficients.

III. COMPUTER CODE

Documentation

The code is written in Fortran IV language. The code listing and a user's manual are available from M. J. Lippmann at Lawrence Berkeley Laboratory.

Spatial Grid

In the model there is no restriction upon choice of basic block (node) shape or numbering of nodes. The geometric configurations of the nodal elements can be arbitrary, and the grid may be one-, two-, or three-dimensional, with rectangular, cylindrical, or spherical symmetry. The dimensions of the nodes and the connections between nodes are required input data. For complex problems, the design of the mesh may create the most difficulty in using the program. Auxiliary computer programs for mesh and input data generation are available for a number of grid systems, including the case with cylindrical or elliptical rings near a well, gradually changing to rectangular nodes in the far field. This mesh is relevant for the simulation of horizontal or inclined fractures intersecting a well (cylindrical or elliptical cross sections) or intersecting other planar fractures within the rock mass (linear cross sections).

Material Properties

For each material the porosity, permeability, specific storage, thermal conductivity, heat capacity, and density of the solid must be specified. These parameters may be constant or may vary with temperature and/or effective stress. The porosity and specific storage can vary with the effective

stress, the permeability with both temperature and effective stress, and the thermal conductivity and heat capacity with temperature only. These relations are specified by tables, interpolated during each time step. Anisotropic permeability can be handled by orienting the grid blocks parallel to the principal axes of anisotropy.

Fluid Properties

Input parameters are the fluid viscosity, heat capacity, density, and compressibility of water. A constant value of the compressibility must be specified; other fluid properties may also be assumed constant. However, the code provides the option of specifying viscosity and heat capacity as functions of temperature and specifying density as a function of temperature and pressure. An empirical formula is used for the density function, and the code interpolates input tables for the appropriate value of the viscosity and heat capacity during each time step.

Sources and Sinks

Mass and energy sources and sinks may be specified for any node. The rate may be constant or vary with time.

Initial Conditions

Initial values of pressure, temperature, and preconsolidation stress must be specified for each grid block. If the restart option is utilized, the specified initial values must correspond to the final values obtained in the last run.

Boundary Conditions

Prescribed potential or flux boundaries may be used. The boundaries can be specified as constant or varying with time. Finite capacity wells (well-bore storage) and heterogeneous flow regimes (fractures) can easily be simulated.

Time Steps and Solution Control

There are several options for selecting the time steps to be taken during the simulation. The maximum and minimum time steps may be specified, or the time steps may be automatically determined on the basis of the maximum desired pressure and/or temperature changes during a time step. The problem is ended when one of several criteria is met. These include attainment of steady state, reaching the specified upper or lower limit for temperature and/or pressure, completing the required number of time steps, and reaching the specified maximum simulation time.

Output

Output is provided according to specified times or specified time steps. The pressure, temperature, and first- and second-order derivatives are printed for each grid block (node). The fluid and energy fluxes are given for each connection. The mass and the energy balance are also included in the output.

IV. VALIDATIONS

The code has been validated against analytic solutions for fluid and heat flow, and against a field experiment for underground storage of hot water. The following is a list of selected problems.

Analytical Solutions (Fluid and Heat Flow)

- (a) Continuous Line Source: The Theis problem (1935) was solved for both early times (transient flow) and long-term steady radial flow.
- (b) Cold Water Injection in a Hot Reservoir: Avdonin's (1964) analytical results were matched for early and later times.
- (c) Doublet Problem: The temperature variations at the production well due to cold water injection were matched against the analytical results of Gringarten and Sauty (1975).
- (d) Conduction Problem: A one-dimensional conduction problem was solved and compared with the analytical solution given by Carslaw and Jaeger (1959).
- (e) Two Node Problem: Transient conduction heat transfer between two nodes was calculated and compared to analytical solutions.
- (f) Buoyancy Flow: The rate of thermal front tilting when hot water was injected into a cold reservoir was calculated and compared to semianalytic results by Hellstrom and others (1979).

Fracture Flow Solutions

- (a) Vertical Fracture: The pressure response in a well intercepting a finite-conductivity vertical fracture was calculated and compared to the semianalytic solution of Cinco-Ley and others (1978).

- (b) Horizontal Fracture: The pressure response in a well intercepting an infinite conductivity horizontal fracture was calculated and compared to the analytical solution of Gringarten (1971).

Auburn University Aquifer Thermal Energy Storage Field Experiment (1979)

Numerical modeling of two cycles of injection, storage, and production of hot water in a confined aquifer yielded results that closely matched temperatures and energy recovery factors observed in the field (Tsang and others 1979a).

V. APPLICATIONS

This model has been applied to problems in the fields of geothermal reservoir engineering, aquifer thermal energy storage, well testing, radioactive waste isolation, and in-situ coal combustion.

Geothermal Reservoir Engineering

- (a) Simulation and reinjection studies have been done using data from the Cerro Prieto geothermal field (Lippmann and others 1978; Tsang and others 1979b; and Lippmann and Goyal 1979).
- (b) Generic studies have been made for injection and production in geothermal reservoirs (Lippmann and others 1977b).
- (c) Theoretical studies have been made of subsidence in geothermal reservoirs due to fluid withdrawal (Lippmann and others 1976, 1977a).
- (d) Studies have been made of flow through fractures in geothermal reservoirs (Bodvarsson and Lippmann 1980).

Aquifer Thermal Energy Storage

- (a) Many generic studies have been performed to demonstrate the feasibility of sensible heat storage in aquifers (Tsang and others 1976, 1978a, 1978b).
- (b) The Auburn field experiments in aquifer storage were modeled successfully (Tsang and others 1979a).

Well Testing

- (a) Studies of well behavior in a two-layered system with a temperature gradient have been made (Lippmann and others 1978; Tsang and others 1979b).
- (b) The effects of an alternative production-injection scheme on the temperature and the pressure response of a geothermal system have been studied (Lippmann and others 1977a; Tsang and others 1978c).
- (c) A study was made of temperature effects in well testing in a single-layer system (Mangold and others 1979).

Radioactive Waste Isolation

- (a) A study was made to examine the conductive heat transfer near a repository (Chan and others 1978).
- (b) A generic study was performed for a fracture system through a repository. These simulations were for periods of up to 10,000 years (Wang and others 1980; Wang and Tsang 1980).

In-Situ Coal Combustion

Calculations were performed to investigate the time required for thermal effects to reach the surface from underground combustion of a coal seam (Mangold and others 1978).

VI. SUMMARY

This model is for the study of fluid flow and heat transfer in deformable formations. The integrated finite-difference method is used to formulate the governing equations and to discretize the saturated medium. Complex geometries and coupled thermohydrologic processes can be modeled.

The code has been well validated and extensively applied to geothermal reservoir engineering, to aquifer thermal energy storage studies, and to field experiments in porous formations. The recent modelings of fracture flows and buoyancy flows are extensions to fractured media and waste repository studies.

MODEL OF DUGUID

This is a finite-element program for two-dimensional isothermal flow in a double-porosity medium. The transient fluid interaction between the fracture and the porous medium and flow acceleration along fractures have been studied. The model is described in Duguid (1973), Duguid and Lee (1973, 1977) and Duguid and Abel (1974).

I. GOVERNING EQUATIONS

In this double-porosity model, the set of governing equations consists of two coupled fluid flow equations with two Darcy-like velocity equations:

$$(1 - \phi^m) \phi^f \beta_P^w \frac{\partial P^{f'}}{\partial t} + (1 - \phi^m) \phi^m \beta_P^w \frac{\partial P^{m'}}{\partial t} + \nabla \cdot \bar{q}^f = \frac{\Gamma(t)}{\rho^w},$$

$$(1 - \phi^f) \phi^m \beta_P^w \frac{\partial P^{m'}}{\partial t} + (1 - \phi^f) \phi^f \beta_P^w \frac{\partial P^{f'}}{\partial t} + \nabla \cdot \bar{q}^m = - \frac{\Gamma(t)}{\rho^w},$$

$$\bar{q}^f = - \frac{k^f}{\mu} \cdot \left(\rho^w \frac{\partial \bar{q}^f}{\partial t} + \nabla P^{f'} \right),$$

$$\bar{q}^m = - \frac{k^m}{\mu} \nabla P^{m'},$$

where $P'(\bar{x}, t) = P(\bar{x}, t) - P_0(\bar{x})$ and the gravitational effect is subtracted. The pressure P^f and the flux velocity \bar{q}^f represent the macroscopic values averaged over the fractures in the vicinity of \bar{x} . P^m and \bar{q}^m are the corresponding values for the rock medium blocks. A rock medium block consists of the rock matrix and the primary pores. In this model it is assumed that the fracture porosity ϕ^f is typically much smaller than the rock medium porosity ϕ^m ,

while the equivalent continuum fracture permeability k^f is much greater than the rock medium permeability k^m . The total pressure is $P = P^f + P^m$.

Fracture-Rock Medium Fluid Interaction

The two fluid flow equations are coupled by the transient mass flux $\Gamma(t)$.

One analytic expression of this fluid interaction term is:

$$\Gamma(t) = \frac{\alpha^{fm}}{\mu} \left[(P^{m'} - p^{f'}) + 2 \sum_{n=1}^{\infty} [(-1)^n P^{m'} - p^{f'}] \exp\left(\frac{-k^m n^2 \pi^2 t}{2L^2 \mu \phi^m \beta_P}\right) \right],$$

where $\alpha^{fm} = 4k^m \phi^f w / \pi b_{1/2} L$, $b_{1/2}$ is the half-aperture of an average fracture, and L is the characteristic half-dimension of a rock medium block. Duguid and Abel (1976) used a slightly different form of $\Gamma(t)$. The form of $\Gamma(t)$ shown here is similar to that used in leaky aquifer analysis (Bredehoeft and Pinder 1970) and represents the mass flux from the rock medium blocks through the fracture surfaces into the fractures. The factor k^m in the flow-coupling constant α^{fm} accounts for the flow in the rock medium blocks, and the factor ϕ^f/b in α^{fm} accounts for the surface areas of fracture-medium interfaces per unit volume. The time constant of the transient exponential in $\Gamma(t)$ depends only on the characteristics of the rock medium blocks (k^m , L) and is independent of the fracture flow. The rock matrix blocks essentially act as the fluid source to the fractures in the model. The quasi-steady fracture-medium fluid interaction Γ is proportional to the pressure difference $P^{m'} - p^{f'}$ (Barenblatt and others 1960).

Porosity Coupling and Consolidation

The fluid flow equations are coupled not only through Γ but also through the time derivatives of pressures. This coupling results from the interchange of the two porosities with time. As the fluid pressures decrease, consolidation can occur through the rearrangement of the skeleton. This rearrangement alters the size of fractures and primary pores. Two mechanisms have been considered for the interchange of the fracture volume with the pore volume. The first mechanism is induced by the changes of fluid density with the pressures in each of the porosities. These contributions are included in the governing equations, as can be shown by the appearance of the fluid compressibility β_P^W in all the storage (fluid capacity) coefficients multiplying the time derivatives of pressures. The second mechanism formally considered by Duguid and Lee (1977) is due to the mechanical deformations of the two porosities. The gradient of rock solid velocity $\nabla \cdot \bar{v}^R$ could be retained in the double-porosity fluid flow equations to account for the effects of rock deformation in a similar manner as in the consolidation theory of single-porosity porous media (Verruijt 1969; Biot 1941, see also Aifantis (1979) for a recent paper on double-porosity equations). The couplings of the inelastic and elastic deformations of fractures and porous media to fluid flow would affect the storage capacities of the double-porosity flow systems.

Fracture Flow Acceleration

The flows in the fractures are usually much faster than the flows through the porous-medium blocks. In this model, Darcy's law for fracture flow is generalized, with the inclusion of the acceleration term $\rho^W \partial \bar{q}^f / \partial t$. The generalized Darcy equation is derived by spatially averaging the Navier-Stokes

equation of motion for incompressible flow inside the individual fractures over a large spherical volume (Lew and Fung 1970). The fractures are represented by tubules with elliptical cross sections. One of the assumptions is that the velocity distribution within the tubule is parabolic (Poiseuille flow). This is valid if the compressible viscous force and the convective term are neglected and a steady-state flow profile is maintained. The inflow through the porous wall around the tubule will not change the parabolic distribution if the inflow is constant along the tubule (Berman 1953; Yuan and Finkelstein 1956; Duguid 1973). Another assumption in the space averaging is that the spherical volume is large enough to contain a representative number of tubules. The intersection of a single elliptical tubule with the spherical surface is assumed to be small enough so that the volume integral can be reduced to an angular integral over the distribution of the direction of tubules. As a result of these assumptions, the equivalent continuum fracture permeability tensor can be formally expressed as

$$\bar{k}^f = \phi \frac{A}{8\lambda^v} b_{1/2}^2 f(\bar{r}, \hat{\Omega}) \hat{\Omega} \hat{\Omega} d\Omega,$$

where A is the cross-sectional area of the tubule and $b_{1/2}$ is the half-width of the minor axis of the tubule or the half-aperture of the fractures. The pore matrix function $f(\bar{r}, \hat{\Omega})$ is defined statistically as the number of oriented tubules per unit area per unit solid angle. λ^v is a parameter for compensating entry and exit effects at tubule intersections. $f(\bar{r}, \hat{\Omega})$ and λ^v are usually unknown. In the model, \bar{k}^f is an input parameter.

Summary of Double-Porosity Couplings

In brief, the governing equations in the model include the effects of the fracture flow acceleration, the transient flow interaction between the fractures and the porous medium, and the coupling of porosity changes. The double-porosity system is described by two pressure fields coupled by flow between the fractures and the porous medium and by the interchange of the two porosities. Each porosity depends on both the fracture pressure and the porous-medium pressure. Within each porosity, the flow flux is driven mainly by its own pressure gradient. For completeness, one could also phenomenologically propose that the fracture flow flux \bar{q}^f depends on both ∇P^f and ∇P^m , and similarly \bar{q}^m on both pressure gradients. The importance of the cross terms due to interdependence of the two pressure fields and the two flow velocity fields may require further study.

II. NUMERICAL SOLUTIONS

Finite-Element Method

The coupled set of equations is solved by the finite-element Galerkin method. The code is capable of solving coupled linear equations with several unknowns at each node. For two-dimensional problems in the x-z plane, there are six equations in six variables. The variables are the incremental pressures P^f and P^m and the components of fluxes q_x^f , q_z^f , q_x^m , q_z^m . Quadrilateral elements are used to divide the planar space. A variable within an element is interpolated in terms of the values of the variable at the four corner nodes. The trial solution is substituted into the differential equations.

The space-differential operators operate on the basis functions used for the interpolation. Isoparametric bilinear polynomial basis functions are used. The residue of the trial solution is integrated over the element weighted by the basis functions. The integration is carried out using 2 x 2 Gaussian integration.

It is of interest to point out that in the governing equations there are only first-order spatial gradients with both pressure and Darcy flux velocity as unknown variables. The Darcy velocity of the porous-medium block \bar{q}^m can be eliminated by substituting \bar{q}^m into the fluid flow equations in the porous medium. This procedure reduces the six unknowns to four unknowns. If the acceleration term in the fracture flux equation is not modeled, the \bar{q}^f can also be eliminated and only two pressure equations need to be solved. In these elimination procedures, second-order gradient terms will appear in the governing equations. These second-order terms are usually treated with Green's theorem in most of the finite-element solutions of fluid flow equations. For the proper treatment of boundary conditions in a double-porosity model, there is a need to maintain the general six first-order equations (see "Boundary Conditions" in next section).

Implicit Time Difference

First-order finite difference is adapted to approximate the time derivatives. A backward-differencing implicit scheme ($\lambda = 1$) or a central-differencing Crank-Nicholson scheme ($\lambda = 0.5$) may be used to construct the implicit matrix equation relating the unknown nodal values at $t + \Delta t$ to those at t .

For m nodes in the flow regime, the $6m \times 6m$ backward-differencing implicit matrix equation is of the form:

$$([A]/\Delta t + [B])\{f\}_{t+\Delta t} = [A]/\Delta t\{f\}_t - \{R\}_{t+\Delta t},$$

where matrix $[A]$ contains the coefficients of the time derivative terms and $[B]$ contains the spatial operators which are associated with the variables. The column vectors $\{f\}$ contain the $6m$ nodal values of the variables, and $\{R\}$ is zero in this formulation unless prescribed flux boundary conditions are applied.

Matrix Solver

The matrix equation is solved by a direct elimination procedure. The matrix $[A]/\Delta t + [B]$ is decomposed into the product of lower- and upper-triangular matrices using the Crout or the Doolittle method. This reduces the matrix equation into two triangular systems which can be solved by backward and forward substitution procedures. Since the fluid interaction $\Gamma(t)$ is transient, $[B]$ is time-dependent. The decomposition of $[A]/\Delta t + [B]$ must be reformulated at each time step.

III. COMPUTER CODE

Documentation

The code listing is available from J. Duguid at the Office of Nuclear Waste Isolation in two versions: IBM-360-91 and CDC 6500 (CYBER 73).

Spatial Grid

The two-dimensional grid consists of four-corner quadrilateral elements. For the solution of two-dimensional aquifer problems discussed later, the

coordinate system was selected parallel to the principal values of the permeability tensor in the fractures. The coordinate system was also assumed to be parallel to the length and thickness of the aquifer.

Material Properties

The two principle values of the equivalent continuum fracture permeability tensor, the isotropic rock medium permeability, the fracture porosity, and the rock medium porosity are input data and can vary spatially with different elements. The average fracture aperture, the characteristic size of the rock medium blocks, and the fracture-medium fluid coupling coefficient are also input parameters for calculating the transient flux $\Gamma(t)$.

Fluid Properties

Water density, viscosity, and compressibility are input parameters. The water compressibility is used in the calculation of the storage coefficients and the transient exponential of $\Gamma(t)$.

Initial Conditions

The initial conditions are zero values of incremental pressures and fluxes.

Boundary Conditions

The boundaries of the system can be applied with prescribed pressure or flux boundary conditions which are constant or time variable. An analytic expression for a leaky flux boundary is used. Since there are two flux velocities in a double-porosity model, the partition of the total flux between the fractures and the rock matrix blocks is not known if only the total flux at the boundary is prescribed. The general program solving all six of the first-

order governing equations simultaneously allows treatment of this type of boundary condition. For prescribed pressure boundary conditions, or when the partition of flux between the two porosities are known, simplified equations, solving only P^m , P^f , and \bar{q}^f can be used. This code allows treatment of the acceleration term in the fracture flow equation and can be further simplified if the acceleration effect is shown to be small.

Time Steps

The time step is small at early times and can be increased logarithmically at each time step.

Output

The calculated results are the pressures and flux velocities representing the macroscopic values averaged over the fractures and over the porous-medium blocks.

IV. VALIDATIONS

The validation of this program is only briefly mentioned in Duguid and Abel (1974). Numerical solutions were obtained for a one-dimensional problem in a finite rod using both central-differencing and backward-differencing schemes. The instability problem for the central-differencing approach and the error-propagation problem for the backward-differencing approach were investigated. Some two-dimensional plane-strain problems were also mentioned in demonstrating the use of the code. It will be of interest to model radial problems and compare the numerical results with known analytic solutions of

well response to double-porosity media. The double-porosity model has been used mainly in well testing analysis.

V. APPLICATIONS

The code has been applied to the solution of problems in a fractured, porous leaky aquifer. The aquifer is confined above by an impermeable boundary and semiconfined below by an aquitard. Leakage from the aquitard is assumed to occur in both the primary pores and the fractures in the aquifer. The horizontal fractured porous aquifer is intersected by a stream (vertical boundary) which is initially in equilibrium with the aquifer. At time $t = 0$ the water level in the stream is instantaneously lowered and the step drawdown is maintained constant thereafter. In an alternative problem, the total discharge rate from the aquifer to the stream is assumed to be constant instead. The first response occurs in fractures which are of larger size than the primary pores. From the numerical solutions of the problems in rectangular coordinates considered in this model, the following conclusions were drawn:

- (a) The flow from the porous-medium blocks to the fractures is important, even when the permeability of the primary pores is small. For the step drawdown problem the transient pressure drop with $k^f = 300 k^m$ (and $\phi^f = 0.017 \phi^m$) is substantially slower than the response with $k^m = 0$. With $k^m = 0$, the flow in the porous-medium blocks is neglected. With the termination of the supply of fluid to the fractures, the rate of response in the fractures increases.
- (b) After very short times, the pressure in the fractures is nearly equal to the pressure in the porous-medium blocks and the gradients of these

pressures are nearly equal. As a result, the discharge is divided between the fractures and the porous-medium blocks according to the ratio of fracture permeability to porous-medium permeability. Large storage coefficients for more compressible formations may prolong the early transient period.

- (c) The response of the aquifer is slowed by the transient interaction term. The slower response is explained by a greater flux at early time flowing from the porous-medium blocks into the fractures when transient interaction is considered. There is, however, only a slight difference between the pressure solutions corresponding to transient and steady-state interaction terms in the problems studied. From the exponent of the transient term Γ , the transient effect is greater for porous-medium blocks having large dimension and low permeability than for small, more permeable blocks. Therefore, the transient interaction may be more important for deep, slightly fractured, low-permeability formations.
- (d) The effect of the acceleration term in the equation of motion of fluid in fractures is small for the problem studied in the model. The acceleration term may be neglected, and the simplified set of equations, with elimination of the velocity terms, can be used.

VI. SUMMARY

This code is for studying isothermal flow in a double-porosity model of a fractured rock mass. The governing equations for the pressure changes in the fractures and in the porous-medium blocks are coupled both through the interdependence of the values of the two porosities and through the transient flux between the two porosities.

With space averaging over an elliptic tubule model for the equation of motion of fluid in fractures, it is shown that the anisotropic fracture permeability tensor can formally be expressed in terms of a pore matrix function for the distribution of the orientation of tubules.

The effect of the acceleration term in the equation of motion can be studied by the finite-element code, which has the capability of solving coupled first-order equations of pressures and fluxes in fractures and pores.

The results of rectangular, two-dimensional modeling of a fractured porous aquifer demonstrate the importance of the flow in the porous medium to the aquifer response, the small difference between the fracture pressure and porous-medium pressure, and the small effects of the transient interaction term and the acceleration term.

The extension to radial well problems and other applications using this model should be continued. Documentation of the code and validation are needed. It will also be of great interest to extend this model for use in solving the coupling of the double-porosity fluid flows with the deformation in the fractures and the consolidation in the porous-medium blocks.

MODEL OF O'NEILL

This is a finite-element model for three-dimensional, nonisothermal, saturated flow in a double-porosity medium. The responses due to hot water injection and the coupling of the temperature equations in the fractures and in the porous medium have been studied. The model is described in O'Neill (1977, 1978).

I. GOVERNING EQUATIONS

In this model there are three governing equations for the fluid flow and heat transfer in a double-porosity medium: one pressure equation and two temperature equations. Each point in space has two temperature values representing the macroscopic values averaged either over the fractures or over the porous-medium blocks. A porous-medium block consists of the rock matrix and the primary pores.

The pressure equation for the combined fluid flow through the fractures and the porous medium is:

$$\rho^w \left(\phi \beta_P^w + \beta_P^p \right) \frac{\partial P'}{\partial t} - \rho^w \phi \beta_T^w \frac{\partial T}{\partial t} - \nabla \cdot \rho^w \left(\frac{\bar{k}^f}{\mu} + \frac{\bar{k}^m}{\mu} \right) \nabla P' = Q_F ,$$

where the porosity ϕ is the sum of the porosity of fractures ϕ^f and the porosity of the pores in the porous medium ϕ^m : $\phi = \phi^f + \phi^m$. The water temperature is the weighted average of temperatures in the fractures and in the pores, $T = (\phi^f T^f + \phi^m T^m) / \phi$. The response of water density and the response of pores to pressure change are assumed to be elastic with constant compressibilities

β_p^w and β_p^p , respectively. The thermal expansivity of water density to temperature change β_T^w is also constant. P' is the incremental pressure above the hydrostatic pressure. The gravitational effect due to water density variation is neglected.

The equations for temperature in the fractures and in the porous medium are:

$$\begin{aligned} \phi^f \rho^w c^w \frac{\partial T^f}{\partial t} + \rho^w c^w q^f \cdot \nabla T^f - \nabla \cdot (K_T^f + \bar{K}_{TD}^f) \cdot \nabla T^f = \\ = h^{fm} (T^m - T^f) + c^w Q_F^f (T^b - T^f), \end{aligned}$$

$$\begin{aligned} [\phi^m \rho^w c^w + (1 - \phi^m) \rho^r c^r] \frac{\partial T^m}{\partial t} + \rho^w c^w q^m \cdot \nabla T^m - \nabla \cdot (K_T^m + \bar{K}_{TD}^m) \cdot \nabla T^m = \\ = h^{fm} (T^f - T^m) + c^w Q_F^m (T^b - T^m). \end{aligned}$$

In this model, the external heat sources are associated with injection of water at temperature T^b . The partition of the fluid mass source Q_F into Q_F^f and Q_F^m is assumed to be according to the permeability ratio $Q_F^f/Q_F^m = k^f/k^m$.

Dispersion

In addition to the thermal conductivities K_T^i , the temperature equations also include the hydrodynamic thermal dispersivities \bar{K}_{TD}^i . In this model, the thermal dispersivities are diagonal tensors and are dependent on the water particle velocities $\bar{v}^i = \bar{q}^i / \phi^i$ according to

$$(\bar{K}_{TD}^i)_{mn} = \begin{cases} (D_T^i)_{mn} (\bar{v}^i)_n & m = n \\ 0 & m \neq n \end{cases}$$

where the constant coefficients of dispersivity \bar{D}_T^{-1} are specified in the input of the program.

Fracture-Porous Medium Heat Interaction

The temperature equations are mainly coupled through the term for heat transfer between fractures and porous media: $\pm h^{fm}(T^f - T^m)$. In the program, h^{fm} is constant in time and is an input parameter in modeling the coupling between the fracture temperature and the porous-medium temperature. The coupling coefficient h^{fm} accounts for the heat conduction from the porous-medium blocks to the fractures and the heat dispersion due to mixing of fluid across the interface between the fractures and the porous medium. In the detailed formulation of these temperature equations by a volume-weighted space-averaging procedure, O'Neill formally expresses the heat transfer from the fractures to the porous medium in terms of surface integrals over the interfaces and then estimates analytically the relative importance of conductive and dispersive contributions. The conductive part is proportional to the thermal conductivity of the porous medium, and inversely proportional to the size of the porous-medium blocks. The dispersive part is proportional to the pore velocity and the correlation of temperature variations and velocity variations over the interface. Moreover, the geometric features in the two contributions to the coupling coefficient are different. The conductive part for heat flow from the porous-medium blocks to the fractures is proportional to the interface area between the fractures and the porous medium with both the solid rock and the primary pores. On the other hand, the dispersive part for fluid mixing is proportional to the interface area between the fractures and the primary pores

only. From estimates with typical thermal and fluid flow properties, O'Neill concludes that h^{fm} is dominated by the conductive contribution from the porous-medium blocks to the fractures.

The temperature equations are also coupled through the flow equation. The flow equation has a time derivative of temperature from the dependence of water density on temperature. The temperature also affects the viscosity of water in both the fractures and the porous medium. The fluid flow equation couples back to the temperature equations through the velocities. The Darcy flux velocities \bar{q}^f and \bar{q}^m from the solutions of the fluid flow equation appear in the convective heat transfer terms and in the dispersive flux terms of the temperature equations.

Double-Porosity Couplings

This model is a generalization of the isothermal double-porosity model of Barenblatt and others (1960) to nonisothermal flow. Between the fractures and the porous media, the quasi-steady transfer $\pm h^{fm}(T^f - T^m)$ in the temperature equations is analogous to the fluid mass transfer term $\pm \alpha^{fm}(P^f - P^m)$ in the isothermal pressure equations. In a thermodynamic description of a double-porosity medium, each point in space is formally characterized by two pressures and two temperatures, one representing the fractures and one the porous medium. In this model for hot water injection, the pressure difference is assumed to equilibrate very quickly and can therefore be neglected.

II. NUMERICAL SOLUTIONS

Hermite Finite-Element Method

The model solves the governing equations with the Galerkin finite-element method using hermite polynomials as the basis functions. The three-dimensional space is decomposed into finite-element domains with eight-corner nodes. The three-dimensional basis functions, used for interpolation, are constructed by multiplying together the one-dimensional hermite polynomials in each coordinate. A hermite polynomial is a cubic polynomial with the property that it is nonzero only in either its value or its derivative at one of the two nodes in a one-dimensional element. There are four independent hermite polynomials: two with unity value, two with unity derivative. Using the four hermite basis functions, a variable within an element can be interpolated in terms of its values and its derivatives at the two nodal points. In the three-dimensional domain, every variable at each node has one value and three partial derivatives with respect to three coordinates. For m nodes in a modeled domain, a variable is expressed in terms of a vector of $4m$ nodal variables. In this model with one pressure equation and two temperature equations, a $4m \times 4m$ matrix equation for the pressure and an $8m \times 8m$ matrix equation for the two temperatures are constructed to represent the governing equations.

The matrix equations are constructed by integrating the residue of the interpolated trial solutions over each element weighted by the basis functions. Most of the element integration is carried out using $2 \times 2 \times 2$ Gaussian quadrature except for the evaluation of the hydraulic conductivity term of

$\rho^w \left(\frac{k^f}{\mu^f} + \frac{k^m}{\mu^m} \right)$ in the fluid flow equation. Since the water viscosities μ^i

depend sensitively on the temperatures, the nodal values of the hydraulic conductivity are first determined by the nodal values of temperature, then linear functions are used to interpolate within the element and a $3 \times 3 \times 3$ Gaussian quadrature is used for the integration. On the other hand for the temperature equations, the Darcy velocities in the convective term and in the dispersive term are more accurately evaluated at Gauss points within an element rather than interpolated from nodal values of pressure. In this case, the use of $2 \times 2 \times 2$ Gaussian integration is sufficient. The products of basis functions and Gaussian weighting factors in the element integrations need be computed only once for each of the elements for all time steps, and can be stored in the program.

Iterative Procedure

A first-order finite difference in time with a backward-differencing implicit or a central-differencing Crank-Nicholson scheme is used to construct the implicit matrix equations relating the variables at $t+\Delta t$ to those at t . Since the pressure solution usually reacts to changes more rapidly than the temperature solution, the pressure equations may be solved first for a number of time steps in succession during the period covered by one step in the temperature equations. Within each temperature time step, the pressure and temperature equations are solved in an iterative procedure. One iteration from the k th step to the $(k+1)$ th step consists of (i) solving the $P_{t+\Delta t}^{k+1}$ with the coefficients determined by $T_{t+\Delta t}^k$, (ii) calculating Darcy velocities with $P_{t+\Delta t}^{k+1}$, (iii) solving $T_{t+\Delta t}^{k+1}$ with the Darcy velocities in the convective and

dispersive terms, and (iv) calculating the hydraulic conductivities and the time derivative of temperature with $T_{t+\Delta t}^{k+1}$. These coefficients are needed for (i) in the next iteration. A given number of iterations are performed for each temperature time step.

Matrix Solver

The matrices have asymmetric nonzero elements and symmetric zero structures. For the solution of the implicit matrix system of either the $4m \times 4m$ pressure equation or the $8m \times 8m$ temperature equation, the algorithms of Eisenstat and Sherman (1974) are incorporated in the program. In the matrix solver, the coefficient matrices are stored in a one-dimensional array in envelope form, with only the matrix elements between and including the first and last nonzero elements in each row retained in storage. A sparse matrix factorization procedure on envelope elements is used.

III. COMPUTER CODE

Documentation

The user's manual with program listing and a sample problem are in the report by O'Neill (1977). The program was run on the IBM 370-158 Virtual Machine at Princeton University.

Spatial Grid

The applications of this program use orthorhombic (three-dimensional rectangular) elements with eight-corner nodes generated in the code. The nodal separations can be nonuniform. The coordinate axes are oriented parallel to the principal directions of the permeability tensors.

Material Properties

For the pressure equation, the input material parameters are the principal values of the permeability tensors and the porosities of the equivalent continuum fractures and the porous-medium blocks. For the temperature equations, the input data are the thermal conductivities, the dispersion coefficients of both porosities, and the rock density and specific heat capacity. All these parameters can vary in space with different elements. The heat transfer coefficient h^{fm} and the pore compressibility β_p^p are constant input data for the whole model domain.

Fluid Properties

The compressibility β_p^w and the thermal expansivity β_T^w of water are required for the pressure equation. The viscosity of water as a function of temperature is calculated in the program according to the relation used by Mercer and others (1975):

$$\frac{1}{\mu} = (5.38 \times 10^{-3} + 3.8 \times 10^{-3}A - 2.6 \times 10^{-2}A^2) \text{ kg/m/sec,}$$

where $A = (T - 150)/100$, $0^\circ\text{C} < T < 300^\circ\text{C}$.

Sources and Sinks

Point source/sink of fluid injection/withdrawal with given temperature can be specified at nodes. An analytic expression for a continuous point-source solution is used for calculating pressure gradients within the first element which encloses the point source.

Initial Conditions

The nodal values and/or the gradients of pressure and/or temperatures can be assigned to all nodes at the initial time or at the restarting time.

Boundary Conditions

Prescribed values and/or gradients of pressure and/or temperatures are specified on boundary nodes.

Time Steps

The heat contents of fracture and rock medium systems can be calculated for each time step. Time stepping can be specified by the size of the first temperature time step, the number of time steps in the solution of the temperature equations, the number of equal time steps in the solution of the pressure equation per temperature time step, or the number of iterations per temperature time step. The temperature time steps can be increased by multiplying each previous step by a common factor.

Output

The values of pressure and temperature and/or their gradients for selected nodes are output at specified time step printing intervals. The values of the variable can also be printed out for points not on the node by interpolating with the hermite basis function.

IV. VALIDATIONS

Several tests of the program are documented. The numerical solutions of linear and spherical radial problems are compared with analytic transient

solutions. The problems solved for validation are listed below:

- (a) Varying Hydraulic Conductivity: The linear flow equation is solved for the case in which hydraulic conductivity is $x^2/(1 + t)$.
- (b) Temperature Coupling: The temperature equations coupled through $h(T^f - T^m)$ are solved for the case in which there are no spatial gradients in the temperature equations.
- (c) Exponential Decay Fluid Source: The linear flow equation is solved with a uniform exponential decay source.
- (d) Temperature Front Movement: The linear temperature front movement in a constant flow field is calculated to test the convective-dispersive equation.
- (e) Point Source of Mass and Heat in Linear, Constant Flow Field: An analytic solution is obtained by O'Neill with the use of coordinate transformation, Fourier transform, and Laplace transform. The numerical solutions downstream from the point source agree with the analytic solution. The temperature up-stream from the source changes steeply and induces some oscillation in the vicinity of the point source.
- (f) Continuous Point Source: The numerical solution is obtained with orthorhombic elements to test the use of a three-dimensional rectangular grid for this spherically symmetric problem and to study the numerical problem near the point source.

V. APPLICATIONS

The program has been applied to the simulation of temperature front movements in fractures and in porous media. Two cases are studied: a linear constant-velocity flow system in response to a step change of temperature at $x = 0$, and a divergent flow system after injection of hot water at a given temperature and flow rate. Most of the results are obtained by solving the coupled temperature equations with the given fluid velocity field. From these simulations, the following effects have been observed:

- (a) The temperature front movement in the fractures slows down. Initially, the fracture front velocity is larger than the porous-medium front velocity. As the two fronts separate, the heat transfer from the hotter fracture water to the porous medium substantially slows down the fracture front and slightly speeds up the porous-medium front. The rate of change of the front movement depends on the heat capacities of the two flow systems. In the cases studied, the heat capacity of the porous medium (pore water and rock matrix) $\phi^m \rho^w c^w + (1 - \phi^m) \rho^r c^r$ is thirty times greater than the heat capacity of fractures $(\phi^f \rho^w c^w)$. Eventually the front velocities converge to a single, common value which is determined by the total heat capacity of the combined flow system.
- (b) The shape of the spreading temperature front is distorted. Without heat transfer between the fractures and the porous medium, each front will develop into a symmetric, normal Gaussian distribution around the temperature front. With heat transfer, the high fracture temperature increases the temperature of the porous medium between the two fronts and results

in a higher and longer tail preceeding the porous-medium front. On the other hand, the slowing down of the fracture front gives conduction and dispersion greater time to spread the fracture front before it reaches a given location. The result of these distortions lowers the temperature at the front of each flow system.

- (c) The front separations behave differently for the linear flow case and the divergent flow case. Initially, the fracture and the porous-medium fronts separate for both flow cases. In the linear case, the front separation monotonically increases and stabilizes to a constant, terminal value. In the radially divergent flow case, the fluid velocities change from high values near the injection point to low values away from the source. After the initial separation of the fronts and the development of large temperature differences between the two flow systems, the spatial gap between the fronts closes and the temperature difference declines when the velocity difference is too small to sustain the initially developed front separations.
- (d) The heat loss in fractures is insensitive to the heat transfer coefficient h^{fm} . For the linear flow case, the percentage change of heat content in the fractures (from time zero to the beginning of terminal velocity) is essentially independent of the value of h^{fm} and the flow velocity. When more heat is input into the fractures with higher fracture velocity through the inflow boundary, more heat will be transferred to the porous medium and will not result in an increase in the percentage of fracture heat input remaining in the fracture system. For the radial flow case,

the ratio of the percent change of heat content in the fractures to that in the porous medium is insensitive to different values of h^{fm} and to different times.

- (e) Thermal dispersion damps out the numerical oscillation. The thermal dispersion terms, included in the model in the temperature equations, are proportional to the intrinsic fluid velocities. In the radial flow case, the high velocities (especially for the fractures) near the injection point greatly increase the dispersion contribution. The dispersion, together with the conduction, is responsible for the spreading of the front and the damping of numerical oscillations. Numerical oscillation (undershoot) in the temperature spatial distributions is noted mainly in the porous-medium front at earlier time on the low-temperature side of the front away from the point source. At early time, the fracture front spreads out quickly. Later in time the fracture front spreads very little over its central portion, while the porous-medium front moves closer to the fracture front and the two fronts converge.
- (f) The anisotropy of the medium results in different rates of front propagation along the principal axes of the permeability. The full capacity of the numerical code is used to solve the fluid flow equation and the temperature equations for an anisotropic case with principal permeability ratio of 25:5:1. The qualitative changes in the front movements and distortions are similar to those noted in the isotropic case.

VI. SUMMARY

This model is intended for the study of fluid flow and, particularly, the temperature fields in a double-porosity model of a fractured rock mass. The temperature equations for the fractures and for the porous-medium blocks are coupled by a heat transfer term $\pm h^{fm}(T^f - T^m)$. The coefficient h^{fm} is mainly determined by the heat conduction from the porous-medium blocks to the fractures. The temperature equations are also coupled to a combined flow equation through the viscosity and density variation with temperature in the flow equation and through velocity-dependent convective and dispersive terms in the temperature equations.

The coupled equations are solved by a three-dimensional finite-element code using hermite basis functions for improving continuity of spatial gradients.

The results of modeling a linear flow system and a divergent flow system with hot water injection indicate the important effect heat transfer between the fractures and the porous medium has upon the changes of the temperature front movements and upon the spreading of the fronts.

The model in its current version is used mainly for the study of temperature effects due to hot water injection. Extension can be made for applications to thermally induced fluid flow movement and nonisothermal well testing analysis.

GW THERM

GW THERM (Ground Water flow with THERMal gradients) is an integrated finite-difference program for two-dimensional, nonisothermal, saturated flow in porous medium. The regional flow patterns around a repository in crystalline rocks have been studied. The code has been used with another thermal stress code. The model, GW THERM, is described in Runchal and others (1979), Runchal and Maini (1980), Dames and Moore (1978), Hardy and Hocking (1978).

I. GOVERNING EQUATIONS

In this model there are two coupled equations: one pressure equation and one temperature equation. In terms of the hydraulic head $h = P/\rho_o^w g + z$, the pressure equation is

$$S_s \frac{\partial h}{\partial t} - \nabla \cdot \left(\bar{K}_F \frac{\mu_o}{\mu} \right) \cdot \left[\nabla h + \left(\frac{\rho^w}{\rho_o} - 1 \right) \hat{z} \right] = q_F,$$

and the corresponding Darcy velocity is

$$\bar{q} = - \left(\bar{K}_F \frac{\mu_o}{\mu} \right) \cdot \left[\nabla h + \left(\frac{\rho^w}{\rho_o} - 1 \right) \hat{z} \right].$$

S_s is the specific storage coefficient. \bar{K}_F is the hydraulic conductivity $\bar{k} \rho_o^w g / \mu_o$ at reference temperature T_o . The viscosity ratio μ_o / μ and the density ratio ρ^w / ρ_o^w couple the pressure field with the temperature field. Boussinesq's approximation has been used in the pressure equation. The effects of density variation are retained only in the buoyancy term to account for the imbalance of gravitational force $-\rho^w g \hat{z}$.

The temperature equation is written as

$$C_H^m \frac{\partial T}{\partial t} + V \cdot (C_H^w \vec{q}T - K_T \nabla T) = Q_H,$$

where C_H^m , C_H^w are the heat capacity per unit volume of the porous medium (rock matrix and pore water) and of water, respectively. The quantity within the parentheses is the combined convective and conductive flux. The convective term is usually expressed as $C_H^w \vec{q} \cdot \nabla T$ instead of $\nabla \cdot C_H^w \vec{q} T$. In finite differencing the temperature equation, the convective term requires first-order treatment.

Trace Element Equation

In this model, the Darcy velocity is also used in the calculation of the mass concentration of a trace element. The trace-element equation is similar to the temperature equation, with retardation of the velocity, diffusion of the concentration, and exponential decay of the trace element taken into account.

II. NUMERICAL SOLUTIONS

Spatial Finite Difference

For the node indexed by i, j for a two-dimensional grid system in x, z - or r, z -coordinates, the spatial gradient of the flux of the form $\partial \vec{F} / \partial x$ is approximated by $(F_{i+1/2, j} - F_{i-1/2, j}) / (x_{i+1/2} - x_{i-1/2})$, where the interface points $i \pm 1/2$ are the midpoints between i and $i \pm 1$. For the thermal conductive flux, the term $K_T \partial T / \partial x$ in the temperature equation, the interface value at $i+1/2, j$ is approximated by $K_{i+1/2, j} (T_{i+1, j} - T_{i, j}) / (x_{i+1} - x_i)$. The arithmetic mean $K_{i+1/2, j} = (K_{i+1, j} + K_{i, j}) / 2$ is used for the interface conductivity as well as

for other coefficients. The hydraulic term in the pressure equation is similarly treated. For the convective flux $C_H^W q_x T$, the interface value is approximated by

$$T_{i+1,j} = \begin{cases} (T_{i+1,j} + T_{i,j})/2, & \text{if } q_x < K_T/0.5(x_{i+1} - x_i)/C_H^W \\ T_{i,j}, & \text{otherwise.} \end{cases}$$

The two approximations correspond to the central weighting and the upstream weighting, respectively. This step change approximation for the treatment of the convective term is used to minimize the numerical oscillation associated with central weighting for large q_x and the numerical dispersion associated with upstream weighting for small q_x .

The final finite-difference equations corresponding to the governing differential equations are written in integrated finite-difference form by multiplying the equations by the volume element of the block, which is the region enclosed by the lines perpendicular to the coordinate axes and passing through the points $i\pm 1/2, j$ and $i, j\pm 1/2$.

Alternating-Direction-Implicit Scheme

In this model, the solutions in time use the alternating-direction implicit procedure. In this scheme the time stepping from t to $t+\Delta t$ is obtained in two half-steps. In the first half-step from t to $t+\Delta t/2$, only the x (or r) components of the spatial differential operators are advanced in time to $t+\Delta t/2$ and the z -components are evaluated at the old time t . By this procedure, the unknown nodal value of the variable at i, j is algebraically related only to the unknown values at $i\pm 1, j$. The algebraic difference equations can be solved

by the tridiagonal matrix algorithm. With the solutions obtained for $t+\Delta t/2$, one can then perform the second half-step from $t+\Delta t/2$ to $t+\Delta t$ in a similar manner, except that the z-components are advanced in time to $t+\Delta t$ instead.

In this model the same time step is used for the solutions of both the pressure equation and the temperature equation. In each half-time step $\Delta t/2$, the pressure field is first solved, the Darcy velocity determined, and then the temperature (and/or concentration) field is solved. Within one time step, there is no iteration between the pressure solution and the temperature solution to update the viscosity and density.

Stream Lines and Particle Tracks

The Darcy velocity \bar{q} and the particle velocity $\bar{v} = \bar{q}/\phi$ are calculated at the block boundaries from nodal pressure values. These velocities are for the calculation of the stream functions and the particle tracks. For steady-state flow, the stream lines, i.e., lines of constant stream function, are the fluid paths or flow lines. The difference between values of the stream function at two points is representative of the volumetric flow between the two points of flow. For the evaluation of stream functions, the velocity field is assumed to be quasi-steady so that the corresponding stream function can be defined. The stream function is calculated by integrating the horizontal component of the velocity along the vertical coordinate and the vertical component along the horizontal coordinate.

The particle track calculation is carried out at the end of each full time step, using the velocity field averaged over the time step. The velocity

at the current particle position is evaluated by linear interpolation from the block boundary values. To calculate the new particle position, the full time step Δt is divided into five subintervals, with the end points of the subintervals at $0.5\Delta x/v_x$, $0.5\Delta z/v_z$, $\Delta x/v_x$, $\Delta z/v_z$, and Δt . This subdivision allows that at least two particle positions are calculated inside every grid block lying across the particle track.

III. COMPUTER CODE

Documentation

The code was developed by Dames and Moore in FORTRAN IV on the CDC 6600. The user's manual with a sample problem is in a company report by Runchal and others (1979). Most input data are read in free format. The free format structure uses words at the beginning of each input data card to identify the property. The numerical value of that property following the key word may be in integer, real, or exponential format and may be located quite freely on the card. The data are stored in common blocks.

Spatial Grid

A two-dimensional, nonuniform grid in either x, z -coordinates or r, z -coordinates is used in this model. The program logic assumes that horizontal x (or r) and vertical z values, which may be positive or negative, algebraically increase with an increase in the corresponding index values.

Material Properties

The material properties can vary in space with different blocks. For the fluid flow, the input data are the specific storage S_s and the components of

hydraulic conductivity \bar{K}_F . The porosity ϕ is also required for the fluid particle velocity calculation. For temperature, the data are thermal conductivity K_T and volumetric heat capacities C_H^m and C_H^w . For calculating tracer element concentration, the retardation factor, diffusion coefficient, and radioactive decay constant are needed.

Fluid Properties

The viscosity ratio of water in the pressure equation is calculated by $\mu/\mu_0 = \exp(B/T - B/T_0)$, where T is in absolute units, T_0 is a reference temperature, and $B = 1436^\circ\text{K}$. The density of water is $\rho = \rho_0 [(T_c - T)/(T_c - T_0)]^\alpha$ where the critical temperature $T_c = 647.3^\circ\text{K}$ and $\alpha = 0.2$. T_0 and the default values of B , T_c , and α can be changed in the input.

Sources and Sinks

The heat source strength can be calculated from a decaying power curve with up to seven components of exponential functions. Heat and fluid input associated with the thermal source can be defined over the grid.

Initial Conditions

Pressure, Darcy velocity, temperature, and trace element concentration can be specified over the grid at the initial time and at the restarting time.

Boundary Conditions

Values of pressure, Darcy velocity components, temperature, and trace concentration can be specified.

Time Steps

The mass and energy balance can be calculated for each time step. The time step is allowed to change in a geometric ratio up to a specified maximum value.

Output

The paths of one or more groups of particles released from user-specified times and positions can be calculated. Several graphic output options are available. The time-history printer plots of pressure, velocity, temperature, and concentration at ten specified points are generated at run termination. Arrays of these solutions, and other material and water properties, can be output as printer plot at specified time-step printing intervals. Contour, vector, stream function, and particle track plots can be generated by a supplemental program SPLOT.

IV. VALIDATIONS

Several numerical solutions have been compared with analytic solutions. There has also been one test calculation for hot water storage. A brief list of the test cases is given below.

Steady-State Solutions

- (a) Uniform Velocity Field: Velocity is calculated for a linear pressure profile.
- (b) Density Variation: The velocity field is calculated for a spatially varying fluid density.

- (c) Linear Temperature Distribution: The temperature distribution between two boundaries is calculated for a case with zero net fluid flow across the boundaries.
- (d) Temperature Distribution in a Uniform Velocity Field: The temperature between two boundaries is calculated for a case with a uniform velocity field across the boundaries.
- (e) Fluid in Rotation: The temperature distribution in a fluid in a state of uniform rotation is calculated within a square excluding the axis of rotation.
- (f) Steady Cylindrical Distribution: The temperature distribution between two radii is calculated.

Transient Solutions

- (a) Exponential Hydraulic Conductivity: The velocity field with time-dependent hydraulic conductivity is calculated.
- (b) Concentration Decay: The exponential decay in concentration is calculated for a radioactive trace element.

Hot Water Storage

Hot-water storage in an aquifer has been modeled. In this simulation, hot water is injected for the first 90 days into a confined aquifer and then pumped out at the same rate for another 90 days. The temperature in the well and the temperature in the aquifer after 90 days and 180 days have been compared with the results by Tsang and others (1977).

V. APPLICATIONS

This model has been applied to the calculation of regional flow around a repository in a generic study in granite, basalt, and shale (Dames and Moore 1978; Runchal and Maini 1980); and in a parametric design study in basalt (Hardy and Hocking 1978; Hardy and others 1979). These calculations are summarized.

Convective Movements

The code has been used in two modes. In the simple mode, only the thermally induced fluid flow field is calculated with this code, and the temperature field is calculated separately by heat conduction calculations (e.g., the use of TRUMP or HEATING, Science Applications, Inc., 1978). The streamlines corresponding to the quasi-steady velocities are plotted to represent the flow patterns. In the coupled mode, the fluid flow field and the temperature field are both calculated. The particle track plots are used to follow the movement of water. The regional and long-term thermal effect on the groundwater movement has the following general features.

- (a) The maximum upward flow occurs between 1000 and 5000 years for a repository 400 - 600 m deep in the generic studies. The upward flow through the repository is largely controlled by the thermal loading and is insensitive to the regional hydraulic gradient, local variations in hydrologic properties, or boundary conditions.
- (b) The flow pattern at the maximum thermal influence is characterized by a large convection cell with upward buoyancy flow through the repository and downward recirculation flow around the repository. In the presence

of a regional hydraulic gradient from recharge zone to discharge zone, the convective pattern is more prominent on the discharge side of the repository than on the recharge side. The shape of the convective cell also depends on the hydraulic conductivities. An overall increase in vertical conductivity tends to stretch the thermal convection patterns in the vertical direction and leads to stronger vertical flows.

- (c) The presence of a vertical fault through the discharge side of the repository promotes the channeling of the downward recirculation flow. A significant increase in the upward velocity is mentioned in the generic studies. Because the fault is located on the discharge side, the channeling of flow through the fault does not change the flow pattern significantly. A fault on the recharge side may lead to significant change in the flow pattern.
- (d) Larger horizontal flows, resulting either from larger horizontal hydraulic conductivities or a larger regional hydraulic gradient, tend to shrink both the convection cells and the influence of thermal buoyancy. A particle entering a very permeable layer, either near surface or at depth, will travel horizontally for a long distance.

Fluid Flow and Thermal Stress

This thermal flow code has been used in tandem with a thermal stress code in the regional repository study in basalt. Some results have been presented mainly to demonstrate the capability. The calculation has the following steps:

- (i) changes in the temperature field induce changes in stress;
- (ii) stress opens or closes the aperture of a fracture;

- (iii) permeability and porosity of the fracture network in the rock are related to the deformation of single fractures; and
- (iv) modified values of these hydraulic properties are used in the continuation of fluid flow and heat transfer calculations until significant change in temperature warrants the return to step (i).

Some of the features in these calculation steps will be briefly outlined.

- (a) After a number of time steps in the thermal and flow calculations, the changes in the temperature field are input to a finite-element, nonlinear, thermally induced stress program DAMSWEL (Williams and others 1979). Linear interpolation is used to interface the finite-difference grid and the finite-element mesh (at Gaussian points within the two-dimensional eight-noded isoparametric quadrilaterals).
- (b) The experimental data of Iwai (1976) and the normal stress-deformation relationship of Goodman (1976) are used to determine the fracture deformation from the thermally induced stress change. The shear dilatations are neglected. Iwai has performed normal stress-fracture deformation laboratory tests on single induced fractures in granite, basalt, and marble. The data are fitted with the nonlinear relationship proposed by Goodman:

$$\frac{\Delta V}{V_{mc} - \Delta V} = A \left(\frac{\sigma_N}{\xi} \right)^t.$$

For the calculation, this relation is used to relate the normal deformation (closure) of the fracture ΔV with the normal applied (thermal) stress σ_N . V_{mc} is the maximum possible normal closure; ξ is the seating stress (weight of the upper rock sample in Iwai's experiments) which defines the

initial condition for measuring the deformation; and A and t are empirical constants determined from the experimental data. The values of A and t depend in general on the loading history because the stress-deformation behavior of fractures exhibits hysteresis and permanent deformation under cyclic loading.

- (c) Permeability and porosity changes are related to single-fracture deformations with the cubic law of fracture flow. The rock formation is assumed to contain one vertical and one horizontal fracture set. The porosity change is directly related to the fracture aperture deformation. Assuming laminar flow between the parallel plates, the cubic relationship between fracture aperture and equivalent continuum permeability is used. The dependence of the permeability on normal stress change is given by the following formula (Iwai 1976):

$$\frac{k_N}{k_\xi} = \frac{1}{\left[1 + A \left(\frac{\sigma_n}{\xi} \right)^t \right]^3}$$

where k_N and k_ξ are the permeabilities at stress σ_N and σ_ξ . The new permeability and porosity are used in the thermal and flow calculations.

- (d) The permeability and porosity changes affect mainly the water movement. However, for most cases in regional repository studies, the fluid flow changes do not significantly affect the temperature field, and the time intervals for interlacing the two codes are determined mainly by heat conduction and thermal loading. For near-field studies, the interaction of the fluid flow and thermal stress is stronger. The pressure field, as well as the temperature field, will deform the fractures.

VI. SUMMARY

This code is for modeling thermally induced flow and heat transfer in porous media. The density buoyancy and the temperature variation of viscosity are taken into account, and the storage coefficients of the pressure equation are specified. The numerical solutions on two-dimensional x,z or y,z grids are obtained by the alternating-direction implicit procedures.

The results of modeling thermally induced flow patterns demonstrate the long-term regional impact of buoyancy flow in a repository. The streamline plots and particle track plots are informative.

The procedure for using this code together with the thermal-stress code is of interest. The inelastic deformation of fractures are important to fluid flow movement.

FINI

FINI 520 is a finite-element program for two-dimensional, nonisothermal, saturated flow in porous media. FINI 500 is the isothermal flow version. The model has been used in fluid flow studies for different time periods for a repository in granite. The stress permeability changes have been calculated with another finite-element code. The model FINI is described in Burgess (1977) and Ratigan and others (1977).

I. GOVERNING EQUATIONS

The FINI 520 model has one quasi-steady pressure equation and one transient temperature equation. In terms of the hydraulic head $h = P/\rho^w g + z$, the pressure equation is

$$-\nabla \cdot \left(\bar{\bar{K}}_F \frac{\mu_o}{\mu} \right) \cdot [\nabla h - \beta_T^w (T - T_o) \hat{z}] = q_F.$$

In FINI 500, a transient term is also included. The Darcy velocity is given by

$$\bar{q} = - \left(\bar{\bar{K}}_F \frac{\mu_o}{\mu} \right) \cdot [\nabla h - \beta_T^w (T - T_o) \hat{z}],$$

and the pore velocity is given by $\bar{v} = \bar{q}/\phi$. The temperature T in the buoyancy term $\beta_T^w (T - T_o)$ and the viscosity ratio μ_o/μ are time-dependent. $\bar{\bar{K}}_F$ is the hydraulic conductivity at reference temperature T_o . The equation of state of water density $\rho^w = \rho_o^w - \rho_o^w \beta_T^w (T - T_o)$ has been used. Boussinesq's approximation is assumed. The effects of density variation are retained only in the imbalance of the gravitational buoyancy force.

The temperature equation is written as

$$\rho^m c^m \frac{\partial T}{\partial t} + \phi \rho^w c^w \bar{v} \cdot \nabla T - \nabla \cdot \bar{K}_T \cdot \nabla T = Q_H,$$

ρ^m and c^m are the bulk density and specific heat of the fluid-filled medium, and ρ^w and c^w correspond to the fluid. The volumetric heat source also includes $\rho^w c^w q_F T^b$ for a fluid source at temperature T^b .

The reference temperature T_0 corresponds to the nonbuoyant condition. For the cases with substantial throughflow, T_0 is fixed at the inflow supply temperature. For natural convection problems without inflow, T_0 is calculated in this model as the average temperature in the modeled region.

II. NUMERICAL SOLUTIONS

Finite-Element Method

The model solves the governing equation by the finite-element Galerkin method. Six-node, planar or axisymmetric, quadratic, isoparametric triangles are used to divide the two-dimensional horizontal-vertical plane. The corresponding three-node flux and external film loading lines are used on the boundary. In the isothermal version, FINI 500, six-node quadratic gap (fracture) elements are also included. Each node has two variable values: the pressure head and the temperature. A variable within an element is interpolated in terms of the nodal values by the quadratic basis functions.

The matrix equations relating the nodal values over the modeled domain are obtained by applying calculus of variations to the Galerkin functional. The functional is constructed by integrating the residue of the interpolated

trial solution over the element weighted by the basis functions. For the triangles, seven numerical integration points are used. The flow velocities are calculated on four of these points inside the element. For the lines on the boundary, three integration points are used.

Implicit Treatment and Solution Scheme

In most finite-element models, first-order finite difference is used to approximate the time derivative to relate the nodal values at t to those at $t+\Delta t$. The values associated with its spatial gradient terms can be calculated explicitly at t with $\lambda = 0$, implicitly at $t+\Delta t$ with $\lambda = 1$, or weighted between with $0 < \lambda < 1$, where λ is the implicit interpolation factor. In this model, instead of the finite-difference method, the Galerkin finite-element procedure with a linear basis function from t to $t+\Delta t$ is used for the time derivative. The derived matrix equations are similar to the usual implicit equations with an equivalent $\lambda = 2/3$. The 2/3 implicit weighting is applied to the second-order hydraulic term and thermal conductive term and to the volumetric sources. However, the first-order buoyancy term $\beta_T^W T$ in the pressure equation and the convective term $\bar{v} \cdot \nabla T$ in the temperature equation are treated explicitly.

In this model, the boundary flux can be of the form $\alpha_p (h - h^b)$ and $\alpha_T (T - T^b)$, where α 's are the film transfer coefficients, and h^b and T^b are the ambient boundary head and temperature outside the film. If α is a fixed constant, the corresponding film transfer is treated 2/3 implicitly. If α is a variable, the film transfer is treated explicitly. The film transfer

boundary condition is used in the study of inflow into a repository with back pressure maintained within the repository.

For steady-state runs, an iterative process is used to obtain the solution. The buoyancy term and the convective term lag one iteration behind the conductive terms and the source and boundary flux terms.

The matrix equation is solved by a triangular symmetric decomposition subroutine, followed by forward and backward substitution.

III. COMPUTER CODES

Documentation

The codes FINI 500, 520 were developed by Acres Consulting Services Limited and were initially installed on the GE415 computer. The user's manuals and sample problems appear in company reports (Skiba 1977; Skiba and others 1977). The program is divided into overlay segments to minimize storage requirements. Disc storage of data is used to pass from overlay to overlay.

Spatial Grid

For each node, the code reads in vertical and horizontal coordinates and the assigned nodal number. Each element is assigned an element type, a material type, and the corner nodal numbers. The element can be planar or axisymmetric 6-node triangles, 3-node lines, or, in FINI 500, 6-node gaps. The principal axes of hydraulic conductivity and thermal conductivity can be oriented away from the coordinate directions by specifying the angle between the vertical mesh axis and the conductivity axes.

Material Properties

The two principal values of hydraulic conductivity, the porosity, the two principal values of thermal conductivity, the bulk density, and the bulk specific heat are input for each material type.

Fluid Properties

Fluid density, fluid specific heat, and the coefficient of thermal expansion are read in together with the material properties. Viscosity is calculated according to the relation used by Mercer and others (1975):

$$\frac{1}{\mu} = (5380 + 3800A - 260A^3) \text{ kg/m/sec,}$$

where $A = (T - 150)/100$, $0^\circ\text{C} \leq T \leq 300^\circ\text{C}$.

Initial Conditions

The pressure head and temperature can be specified at nodes either at the initial time or at restarting times. Disc storage is usually used between stop and restart.

Source and Sinks; Boundary Conditions

For both pressure head and temperature field, the specified nodal values, nodal source, element area source rate, line normal flux, line film transfer coefficients, and ambient value outside the film can be specified. All the values and sources can independently vary linearly over time spans of one to several time steps.

Time Steps

For each time span in the analysis, the number and size of time steps are specified. Since the pressure head equation is quasi-steady, there is only one time step, that for the temperature transient.

Output

Pore velocities are computed and written to disc for each time step in the time span. Meshes, isotherms, equipotentials of pressure head, and pore velocities are plotted with a follow-up program FINI 511, using the data on the disc files produced by the main code.

IV. VALIDATIONS

- (a) Temperature Front Movement: The linear temperature front movement in a constant flow field is calculated to test the convective-dispersive temperature equations.
- (b) Steady Potential with Sinusoidal Potential Boundary: A two-dimensional distribution of potential is calculated to test the steady-state pressure equation.

V. APPLICATIONS

The codes have been used in the study of groundwater movements around a repository in the Precambrian bedrock of Sweden for the Swedish Nuclear Fuel Safety Project (Karnbranslesakerhet or KBS). The results of calculations with these fluid flow codes and with other stress codes (RSI of RE/SPEC) are in the KBS technical reports 54:1-6 (Stille and others 1977; Ratigan 1977a,b; Burgess 1977; Ratigan and others 1977; Lindblom and others 1977; see also Burgess and

others 1979). Currently, this code is being used in the Atomic Energy of Canada, Limited (AECL) project for a granite repository. Some of the results from the KBS studies are qualitatively summarized.

Initial Groundwater Flow

- (a) The effect of an inclined high-conductivity gap embedded in a regional flow field has been modeled. If the gap exits near the seashore, regional flow from the inland mountain recharge areas to the coastal discharge areas will be channeled by the gap and result in high discharge velocity. If the gap dips in the other way, the flow is attracted to greater depth.
- (b) If the hydraulic conductivity decreases with depth, a quiescent zone with slow groundwater flow is developed at depth. This feature is more evident when the horizontal conductivity is greater than the vertical conductivity. The empirical conductivity depth relationship used in some cases is

$$\log K_F(\text{m/sec}) = -5.57 + 0.362(\log D) - 0.978(\log D)^2 + 0.167(\log D)^3,$$

where D is the depth in meters.

Excavation and Thermal Effects

- (a) The excavation of tunnels for a repository results in an increased compressive stress which is tangential to the tunnel wall and which in turn closes the fractures and decreases the hydraulic conductivity normal to the wall. The normal stresses are zero at the tunnel periphery and steeply increase to in-situ values over short distance into the rock, resulting in high tangential conductivity near the tunnel. The

conductivity-normal stress relationship used in the calculations is the same as the conductivity-depth relationship (above) with $\log D$ substituted by $\log \sigma_N / \sigma_o$, where σ_o is the overburden stress from 1 m of rock.

- (b) After emplacement of the waste, the perturbations due to thermal stresses and viscosity changes on hydraulic conductivity are less significant than the perturbations due to construction of the repository. Inflows to the repository, with or without the development of back pressure in the repository, have been modeled.
- (c) In the absence of regional groundwater flow, the waste heat induces convection cells around the repository. With regional cross flow, the cells are suppressed and become minor perturbations to the natural flow patterns.

Long-Term Effects After Thermal Impact

- (a) The flow patterns around a repository have been modeled for a zone with a local groundwater table peak above the repository and bounded by vertical boundaries representing major fault zones. The flow is generally downward from the surface to the repository and laterally toward the vertical boundaries. For the case where horizontal hydraulic conductivity decreases with depth and with small vertical conductivity, the local groundwater table variation has little effect on the flow patterns at depth.
- (b) If the repository rooms are left void or loosely backfilled with original material, the flux and pore velocities in the repository area differ considerably from the natural conditions before the repository existed. The travel times from the repository to the vertical boundaries have been calculated for different cases.

VI. SUMMARY

This code is designed for modeling thermally induced flow in porous media. The time-dependent temperature equation is combined with the quasi-steady pressure equation to account for the density-buoyancy effect. The numerical solutions on vertical-horizontal planar or axisymmetric grids are obtained by the finite-element method.

The results of modeling steady flow patterns before and after the thermal impact of a repository, and the results of thermally induced flow patterns, are of interest. The effects of permeability-depth dependence, regional groundwater flow, stress-permeability perturbations, and the presence of fault gaps have been studied for a hypothetical repository in granite.

CFEST-FE3DGW

The model FE3DGW (Finite Element 3-Dimensional Ground-Water) is for isothermal, saturated flow in multilayered porous media. The model has been used in simulations of regional groundwater basins and in repository generic studies. CFEST (Coupled Flow, Energy, and Solute Transport) is an extension of FE3DGW to include heat and solute transport. FE3DGW is described in Gupta and others (1979) and Cole and Gupta (1979). The early versions of FE3DGW are described in Gupta and others (1975) and Gupta and Tanji (1976, 1977). CFEST is described in Gupta and others (1980).

I. GOVERNING EQUATIONS

In the FE3DGW model, the governing equation is

$$(\phi \beta_h^w + \beta_h^p) \frac{\partial h}{\partial t} = \nabla \cdot \bar{K}_F \cdot \nabla h - q_F'$$

The variable is the hydraulic head

$$h = \int_{P_0}^P \frac{dP}{\rho^w(P)g} + z.$$

The Darcy velocity is

$$\bar{q} = - \bar{K}_F \cdot \nabla h.$$

The responses of fluid density ρ^w and porosity ϕ to head changes are assumed to be elastic, with constant compressibilities β_h^w and β_h^p , respectively. \bar{K}_F is the hydraulic conductivity, and q_F' is the strength of the withdrawal rate. The hydraulic head h is also used as the variable of the fluid flow equation in CFEST.

In CFEST, the fluid flow equation is derived from the conservation of total fluid mass:

$$\frac{\partial}{\partial t} (\phi \rho^W) = \nabla \cdot \rho^W \bar{K}_F \cdot \nabla h - Q_F^i.$$

The transfer of energy by conduction and convection is given by

$$\frac{\partial}{\partial t} [\phi \rho^W U + (1-\phi) \rho^R c^R T] = -\nabla \cdot (\rho^W c^W q_T) + \nabla \cdot \bar{K}_T \cdot \nabla T - Q_F^i c^W T^b - Q_L^i.$$

Solute transport by diffusion (dispersion) and convection is given by

$$\frac{\partial}{\partial t} (\phi \rho^W C) = -\nabla \cdot (\rho^W q_C) + \nabla \cdot \bar{K}_C \cdot \nabla C - Q_F^i C^b.$$

Q_F^i ($= -Q_F$) is the fluid mass sink/source and Q_L^i is the rate of heat loss. The injection of fluid at temperature T^b and concentration C^b are included.

The final forms of the equations are derived by substituting the following relations:

$$\psi(h_p) = \psi_0 [1 + \beta_h^P (h_p - h_{p_0})],$$

$$\rho^W(C, T, h_p) = \rho_0^W + \rho_0^W \beta_h^W (h_p - h_{p_0}) - \rho_0^W \beta_T^W (T - T_0) + [\rho^W(1, T_0, h_{p_0}) - \rho_0^W] C,$$

$$U(T) = U_0 + c^W (T - T_0),$$

where h_p is the pressure head component of h and β_h^W is the pressure head compressibility. The thermal expansivity β_T^W and the specific heat c^W characterize the linear responses of the fluid density ρ^W and the internal energy U to the temperature change. The change of ρ^W is also proportional to the concentration C . With the substitution of these relationships, the fluid flow, energy transfer, and solute transport equations are expressed in terms of the head h , temperature T , and concentration (mass fraction of solute) C .

II. NUMERICAL SOLUTIONS

Spatial Finite-Element Method

The models reduce the governing partial differential equations to systems of algebraic equations through the use of the Galerkin finite-element method. The three-dimensional space is decomposed into finite-element domains with eight corners. FE3DGW uses mixed order isoparametric elements. The corner nodes can be joined either by straight lines with linear basis functions or by curved lines with quadratic or cubic basis functions. In CFEST, only linear elements are used. A variable within an element is interpolated in terms of the values of the variable at the nodes on the element boundary. The trial solution is substituted into the differential equations. The space-differential operators operate on the basis functions used for interpolation. The residue of the trial solution is integrated over the element weighted by the basis functions. The integration is carried out using 2, 3, or 5 Gaussian integration points in each dimension.

Implicit Time Difference

First-order finite difference is adapted to approximate the time derivative. The backward-differencing implicit scheme is used to construct the implicit matrix equation relating the unknown nodal values at $t+\Delta t$ to those at t . The intermediate results of the products involving basis functions at Gaussian points are computed and stored on disc until the coefficient matrix is altered due to a change in time step or hydraulic properties.

Iterative Scheme

In CFEST, the three equations are solved in a cyclic-uncoupled solution scheme in which the dependent variables (head h , temperature T , concentration C) are treated as unknowns only when their respective equations (fluid flow, energy transfer, solute transport) are being solved. Thus when the fluid flow equation is solved for head, the temperature and concentration are assumed known from the most current estimates of these variables in the evaluation of nonlinear coefficients and loading functions. The energy transfer and solute transport equations are treated similarly. The cyclic sequence of the solution proceeds from fluid flow to energy and finally to solute transport. If successive iterations of this cycle fail to yield compatible results, the cycle is repeated.

Matrix Solver

The solution of the matrix equation uses an in-core, compressed-matrix solver (Gupta and Tanji 1977). The nonzero coefficients are stored in one array and their corresponding column indices in another array. First the code locates the element with the largest absolute magnitude in the row containing a minimum number of nonzero elements. Then the elements in this row are normalized with this element. The row is used to eliminate the elements in remaining rows. The elimination loop proceeds until an upper-triangular system is obtained. The triangular equation is solved by the backward substitution procedure.

III. COMPUTER CODE

Documentation

FE3DGW is written in FORTRAN IV and was initially developed on Burroughs B6700 at the University of California, Davis. The code also has been run on CDC 7600 at Lawrence Berkeley Laboratory and at Rockwell. The current development of FE3DGW and CFEST is mainly using the PDP 11/45 at Battelle Pacific Northwest Laboratory for the Assessment of Effectiveness of Geologic Isolation Systems Program. The user's manual and code listing of FE3DGW are in the reports by Gupta and others (1975, 1980). The following subsections are limited to FE3DGW. The documentation of CFEST is underway.

Spatial Grid

The grid design for a multilayer system proceeds in two steps: subdivision of the surface region, and well-log descriptions at each surface node. The surface of the modeled region is divided into two-dimensional mixed-order elements with linear, quadratic, or cubic order sides. Major features on underground hydrogeologic units, together with surface-water boundaries and well locations, are identified by discrete nodes on the surface. For each surface node, the vertical log detail for the layers is provided by the user. For the well nodes, the well data itself can be used. For other nodes, interpolation from contour maps of thickness or elevation of each formation can be used to provide the information. With the log description, the code generates the three-dimensional grid within the program.

Material Properties

The principal directions of hydraulic conductivity are assumed to be oriented parallel to the $x, y,$ and z coordinates. For each material, the values of hydraulic conductivities can be (i) read-in constants; (ii) calculated with $\bar{k}_p^w g/\mu$ using read-in \bar{k} , density and viscosity from temperature-depth relationships for salt-free water; or (iii) estimated from read-in salt concentration at all the nodes. The hydraulic conductivities can change from element to element. Other properties for each material are the porosity, the reference pressure at which the porosity is measured, and the compressibility of the porous medium.

Fluid Properties

The compressibility of fluid is read in together with the material properties.

Sources and Sinks

Nodal and/or element sources and sinks can be specified.

Initial Conditions

The head values for all the nodes can be specified at the initial time or at restarting time.

Boundary Conditions

Prescribed head (water level) and prescribed flux (vertical infiltration) boundaries can be specified.

Time Steps

The number and the size of time steps are specified by the user.

Output

The grid values, contour maps, and three-dimensional plots of input data and calculated results can be generated with supporting programs. PLOTEL plots the location of each node, two-dimensional surface elements, and the vertical log at each location. GRIDIT, GRIDIN, or GRIDH are used to produce contour and three-dimensional plotting of top elevation, thickness, and head of each material after the finite-element grid values are interpolated to regular grid locations. Interactive graphic terminals can be used.

IV. VALIDATIONS

FE3DGW:

- (a) Continuous Line Source: The Theis solution (1935) for radial flow to a well pumping at a constant rate in an infinite, anisotropic aquifer.
- (b) Potential Distribution: Regional potential distribution in an aquifer system having an initial uniform gradient, large remote radial boundary, and cavernous cylindrical reservoirs.
- (c) Drawdown Distribution: Drawdown in the vicinity of a steady well draining an elastic strata.

CFEST:

- (a) Temperature Front Movement: The linear temperature front movement in a constant flow field is calculated to test the convective-dispersive equation.
- (b) Flux Boundary Problem.
- (c) Radial Transport Solution.

V. APPLICATIONS

The model has been used in the simulation of multiaquifer systems at Sutter Basin, California, and Long Island, New York. The code is currently being used in simulations for waste repositories in salt and in hard rock.

- (a) Sutter Basin: A vertical fault zone in the basin is the channel through which the connate water rises from depth. The heads are higher near the fault zone at the bottom of a near-surface nonmarine deposit.
- (b) Long Island: A three-dimensional, wedge-shaped model was constructed for the ground-water system with complex stratification. The model was used to evaluate alternative schemes for water supply and waste-water treatment. Historical data were used for steady-state and transient validations.
- (c) Salt Repository: A hypothetical repository is assumed to be located 600 m deep in a generic salt formation below a nonprolific aquifer. The vertical ground-water potentials were calculated to examine the consequences of the accidental release of radionuclides from the repository to a river on the ground surface 5 km from the center of the repository.
- (d) Hard Rock Repository: The flow paths and travel times to the surface lakes and rivers from a reference repository in granite were determined. In the simulation of flow through the fractures, the major fracture zones are represented by discrete elements with two additional thin elements to provide a transition zone from fractures to rock matrix.
- (e) Hard Rock Mine: The pumping requirements and the zone of influence of drawdown were studied for a mine in a Precambrian crystalline rock site.

VI. SUMMARY

FE3DGW was developed for modeling large ground-water basins. It is being extended, in the new CFEST, to model the hydraulic head, temperature, and concentration.

The numerical solutions in three-dimensional space were obtained by the Galerkin finite-element method with mixed-order basis functions. The mesh is generated using subdivision of the surface region and the well-log descriptions at surface nodes. Graphic output capability and interactive modeling applications are emphasized in the recent development.

FE3DGW has been used in the simulations of two large ground-water basin studies. Detailed documentation of the recent applications in generic and site-specific repository studies will be of interest.

SWIFT

SWIFT (Sandia Waste Isolation Flow and Transport) is a finite-difference program for three-dimensional fluid flow, heat, and inert solute transfer in saturated porous medium. The model has been used in radioactive waste transport calculations for salt and other formations. Different versions of the model are described in Dillon and others (1978), U. S. Department of Energy (1979), and in the report of the program SWIP (U. S. Geological Survey 1976).

I. GOVERNING EQUATIONS

In this model there are three coupled equations: one pressure equation, one temperature equation, and one concentration equation. The set of governing equations is formally written in the form of conservation equations. The continuity equation for the fluid flow is:

$$\frac{\partial}{\partial t} (\phi \rho^w) = \nabla \cdot \left[\frac{\rho^w \bar{k}}{\mu} \cdot (VP - \rho^w gVD) \right] - Q'_F.$$

The energy balance between the change of internal energy U and the net flux of enthalpy H is described by:

$$\begin{aligned} \frac{\partial}{\partial t} [\phi \rho^w U + (1 - \phi) \rho^r c^r T] &= \\ &= \nabla \cdot \left[\frac{\rho^w H \bar{k}}{\mu} \cdot (VP - \rho^w gVD) \right] + \nabla \cdot (\bar{k}_T + \bar{k}_{TD}) \cdot \nabla T - Q'_H - Q'_F H - Q'_L. \end{aligned}$$

The material balance equation for a solute (e.g., salt) is:

$$\frac{\partial}{\partial t} (\phi \rho^w C) = \nabla \cdot \left[\frac{\rho^w C \bar{k}}{\mu} \cdot (VP - \rho^w gVD) \right] + \nabla \cdot \rho^w (K_C + \bar{k}_{CD}) \cdot \nabla C - Q'_F C.$$

The material equation is needed for cases in which additional fluid movement is induced by the density difference between concentrated salt water and fresh water. The explicit gradient expression of the Darcy velocity,

$$\bar{q} = -\frac{\bar{k}}{\mu}(\nabla P - \rho^W g \nabla D) ; \quad D = \text{depth},$$

has been used for the flux terms in all three governing equations. The Q'_F ($= -Q_F$) in the equations is the fluid mass withdrawal rate. In the temperature equation, Q'_H is the heat withdrawal rate and Q'_L is the heat loss to surrounding strata.

The governing equations can be explicitly expressed in terms of pressure P , temperature T , and concentration C by relating the density ρ^W , porosity ϕ , internal energy U , and enthalpy H to these variables. With the initial pressure and temperature at some point in the aquifer as the reference conditions:

$$\phi = \phi_0 [1 + \beta_P^D (P - P_0)],$$

$$\rho = \rho_0 [1 + \beta_P^W (P - P_0) - \beta_T^W (T - T_0)] + a_C C,$$

$$U = U_0 + c^W (T - T_0),$$

$$H = H_0 + c^W (T - T_0).$$

In this code, a modeled domain is characterized by a constant compressibility of pores β_P^D for response of the porosity to pressure change, and by a constant compressibility β_P^W , a constant thermal expansivity β_T^W , and a constant $a_C = (\partial\rho/\partial C)_{C=0}$ for the responses of fluid density to pressure,

temperature, and concentration changes. The fluid energies are linear functions of temperature. c^w in the equations for U and H is the heat capacity of water.

Dispersion

In addition to the thermal conductivity $\bar{\bar{K}}_T$ and molecular diffusivity K_C , the energy equation and the solute equation also include the hydrodynamic dispersivities $\bar{\bar{K}}_{TD}$ and $\bar{\bar{K}}_{CD}$, respectively, in the diffusion terms. The hydrodynamic dispersion is described as a linear function of fluid velocity. In terms of either the longitudinal dispersivity α_ℓ or the transverse dispersivity α_t , the hydrodynamic dispersivities can be expressed as

$$K_{TD} = \phi \alpha v,$$

$$K_{CD} = \frac{\phi \alpha v}{C_H^w},$$

where v is fluid particle velocity $v = q/\phi$ and C_H^w is the heat capacity per unit volume of fluid. When $\alpha_\ell \neq \alpha_t$, the temperature (or concentration) gradient in one direction will induce dispersive flux in another direction and cross-derivative terms (such as $\partial(K_{xy} \partial T / \partial y) / \partial x$) will appear in the energy and solute equations. The use of the same dispersivity α in the energy and solute equation expresses the concept that the microscopic heterogeneity in convective flow creates the same dispersive effect in temperature as it does in a material concentration. It should be noted that the product $\phi \alpha$ has often been used by other models for the term "dispersivity."

Radioactive Trace Element Transport

After solving the coupled equations describing the fluid flow, energy, and an inert solute transfer, the flow solution is then used to solve radioactive/trace component equations at the end of each time step. The equation for a radioactive component is similar to the concentration equation of the inert solute with additional sink/source terms for the radioactive decay and generation from other nuclides. The equation of a parent nuclide is solved before those of its daughters. A decay chain with a parent decay into several daughters can be treated by specifying the branching fractions.

II. NUMERICAL SOLUTIONS

Spatial Difference

The governing equations are solved by a finite-difference method for a grid in three-dimensional x, y, z -coordinates or in two-dimensional r, z -coordinates. For the node i, j, k for the x, y, z grid, the finite-difference approximation for the x differential term of $\nabla \cdot (\rho^w k / \mu) \cdot \nabla P$ is of the form

$$U_{i+1/2, j, k} (P_{i+1, j, k} - P_{i, j, k}) - U_{i-1/2, j, k} (P_{i, j, k} - P_{i-1, j, k})$$

The interface transmissibility (conductance) at the interface $i+1/2, j, k$, midway between i, j, k and $i+1, j, k$, is evaluated as

$$U_{i+1/2, j, k} = \frac{2\Delta y_j \Delta z_k}{\left(\frac{\Delta x}{k_x}\right)_i + \left(\frac{\Delta x}{k_x}\right)_{i+1}} \left(\frac{\rho^w}{\mu}\right)_{i+1/2, j, k}$$

with harmonic mean for k_x and arithmetic mean for ρ^w / μ . The block lengths are $\Delta y_j = y_{j+1/2} - y_{j-1/2}$, and Δz and Δx are similarly defined.

In finite differencing, the differential equation has been multiplied by the volume of the nodal block $\Delta x_i \Delta y_j \Delta z_k$ to express it in the integrated finite-difference form. If the principal axes of the permeability are oriented along the coordinate system, the finite-difference approximation of $\nabla \cdot (\rho \bar{k} / \mu) \cdot \nabla P$ is the sum of the x, y, and z differences. Other conductive terms $\nabla \cdot \bar{K}_T \cdot \nabla T$ and $\nabla \cdot \rho \bar{K}_C \cdot \nabla C$ in the energy and solute equations can be similarly approximated. For the dispersive terms $\nabla \cdot \bar{K}_{TD} \cdot \nabla T$ and $\nabla \cdot \rho \bar{K}_{CD} \cdot \nabla C$ with anisotropic dispersivities, additional difference terms for the cross-derivatives will be included. If a simulation is performed in a two-dimensional r, z grid, the term $2\Delta y_j \Delta z_k / (\Delta x_i + \Delta x_{i+1})$ in the difference equation becomes $2\pi \Delta z_k / \ln(r_{i+1}/r_i)$.

The first-order convective terms $\nabla \cdot \rho \bar{W} \bar{H} \bar{q}$ and $\nabla \cdot \rho \bar{W} \bar{C} \bar{q}$ in the energy and solute equations can be approximated either with central weighting or with upstream weighting. The central weighting (central difference in space) has no second-order space-truncation error. However, the solution may oscillate artificially if block sizes exceed certain limitations. On the other hand, the upstream weighting (backward difference in space) introduces a space-truncation error which is virtually identical to the physical diffusion. To limit the numerical oscillation or numerical diffusion, the grid size is limited in either weighting method. The instability consideration and numerical diffusivity also depend on the choice of schemes for finite differencing in time (Lantz 1971).

Semi-Implicit Time Difference

First-order finite difference in time is used. A time derivative $\partial\chi/\partial t$ is approximated by $\delta\chi/\delta t$ with $\delta\chi \equiv \chi_{t+\Delta t} - \chi_t$. It is noted from this definition that $\delta(\chi^1 \chi^2) = \chi_{t+\Delta t}^1 \delta\chi^2 + \chi_t^2 \delta\chi^1$. With this rule, $\partial(\phi\rho^W)/\partial t$, $\partial(\phi\rho^W U)/\partial t$ and $\partial(\phi\rho^W C)/\partial t$ of the governing equations can be approximated. The $\delta\phi$, $\delta\rho^W$, δU can further be expressed in terms of δP , δT , and δC :

$$\delta\phi = \phi_o \beta_P^P \delta P, \quad \delta\rho^W = \rho_o^W \beta_P^W \delta P - \rho_o^W \beta_T^W \delta T + a_C \delta C, \quad \text{and } \delta U = c^W \delta T.$$

Then the system of three difference equations is algebraically reduced to a triangular system with only δP appearing in one equation, δP , δT in the next, and all of δP , δT , δC on the third equation (Gaussian elimination). This allows the sequential solution of δP , δT , and δC within an outer iteration (Coats and others 1974).

The dependent variables, P , T , and C , appearing in the space derivatives can be the values at the new time $t+\Delta t$ (backward-differencing implicit scheme) or be the averages of the values at the new time and the values at the old time t (central-differencing Crank-Nicholson scheme). In this model, the pressure equation is treated implicitly, but the temperature equation and the concentration equation can be solved by either scheme. Within one time step, δP , δT , and δC are solved iteratively. One iteration consists of solving δP , updating the ρ^W and ϕ ; solving δT , updating ρ^W ; and solving δC , updating ρ^W . The iteration stops when the convergence criteria are satisfied. A tolerance of 0.001 is used on the maximum fractional change in density $(\Delta\rho_T^W + \Delta\rho_C^W)/\rho_o^W$ over the grid block in one iteration. The temperature or concentration

calculation can be bypassed if the corresponding fractional change in density is less than 0.0005.

The interface transmissibilities corresponding to the terms $\rho^w \bar{k}/\mu$, $\rho^w \bar{hk}/\mu$, $(\bar{K}_T + \bar{K}_{TD})$, and $\rho^w (\bar{K}_C + \bar{K}_{CD})$ are treated explicitly; i.e., the values of these coefficients at old time t are used in solving P , T , C of the new time $t+\Delta t$. At the end of the iteration, enthalpy H is calculated by $H_{t+\Delta t} + c^w \Delta T$, viscosity is calculated with the new temperature and concentration, and the new flow velocity field is determined. During the iterations, cross-derivative terms originating from the anisotropic dispersive heat and solute fluxes (off-diagonal terms) can be treated either by lagging one iteration behind the diagonal terms or by approximating the cross terms by adding the off-diagonal dispersivities to the diagonal component along the x,y,z -coordinate axis.

Solution Schemes

Within one iteration, the solution of implicit equations for δp or δT or δC is obtained either by the reduced-band-width, direct-solution method ADGAUSS (Price and Coats 1974) or by the two-line successive-overrelaxation iterative method L2SOR. ADGAUSS uses an alternating diagonal ordering scheme for the nodal numbering to reduce the storage requirement and computing time in the direct Gaussian elimination procedure. For the example of the two-dimensional grid (i,j) , the ordering is $(1,1)$, $(1,3)$, $(2,2)$, $(3,1)$, ..., $(1,2)$, $(2,1)$, ... This ordering scheme partitions the matrix into upper and lower halves, with the upper half in upper triangular form. The elimination proceeds half a matrix at a time. For small problems, ADGAUSS may be more efficient than

iterative methods. For large problems, iterative methods with smaller storage requirements are recommended. The L2SOR is a block iterative method. The block matrix to be inverted each iteration has five diagonals. The acceleration factor for the overrelaxation is determined by the spectral radius of the matrix, which is estimated by the successive-overrelaxation iterative technique.

III. COMPUTER CODES

Documentation

The code was developed by Intera Environmental Consultants, Inc. The user's manual for the model version developed for the U. S. Nuclear Regulatory Commission is in Dillon and others (1978). The code is available from National Technical Information Service (NTIS) and has been adapted to a number of computer systems at Sandia, Rockwell, U. S. Geological Survey, Lawrence Livermore Laboratory, and others.

Spatial Grid

The partition of space can be either a three-dimensional, rectangular, nonuniform grid in x,y,z -coordinates, or a two-dimensional grid in r,z -coordinates. For the x,y,z grid, dip angles in x - and y -directions can be specified. For the r,z grid, the blocks can be divided on an equal $\Delta \log r$ basis or each block center can be specified. The Δz can be nonuniform.

Material Properties

The hydraulic conductivities, the porosity, and the rock heat capacity can vary spatially in different regions of grid blocks. Other required input data are the thermal conductivities \bar{K}_T along x,y,z-directions, the molecular diffusivity K_C , the dispersivities α_L, α_T , the rock density ρ^R , and pore compressibility β_P^P . The x,y,z-transmissibilities, as well as the depth and thickness of the blocks, can also be modified independently within a region. If trace element concentration calculations are performed, the half-life, the adsorption coefficient for each rock type, the daughter-parent relationship, and the branching fractions for each component are required data (from cards or disk).

Fluid Properties

For injection of waste fluid into natural aquifers, both the density of fresh fluid ($C = 0$) and the density of contaminated fluid ($C = 1$) at the same reference temperature and pressure are required input parameters. Other parameters are the compressibility β_P^W , the thermal expansivity β_T^W , and the heat capacity c^W . The water density is calculated as a linear function of pressure, temperature, and concentration. At least one value of viscosity is required at $C = 0$ and one at $C = 1$. One should enter as much data (in tables) as is available for viscosity versus temperature and/or concentration. The basic viscosity dependence on temperature and concentration is

$$\mu = \mu_0(C) \exp[B(C)(1/T - 1/T_0)].$$

If only one viscosity point is available, the program obtains the values at other temperatures according to the generalized chart of Lewis and Squire.

Sources and Sinks

A wellbore model can be used with the reservoir model if the surface conditions instead of the bottom-hole conditions at aquifer formation layers are specified. The wellbore model solves iteratively a steady-state energy balance equation, with heat loss to formations surrounding the wellbore taken into account. The pressure and temperature differences between the wellbore and the grid block center are calculated with steady radial flow equations. The specified discharge rate of fluid, heat, and contaminant can be allocated between different aquifer layers either on the basis of mobility k/μ alone or with mobility and specified or calculated pressure drop between the wellbore and the grid block. The rate can be expressed explicitly or semi-implicitly with $(dq/dP)\delta P$ added to the explicit flow rate.

Initial Conditions

The reference pressure, temperature, and concentrations in the aquifer, and the natural flow velocity along the x-direction, can be specified at $t = 0$. The problem restarts by reading intermediate results and data from tapes or disk. The table of initial temperature versus depth can be input.

Boundary Conditions

The heat loss to layers of overburden and underburden can be calculated by specifying the thickness, thermal conductivity, and heat capacity of the layers. The aquifer outer boundary can be maintained at constant pressure, temperature, and concentration. The influx can be steady or time-dependent. The time-dependent flux can be determined by the pressure change in the peripheral blocks, or it can be calculated with the dimensionless pressure-time

curves for treating the finite model region surrounded by an aquifer of infinite or finite extent (Carter and Tracy 1960; Van Everdingen and Hurst 1949).

Time Steps

The size of the time step can be controlled by specifying the desired maximum changes in pressure, temperature, and concentration. The number of time steps and the number of iterations per time step can be specified. Material and heat balances are calculated.

Output

The cumulative production/injection in the aquifer and in the wellbores, the heat loss, and the fluxes across the boundaries can be output at specified time-step printing intervals. Contour maps of pressure, temperature, and concentration on the x,y- or r,z-plane can be output on the printer. The calculated values and the measured data of pressure, temperature, and concentration in each layer in a well or on the surface can be plotted as a function of time. The Darcy velocity and other material and fluid properties can be output at a given time.

IV. VALIDATIONS

Since SWIFT was developed from SWIP, the comparison of numerical results with analytic solutions for SWIP will be briefly summarized below. Other tests for the wellbore model, heat loss calculation, aquifer time-dependent boundary condition, and fluid property calculation can be found in the SWIP report (U. S. Geological Survey 1976), and the test for radioactive trace

component transport can be found in the SWIFT report (Dillon and others 1978).

The documented tests for the aquifer model are:

- (a) Continuous Point Source: The Theis problem with production and shut-in is solved either with 16 nodes in radial coordinates or with 11 x 11 or 13 x 13 nodes in rectangular coordinates.
- (b) Temperature (concentration) Front Movement: Both linear and radial front movement in a given flow field are calculated to test the convective dispersive equation.
- (c) Salt Water Intrusion: The linear concentration profiles are calculated for comparison with the steady-state profile.

V. APPLICATIONS

The model was developed by Intera for Sandia Laboratories supported by the U.S. Nuclear Regulatory Commission (NRC). A different version of the model was used in the Draft Environmental Impact Statement (U.S. Department of Energy 1979) for the Waste Isolation Pilot Plant (WIPP) in bedded salt. The code is being used for work with the Atomic Energy of Canada on a granite repository; with Elsam Arbejde, Denmark, on a salt dome repository; with the Institute fur Tieflagerung, GSF, West Germany, on ASSE mine waste disposal; with the Technical University of Berlin for Gorleben salt dome site; and with Rockwell for Basalt Waste Isolation Plant (S. B. Pahwa, personal communication 1980).

WIPP

The modeling for WIPP is mainly the analysis of different scenarios for radionuclide transport through hydraulic communication between the repositories

(700 m and 900 m deep) and near-surface aquifers and/or a deep aquifer. The deep aquifer has greater hydraulic potential and provides a driving force for upward flow into the shallow aquifers. The temperature rise in the two aquifers is small (Pahwa and Wayland 1978).

Conduction and Convection

A hypothetical repository in salt, sandwiched between sandstone formations above and below, has been simulated with or without regional groundwater flow. The groundwater flow lowers the temperature in the repository, distorts the temperature contours, and essentially diminishes the temperature rise in the aquifers, especially in the more permeable overlying sandstone formations.

VI. SUMMARY

This code models fluid flow, heat transfer, and solute transport of an inert dissolved material. The concentration calculations for radioactive trace components in decay chains have been implemented in the program.

The numerical solutions on a three-dimensional x,y,z grid, or a two-dimensional r,z grid, are obtained by a finite-difference method. Different choices of weighting schemes in space, differencing schemes in time, and matrix solvers are available. Automatic time step control is used. The code can handle various aquifer boundary conditions and wellbore treatments but it requires a thorough familiarity with detailed procedures for setting up data and a full understanding of the model's capabilities.

The code has been used for geosphere transport analyses and in salt repository far-field studies. Recent applications of this code to different formations will be of interest for repository studies.

MODEL OF COATS

This is a finite-difference program for three-dimensional, two-phase, steam-water flow and heat transfer. The model is designed for geothermal well and reservoir simulations. Two-phase well testing analysis and natural convection in fractured matrix geothermal reservoirs have been modeled. The model is described in Coats (1977), Coats and others (1977), and Aydelotte (1980).

I. GOVERNING EQUATIONS

In this model, the primary equations of mass balance and energy balance are expressed in terms of pressure and temperature for single-phase regions containing either liquid water or superheated steam, and in terms of pressure and saturation if both liquid phase l and vapor phase v are presented. In two-phase mixtures, the temperature is determined by the pressure, $T = T_S(P)$, where the subscript S denotes the saturated condition.

The mass balance equation for combined liquid and vapor phases is:

$$\frac{\partial}{\partial t}(\psi S^l \rho^l + \phi S^v \rho^v) = \nabla \cdot \left[\frac{\bar{k}k_r^l \rho^l}{\mu^l} \cdot (\nabla P^l - \rho^l g \nabla D) + \frac{\bar{k}k_r^v \rho^v}{\mu^v} \cdot (\nabla P^v - \rho^v g \nabla D) \right] - Q'_F.$$

In this model, the capillary pressure difference between vapor phase pressure P^v and the liquid phase pressure P^l can be taken into account. The liquid phase pressure P^l is expressed as $P^l = P^v - P_c$, where the capillary pressure P_c is a single-valued function of vapor saturation S^v . The saturations are related by $S^l + S^v = 1$.

The energy balance between the change of internal energy U and the net flux of enthalpy H is:

$$\frac{\partial}{\partial t} [\phi S^{\ell} \rho^{\ell} U^{\ell} + \phi S^v \rho^v U^v + (1 - \phi) \rho^r c^r T]$$

$$= V. \left[\frac{\bar{k}^{\ell} \rho^{\ell}}{\mu^{\ell}} H^{\ell} \cdot (VP^{\ell} - \rho^{\ell} g VD) + \frac{\bar{k}^v \rho^v}{\mu^v} H^v \cdot (VP^v - \rho^v g VD) \right] + V. (\bar{K}_T \cdot VT) - Q_H' - Q_L'$$

The potential and kinetic energy terms are ignored.

Thermodynamic and Constitutive Relationships

For the evaluation of the fluid properties, the model uses steam tables for two-phase mixtures and formulas for single-phase regions. The Steam Tables of Keenan and others (1969) are used for the internal energy U^{ℓ} , U^v and the density ρ^{ℓ} , ρ^v as single-valued functions of temperature in the two-phase region. For the single-phase liquid water, U^{ℓ} is assumed to be a single-valued function of temperature. The density is calculated as

$$\rho^{\ell} \cong \rho_S^{\ell}(T) \left[1 + \rho_S^{\ell}(T) s(T) (P - P_S(T)) \right],$$

$\rho_S^{\ell}(T) s(T)$ is the compressibility, with the temperature dependence of the function $s(T)$ determined from a tabulation of specific volume in the Steam Tables.

For the steam phase:

$$\rho^v \cong \rho_S^v(P^v) \frac{T_S(P^v) + 460^{\circ}\text{F}}{T + 460^{\circ}\text{F}},$$

$$U^v \cong U_S^v(P^v) + c^v [T - T_S(P^v)],$$

where the heat capacity c^v is constant. The viscosities μ^{ℓ} and μ^v are evaluated as single-valued functions of temperature equal to their respective

saturated values. The enthalpies H^α are related to the internal energies U^α and the densities ρ^α by the definitions $H^\alpha = U^\alpha + P^V/\rho^\alpha$. The model uses P^V as the pressure variable in all relationships.

In addition to the fluid properties, the following material properties also depend on the variables P^V, T or P^V, S^V . The porosity is calculated from

$$\phi = \phi_0 \left[1 + \beta_P^P (P^V - P_0^V) \right],$$

where the constant β_P^P is the compressibility of pores. The reservoir thermal conductivity K_T and the rock heat capacity $\rho^R c^R$ are independent of the pressure, temperature, and saturation.

The relative permeability k_r^L or k_r^V at a given saturation and pressure is calculated from the formula $k_r = k_{rr} \bar{S}^n$, where \bar{S} is the normalized saturation, n is a pressure-dependent exponent, and k_{rr} is the value of relative permeability at $\bar{S} = 1$. One example of the relative permeability curves used in the model is:

$$k_r^L = \left[\frac{S^L - 0.2}{1 - 0.2} \right]^2 \quad \text{and} \quad k_r^V = 0.5 \left[\frac{S^V}{1 - 0.2} \right]^2,$$

with an irreducible liquid saturation $S_r^L = 0.2$, and with $k_{rr}^V = 0.5$,
 $n^L = n^V = 2$.

II. NUMERICAL SOLUTIONS

Finite-Difference Method

The governing equations are solved by the finite-difference method for a grid in three-dimensional x, y, z -coordinates or r, θ, z -coordinates. The variables (P^V , T , or S^V) at grid blocks i, j, k are algebraically connected to the adjacent blocks $i \pm 1, j, k$, $i, j \pm 1, k$, and $i, j, k \pm 1$. For the interblock transmissibilities (conductances) relating the fluxes with the variable gradient, the interblock values of ρ/μ and ρg are evaluated as arithmetic means of their values in the two grid blocks. The relative permeabilities k_r and enthalpies H are assigned the upstream value (i.e., the value at the grid block having the higher fluid potential).

Fully Implicit Scheme

Time is discretized fully implicitly as a first-order finite difference. With the transmissibilities and source terms depending on the variables, the implicit system of equations is nonlinear. The set of equations is linearized using a residual formulation with Newton-Raphson iteration. If the set of two nonlinear, implicit, finite-difference equations of the nodal unknown vector \bar{x} for each grid block is expressed as $\bar{F}(\bar{x}) = 0$, the Newton-Raphson procedure approximates the nonlinear equations at each iteration with a Taylor series expansion about the old solution:

$$\bar{F}(\bar{x}) \approx \bar{F}(\bar{x}^k) + \sum_i \left(\frac{\partial \bar{F}}{\partial x_i} \right)^k \left(x_i^{k+1} - x_i^k \right).$$

The partial derivatives are evaluated at the latest iterative value x_i^k . Each

nodal value of the variables is successively updated until the maximum absolute changes of pressure, temperature, or saturation over all grid blocks are less than the desired convergent criteria. Generally the tolerances of 0.1 psia, 1°F, and 1% saturation are used.

Matrix Solver

The linearized system of equations is solved by the reduced-bandwidth direct method (Price and Coats 1974). The solver uses an alternating-diagonal ordering scheme for the nodal numbering to reduce the storage requirement and computing time in the Gaussian elimination procedure. The nodal points are numbered in the order 1st, 3rd, 5th, ..., followed by 2nd, 4th, ..., diagonal planes for a three-dimensional grid and diagonal lines for a two-dimensional grid. The ordering scheme partitions the matrix into upper and lower halves, with the upper half in upper-triangular form. Elimination of the upper half creates a lower matrix of limited bandwidth.

III. COMPUTER CODE

Documentation

The code was developed by K. H. Coats of Intercomp for geothermal applications. The following code characteristics are deduced from the sample applications documented in Coats (1977), Coats and others (1977), and Aydellotte (1980).

Spatial Grid

The grid can include blocks of zero porosity representing hard rock with no pressure calculated, and blocks with unity porosity representing either fractures or wellbores. The model applies to one-, two-, and three-dimensional grids in either x, y, z rectangular coordinates or r, θ, z cylindrical coordinates. For the radial grid the geometric spacing $r_i = \alpha r_{i-1}$ with $\alpha = (r_e/r_w)^{1/N}$ for N radial increments from the wellbore radius r_w to the external radius r_e , has been used in some problems.

Material Properties

The permeability, porosity, reservoir and overburden thermal conductivity and heat capacity, rock compressibility and relative permeability equations or data are the material properties listed in the problems modeled by this code.

Fluid Properties

The fluid properties are evaluated with steam tables or formulas in the code. No data corresponding to the fluid properties are listed in the tables describing the modeled problems.

Sources and Sinks

The model includes heat source/sink terms necessary in simulating free convection cells. For the production of two-phase flow, the model can either incorporate the wellbore in the reservoir grid system or use a wellbore model.

The implicit well treatment with small wellbore blocks can automatically model the crossflow between open layers and reverse flow from wellbore to

some of the layers in a producing well. However the small volumes of the wellbore blocks may limit the time step sizes.

The two-phase flow, vertically within or laterally from the column of wellbore grid blocks, also requires special modeling treatment. At normal rates of geothermal wells, turbulent flow is fully developed in the wellbore and the no-slip two-phase flow is a good assumption. The no-slip condition with volumetric fractional flow equaling saturation can be modeled either with vertical pipe flow correlations or with the usual Darcy flow expressions modified by pseudo relative permeabilities.

To avoid the small volume blocks, a wellbore model can be incorporated in the code to allow the use of grid blocks of large areal dimensions enclosing the wells. The implicit treatment of a well produced at a given target flow rate from a multilayer reservoir is very complicated when the wellbore pressure is not low enough to allow free-flowing and to sustain deliverability. The difficulty is due to the interdependence of the flow rates of different layers through the wellbore pressure drop. A significant simplification results if the wellbore pressure differences between layers are treated explicitly. The various implicit and semi-implicit treatments of the wellbore model were discussed in detail by Coats (1977).

Initial Conditions

The initial pressure, temperature, and saturation are listed in the tables describing the modeled problems.

Boundary Conditions

The heat transfer above and below the reservoir are included in the modeling of natural convection in the permeable formation. The lateral water influx from an aquifer extending beyond the reservoir grid is treated with the Carter and Tracy (1960) or simpler approximations.

Time Steps

Large time steps are used in most of the modeled problems to demonstrate the stability of the implicit formulation.

Output

Pressure, temperature, saturation, quality, and flow rates in different directions are tabulated or plotted to present the modeling results.

IV. VALIDATIONS

The code was developed with the hope that the implicit model formulation would give unconditional stability with no time-step restrictions other than that imposed by time-truncation error. A number of problems have been run to evaluate the stability and time-step tolerance and to compare the numerical results with analytic solutions, other numerical solutions, and laboratory experiments. The problems are listed below.

Analytic and Numerical Solutions

- (a) Well Deliverability: A radial problem with nine grid blocks was used to compare the calculated deliverability with an analytic solution that was derived for two-phase flow, taking into account the water flashing and steam expansion between the wellbore and the external boundary (Coats 1977).

- (b) Drawdown Test: The wellbore pressure drop was matched with the solution of a two-phase drawdown test presented by Garg (1978) for a well produced at a constant mass rate from an initially undersaturated reservoir.
- (c) Saturation Distribution: The calculated saturation values over a two-dimensional grid were compared with the numerical results of Toronyi and Farouq Ali (1977) and Thomas and Pierson (1978) for a reservoir production problem for a vapor-dominated reservoir.

Implicit Stability and Throughput Ratio

- (a) One-dimensional Test: The radial problem with nine grid blocks was also used to test the stability and time-truncation error. The implicit stability is expressed in terms of a throughput ratio which is defined as the total volume of flow passing through the grid block in one time step divided by the volume of the block. The throughput ratio is proportional to the maximum stable time step. For an acceptable time-truncation error with time step of 1000 days, the throughput ratio with implicit treatment is two orders of magnitude larger than that with semi-implicit treatment.
- (b) Two-dimensional Test: Two-dimensional problems are generally better indicators of model competence than one-dimensional tests. A five-layer, cylindrical grid with wellbore included was used to achieve a stable throughput ratio the order of 10^8 and producing cell steam saturation changes of 80 to 100%. The corresponding semi-implicit treatment can achieve only a 20,000 throughput ratio and 3 to 10% saturation changes. It is of interest to note that this five-layer problem has employed a pseudo straight-line capillary pressure curve corresponding to the thickness of one layer.

(c) **Partial Perforation Effect:** The two-dimensional grid was also used to study the effects of partial perforation with well completion (open) interval shorter than the reservoir thickness. The heat and mass productions are sensitive to the location of the open interval. Only the portion of the reservoir formation above the open interval can be effectively drained.

Stanford Bench Experiment

The code was used to simulate a two-phase depletion experiment in a synthetic porous-medium core (Kruger and Ramey 1974). To supplement the experimental information, hypothetical relative permeability curves and steady-state boundary heat-transfer equations (Thomas and Pierson 1978) were used to yield good agreement between the calculated and the measured profiles of pressure and temperature. The saturation profile was also compared with the results of the implicit pressure-explicit saturation model of Thomas and Pierson. The discrepancies between the results may be due to the difference in the implicit-explicit evaluation of saturation-dependent coefficients.

V. APPLICATIONS

The model has been applied to fractured-matrix reservoir performance, well test analysis, extraction of energy from hot dry rock, and natural convection problems in fractured geothermal reservoirs.

Fractured-Matrix Reservoir Performance

A cylindrical discrete fracture model was simulated. In this model, the set of horizontal fractures sandwiched between matrix blocks was connected by

a cylindrical vertical fracture. A large permeability was used for the fracture to render viscous forces negligible relative to the gravitational forces. A zero capillary pressure was used for the fractures and a linear relation for the porous medium. Because of the discontinuity in the capillary pressure between blocks and horizontal fractures, there was poor recovery of water from the matrix blocks. The horizontal fracture rapidly approached 100% steam. The water drained vertically downward from the blocks into the horizontal fracture instead of moving laterally into the vertical fracture. In comparison with porous-medium results, the two-phase transition zone is lower for the fracture-porous simulation.

Well Test Analysis

- (a) Fracture Effects: Simulation of a single-phase flow, pressure drawdown test in a tight formation with horizontal fractures showed upward concave curvature in the semilog plots of pressure drawdown versus time. This departure from the linear curve is due to the vertical flow from the matrix into the fractures. The degree of the upward curvature increases with decreasing matrix permeability and decreasing horizontal fracture spacing.
- (b) Two-phase Effects: The large apparent compressibility due to the steam phase and the heat transfer between the flowing fluid and the rock are two problems encountered in two-phase well-testing solutions. This geothermal reservoir and wellbore model was used in the history-matching simulations for test wells in Cerro Prieto, Mexico, and in Hawaii. The

difficulties associated with simulation of the fracture effects in two-phase geothermal well tests were studied (Aydelotte 1980).

Hot Dry Rock

A 5 x 5 x 5 grid was used to simulate a vertical fracture imbedded in a hot dry rock formation. In the 5 x 5 fracture plane, cold water was injected in the lower portion and hot water was produced in the upper corner. The fracture permeability was varied over a number of runs from 10 darcies to 800,000 darcies. The fracture permeability had no effect on calculated energy recovery and producing well temperature but had remarkable effect on the flow patterns. Circulatory convection cells do not appear for permeabilities less than 100,000 darcies but complex flow distribution and laterally alternating temperature changes exist for 800,000 darcies.

Convection in Fractured-Matrix Formation

The convective cell patterns were studied for a vertical fracture of rectangular shape imbedded in a hard-rock formation. The heat conduction above and below the permeable fracture were included in the simulations. The temperature profiles and the cell patterns depend on the lateral extent of the fracture and the initial perturbations which trigger the convective motion. For an initially two-phase formation with a superheated steam zone overlying an undersaturated liquid zone, superheated steam circulatory convection did not occur in the simulation. The conduction reduced the superheated temperature to saturation temperature. The steam moved uniformly upward and condensed at the formation top and the liquid moved downward in the saturated steam zone.

VI. SUMMARY

This is an implicit, three-dimensional geothermal model. The model simultaneously solves the pressure and saturation under two-phase conditions and the pressure and temperature for single-phase regions. The capability to accommodate large time steps and small grid blocks is the aim in the development of the highly implicit model. The various implicit and semi-implicit treatments associated with allocation of well rates among the multiple open intervals were studied.

The influence of fractures on two-phase flows requires extensive modeling effort. The applications of the model to reservoir performance, energy recovery, and natural convection in fractured-matrix formations indicate that the flow in the matrix, steam expansion, capillary pressure, and heat conduction in the rock are important factors for the determination of the two-phase flow in fractures.

MODEL OF FAUST-MERCER

This is a finite-difference program for three-dimensional, two-phase, steam-water flow and heat transfer in porous media. The model was developed for geothermal simulations. An areal model has also been developed by vertical integration of the three-dimensional equations and applied to the hydrothermal field at Wairakei, New Zealand. The models are described in Faust and Mercer (1979a,b), Mercer and Faust (1979), and also in Faust (1976), and Faust and Mercer (1975, 1976, 1977a,b).

I. GOVERNING EQUATIONS

In this model, there are two nonlinear partial differential equations formulated in terms of pressure P and enthalpy H. The first equation is based on the mass balance for the liquid phase l and vapor phase v combined:

$$\frac{\partial}{\partial t} (\phi \rho) = \nabla \cdot \left[\frac{\bar{k} k_r^l \rho^l}{\mu^l} \cdot (\nabla P - \rho^l g \nabla D) \right] + \nabla \cdot \left[\frac{\bar{k} k_r^v \rho^v}{\mu^v} \cdot (\nabla P - \rho^v g \nabla D) \right] + Q_F,$$

where ρ is the density of the liquid-vapor mixture, $\rho = S^l \rho^l + S^v \rho^v$, with $S^l + S^v = 1$. In the mass balance equation, the capillary pressure effects are neglected and the Darcy velocities for both phases are expressed in terms of a single fluid pressure P. The second governing equation is based on the energy balance for the liquid, vapor, and rock r:

$$\begin{aligned} \frac{\partial}{\partial t} [\phi \rho H + (1 - \phi) \rho^r H^r] = & \nabla \cdot \left[\frac{\bar{k} k_r^l \rho^l}{\mu^l} H^l \cdot (\nabla P - \rho^l g \nabla D) \right] \\ & + \nabla \cdot \left[\frac{\bar{k} k_r^v \rho^v}{\mu^v} H^v \cdot (\nabla P - \rho^v g \nabla D) \right] + \nabla \cdot \left[K_T \left(\frac{\partial T}{\partial P} \right)_H \nabla P + K_T \left(\frac{\partial T}{\partial H} \right)_P \nabla H \right] + Q_H, \end{aligned}$$

where H is the total enthalpy: $H = (S^l \rho^l H^l + S^v \rho^v H^v) / \rho$. The local thermal equilibrium among the liquid, vapor, and rock is assumed. The lumped conduction-dispersion term is expressed in terms of an isotropic coefficient K_T and the gradients of the temperature $T(P, H)$. In the energy balance equation, the kinetic energy (viscous dissipation), potential energy, and the pressure material derivative from compressible pressure work are neglected.

Areal Model

From the three-dimensional equations, an areal model has been derived by partial integration in the vertical dimension over the thickness of the reservoir. The basic assumption is that the reservoir has good vertical communication and that vertical equilibrium between the steam and water is achieved. In the absence of significant capillary pressure, gravity segregation between the vapor and liquid produces a two-phase steam cap with residual water saturation above the liquid water. The governing equations for the areal model are expressed in terms of the vertically averaged pressure and enthalpy. With the assumption that the pressure varies hydrostatically in each phase, the vertically averaged pressure and enthalpy can be algebraically related to the pressure and the elevation of the interface contact. In the model, the interface pressure and elevation, together with the liquid and vapor densities and enthalpies, are calculated from the values of the vertically averaged pressure and enthalpy. The mass and energy leakage to confining beds are taken into account, with additional mass and energy flux terms evaluated at the top and the bottom of the reservoir. The effects of a sloping reservoir with variable thickness are also included. The validity of the assumptions of the areal model can be checked with the three-dimensional model.

Thermodynamic and Constitutive Relationships

The fluid properties of liquid water and steam are calculated from analytic formulas of P and H. The analytic formulas are obtained by least-squares regression applied to data from steam tables (Meyer and others 1968; Keenan and others 1969). The derivatives of the functions are directly obtained from the analytical formulas. The dependence of the fluid properties on the variables is described as follows: The saturated liquid enthalpy H^l and the saturated steam enthalpy H^v are treated as functions of pressure. Temperature is treated as a function of pressure and enthalpy for the liquid water region and for the superheated steam region, and is treated as a function of pressure in the two-phase region. The vapor density ρ^v and the liquid density ρ^l are considered functions of pressure and enthalpy. The liquid water saturation S^l in the two-phase region is

$$S^l = \frac{\rho^v (H^v - H)}{H(\rho^l - \rho^v) - (H^l \rho^l - H^v \rho^v)}, \quad \text{and} \quad S^v = 1 - S^l.$$

The viscosities are considered functions of temperature. The relative permeabilities are:

$$k_r^l = \bar{S}^4 \quad \text{and} \quad k_r^v = (1 - \bar{S})^2 (1 - \bar{S}^2),$$

where \bar{S} is the normalized saturation: $\bar{S} = (S^l - S_r^l) / (1 - S_r^l - S_r^v)$ for a formation with residual saturations S_r^l and S_r^v (Corey and others 1956).

For the formation property, the porosity is calculated from

$$\psi = \psi_0 [1 + \beta_P^P (P - P_0)],$$

where β_p^P is the constant intergranular vertical compressibility coefficient.

The rock enthalpy is a linear function of temperature, given by: $H^R = c^R T$.

II. NUMERICAL SOLUTIONS

Finite-Difference Method

The finite-difference method is used for solving the unknowns on a rectangular, irregular grid. For the evaluation of the interblock transmissibilities (conductances), the density, the viscosity, and the derivatives $(\partial T / \partial p)_H$ and $(\partial T / \partial H)_p$ are evaluated as arithmetic averages of values in adjacent blocks. Relative permeabilities and enthalpies are assigned the upstream value. Permeability, thermal conductivity, and other space-dependent terms are determined as harmonic means of the values in adjacent blocks.

Implicit Schemes

The system of $2N$ nonlinear implicit finite-difference equations over N grid blocks is solved by Newton-Raphson iteration in the three-dimensional version of this model. Each grid block is connected to six adjacent blocks, so that each equation has a maximum of 14 unknowns (7 pressure, 7 enthalpy). The set of nonlinear equations is approximated with a Taylor's series expansion about an assumed solution. The linearized matrix equation is solved and iterated. Convergence is checked by calculating global mass and energy balance errors and comparing them to specified criteria. The three-dimensional model is fully implicit with Newton-Raphson iteration applied to the transmissibility, accumulation, and source terms. For the two-dimensional areal model,

only accumulation and source terms are treated implicitly; the transmissibility terms are treated by the Picard iteration scheme to update each iteration.

Matrix Solvers

For the three-dimensional model, the nonsymmetric, linearized matrix equations are solved by the slice-successive overrelaxation iterative method imbedded in the Newton-Raphson iteration. Each slice or matrix block corresponds to a vertical cross section of the grid. Each slice has 10 unknowns per equation, and the matrix is solved directly by Gaussian Doolittle elimination. The remaining 4 (out of 14) coefficients are treated iteratively. The bandwidth of the matrix equation for each slice is approximately four times the number of horizontal layers. A convergence criterion of 0.001 is used on the maximum fractional changes in pressure ($\Delta P^k / \Delta P^1$) and in enthalpy ($\Delta H^k / \Delta H^1$) over the grid block in the k th iteration. An overrelaxation parameter between 1.0 to 1.7 is normally used.

For the two-dimensional areal model, the use of Newton-Raphson iteration on only the accumulation and source terms allows the reduction of the $2N \times 2N$ matrix equation to two $N \times N$ symmetric matrix equations after Gaussian elimination to triangularize the 2×2 nodal equations (Coats and others 1974). The symmetric equations are solved using Gaussian Doolittle decomposition with the alternating direction D4 ordering scheme (Price and Coats 1974).

III. COMPUTER CODES

Documentation

The model was developed at the U. S. Geological Survey by C. Faust and J. Mercer. The user's manual and the Fortran IV code listing of a two-dimensional version is in Faust and Mercer (1977b). The following code characteristics are mainly for the two-dimensional areal model.

Spatial Grid

The reservoir can be simulated either with a nonuniform x,y,z grid or an areal x,y grid. For the two-dimensional model, the reservoir thickness can be specified individually for each areal block.

Material Properties

For the two-dimensional model, the x and y permeability and the initial porosity can be specified for each areal block. Other material properties required for the simulation are the reservoir thermal conductivity, confining bed thermal conductivity, rock specific heat, rock density, and reservoir compressibility.

Fluid Properties

The fluid properties are evaluated with regression formulas which are based on steam table data for a temperature range of 10°C to 300°C. No data corresponding to the fluid properties are required in the input. For the two-dimensional model, the fluid properties are assumed either to be uniform with depth or to be determined with the vertical equilibrium condition.

Sources and Sinks

The strength of fluid source/sink is specified for each well block.

Initial Conditions

Although the unknown dependent variables are pressure and enthalpy, the user can read in either initial pressures and temperatures or initial pressures and enthalpies. If temperatures are read, they are converted in the program to enthalpies. If the initial conditions of the reservoir are two-phase, the enthalpies must be read in.

Boundary Conditions

The loss and gain of heat to the base and cap rock are incorporated into the reservoir model. The one-dimensional, heat-conduction equation is solved at each grid block for each iteration. The confining bed thickness is divided into ten linear elements that double in size with distance from the reservoir boundary. The temperature difference across the small element adjacent to the reservoir is used to compute the heat flux through the cap rock-reservoir boundary. The heat leakage to the base rock is assumed to be equal to the flux computed at the caprock-reservoir boundary.

Time Steps

The size and the maximum number of time steps are specified by the user. The mass and energy balance is computed for each time step.

Output

On a successful run, the pressure values, the enthalpy values, and the mass and energy balance are printed every time step. In addition, the water saturation, temperature, and density can be printed at selected steps.

IV. VALIDATIONS

A number of problems have been simulated to validate the model and to compare different numerical methodologies. The primary objective of many of the simulations was to test the validity of the vertically averaged model.

Water Injection Solution

The temperature profile of the injection front was compared with the analytic solution of Avdonin (1964) for linear, single-phase flow through a confined aquifer. Both midpoint weighting and upstream weighting of enthalpy were used in the simulation. The midpoint weighting approximates the temperature front well but exhibits oscillations behind the front. Upstream weighting smears the front out by numerical diffusion and does not exhibit oscillations. It was also noted that the finite-element results with linear, quadratic, and hermite cubic basis functions all exhibit oscillations and produce a steeper front than the finite-difference method for this problem.

Stanford Bench Experiment

Experimental data obtained in a synthetic sandstone core (Kruger and Ramey 1974) were used to verify the models for two-phase problems. In this verification an implicit, one-dimensional finite-element model is used with upstream weighting for the relative permeabilities and diagonal lumping for the accumulation terms. To accommodate the boundary conditions not available in the experimental data, a steady-state conductive heat flux was assumed at the sides of the core (Garg and others 1975b). The calculated temperature profiles were shown to be insensitive to variations in the form of the relative permeability functions.

Justification of Vertically Integrated Model

- (a) Vertical Equilibrium Assumption: A hypothetical one-dimensional model with 8 grid blocks was compared with cross section models of either 8 x 6 or 8 x 10 grid blocks. For the one-dimensional grid, the thermodynamic properties were assumed to be either vertically uniform or in vertical equilibrium. It was shown that the vertical-equilibrium model reproduced the two-dimensional results better than the uniform model in simulating the two-phase pressure depletion and saturation change. The vertical-equilibrium model works best for reservoirs less than 500 m thick with relatively high permeability and a thin steam cap. It can also be applied to problems with vertical to horizontal anisotropy when permeability is sufficiently high.
- (b) Reservoir Depletion: An 8 x 10 areal model for a heterogeneous reservoir of variable thickness was compared with an 8 x 10 x 5 three-dimensional model. The two models gave similar results showing rapid pressure decline and two-phase development for a reservoir without mass recharge or reinjection.

V. APPLICATIONS

The areal model was applied to the hydrothermal field at Wairakei, New Zealand. Steady-state behavior was reproduced and used as initial conditions for a history match from 1953 to 1973 and a prediction from 1974 to 2000.

There are 150 blocks covering an area of approximately 74.5 km². The reservoir model of variable thickness is overlain and underlain by leaky

confining beds. The steady-state simulation matched the observed direction and rate of natural discharge by adjusting the pressure distribution and the vertical permeability through the upper confining bed. The temperature distributions are considered known from downhole temperature measurements. The steady-state modeling results indicated that portions of the reservoir had a steam cap prior to exploitation.

To simulate the transient effects of exploitation, well discharge rates were incorporated into the model. In addition to the steady-state leakage, transient recharge through underlying confining beds was required to match the slow decline of pressure data. The remaining discrepancy between the location of the observed and the computed maximum pressure drop was attributed to possible reduction in the permeability associated with formation compaction or subsidence. As production progressed, the modeling results indicated that the steam cap increased both areally and in thickness. When the contact between the two-phase zone and the single-phase (liquid) zone dropped below the open intervals of the wells, a mixture of steam and water was removed from the reservoir and reservoir temperature dropped.

The predictive simulation indicated that the field could maintain production rates to the year 2000. The main uncertainties in the prediction are due to the lack of information on the leakage properties of the confining beds.

VI. SUMMARY

This is a geothermal reservoir model formulated in terms of fluid pressure and enthalpy for two-phase flow in porous media. A three-dimensional version has been used mainly to validate the assumptions used in the vertically integrated, two-dimensional, areal model. The areal model assumes vertical equilibrium (gravity segregation) between steam and water and can be applied to reservoirs with good vertical communication.

The applications of the areal model to the hydrothermal field at Wairakei, New Zealand, indicate that the two-phase pressure decline in a geothermal reservoir is sensitive to the recharges through the confining beds. Although the computed results match observed data over 20 years, the long-range predictions over 20 years may be unreliable due to the lack of information on the leakage properties of the confining beds.

MUSHRM

MUSHRM (Multi-Species Hydrothermal Reservoir Model) is a finite-difference program for the three-dimensional, two-phase, multicomponent fluid flow and heat transfer in porous media. Different equation-of-state packages have been developed to evaluate the effects of salt precipitation around geothermal wells and of methane evolution in geopressured reservoirs. The model has been applied to history matching of the Wairakei geothermal field and generic studies in other geothermal systems. Interactions between the fluid mass-energy transport and the rock stress-strain response have been studied. The model is described in a number of papers (Brownell and others 1977; Garg and Pritchett 1977, 1978; Garg and others 1975b; Pritchett and Garg 1978; Pritchett and others 1976a, 1980; Riney and others 1977), and in the series of reports on geohydrological environmental effects of geothermal production (Pritchett and others 1975, 1976b; Pritchett 1978) and on geopressured geothermal reservoir simulation (Garg and others 1977b, 1978, Pritchett and others 1979).

I. GOVERNING EQUATIONS

In this model, the governing equations are formulated in terms of fluid density ρ and internal energy U . The mass balance equation is:

$$\frac{\partial}{\partial t} (\phi \rho) = -\nabla \cdot (\phi S^l \rho^l \bar{v}^l + \phi S^v \rho^v \bar{v}^v) + Q_F.$$

The general form of the energy balance equation in this model is:

$$\begin{aligned} \frac{\partial}{\partial t} [\phi \rho U + (1-\phi) \rho^r U^r] = & -\nabla \cdot (\phi S^l \rho^l U^l \bar{v}^l + \phi S^v \rho^v U^v \bar{v}^v) + V \cdot K_T \nabla T + Q_H \\ & -\nabla \cdot (\phi S^l \rho^l \bar{v}^l P + \phi S^v \rho^v \bar{v}^v P) + \phi (S^l \rho^l \bar{v}^l + S^v \rho^v \bar{v}^v) \cdot \bar{g}. \end{aligned}$$

The last two terms on the right-hand side of the energy equation are the pressure-work/viscous-dissipation contributions to the energy balance, which are usually neglected. Local thermal equilibrium is assumed among the liquid phase l , vapor phase v , and rock r . The capillary pressure difference between liquid and vapor is neglected. Darcy's equation for the fluid phases is

$$\phi S_{\alpha}^{\alpha} = - \frac{\bar{k}_r^{\alpha}}{\mu^{\alpha}} (\nabla p - \rho^{\alpha} g), \quad \alpha = l, v.$$

In the equations, the phase densities ρ^l , ρ^v , and internal energies U^l , U^v can be expressed in terms of the mixture density ρ , internal energy U , steam quality Q^v (mass fraction of vapor), and vapor saturation S^v (volume fraction of vapor) as:

$$\rho^l = \rho \left(\frac{1 - Q^v}{1 - S^v} \right); \quad \rho^v = \rho \frac{Q^v}{S^v};$$

$$U^l = U - Q^v U_{\text{vap}}; \quad U^v = U + (1 - Q^v) U_{\text{vap}};$$

where U_{vap} is the heat of vaporization.

Equation-of-State Packages

Several equation-of-state subroutines have been developed for single- or multiphase and single- or multicomponent systems. For two-phase flow of vapor and liquid water, the independent variables, or calling arguments, are the fluid density ρ and the internal energy U . The equation-of-state package returns values for the pressure P , temperature T , quality Q^v , saturation S^v , heat of vaporization U_{vap} , derivatives of P , T , U_{vap} with respect to ρ and U ,

viscosities μ^l , μ^v , and thermal conductivities K_T^l , K_T^v . The liquid and vapor conductivities are used in determining the mixture thermal conductivity K_T . Within the package, quantities are calculated by interpolation and extrapolation of tabular values and by analytic equations derived by fits to data. The phase diagram is divided into computational regions. For both liquid and vapor phases, the pressure and temperature at a given density are calculated from:

$$P - P_{\text{ref}} = \left(\frac{\partial P}{\partial U} \right)_{\rho} (U - U_{\text{ref}}) ; \quad T - T_{\text{ref}} = \left(\frac{\partial T}{\partial P} \right)_{\rho} (P - P_{\text{ref}}).$$

The P_{ref} , U_{ref} , and T_{ref} are functions of specific volume along reference curves. Along the saturation curve separating the liquid and vapor from the two-phase region, the tabular values from ASME Steam Tables (Meyer and others 1967) are used for the reference values. Along the isobars of $P = 1$ bar for single-phase liquid and vapor, and on the Hagoniot curve for compressed liquid with density greater than that at 25°C and 1 bar, analytic formulas are used for the reference values. The coefficients $(\partial P / \partial U)_{\rho}$ are determined by tabular fitting in the $P - U$ diagram above the saturation curve. The coefficients $(\partial T / \partial P)_{\rho}$ are given as functions of the specific volume. With (P, T) determined from (P, U) , the viscosities, thermal conductivities, and other fluid properties can be calculated with analytic or tabular fits.

For water-salt (NaCl) solutions, the salinity is an additional independent variable. For most of the fluid properties, analytic correction factors as functions of salinity are included in the package. In order to determine the mass fractions of solid, liquid, and vapor components, the solubilities of salt in the liquid and vapor phases are calculated. If the input salinity is greater than the saturation value, solid salt will precipitate out of solution.

The mass fraction of solid precipitate is determined by an iterative procedure. The internal energy of solid salt is approximated as a function of temperature only, and the specific volume is calculated as a function of pressure.

For applications in geopressed reservoirs, a package for water/methane mixtures has been developed. The water (or brine) is assumed to be present only in the liquid phase. The methane is either dissolved in the liquid or in gaseous phase in equilibrium with a saturated solution. The mass fraction of methane is the additional calling argument. Within the package, quantities are calculated as functions of pressure, temperature, and/or salinity. The solubility of methane declines with increasing salinity.

Constitutive Relationships

When detailed experimental data are unavailable, the relationship of Budianski (1970) is used to approximate the mixture thermal conductivity K_T :

$$(1 - \phi) \left[\frac{2}{3} + \frac{1}{3} \left(\frac{K_T^r}{K_T} \right) \right]^{-1} + \phi \left\{ S^l \left[\frac{2}{3} + \frac{1}{3} \left(\frac{K_T^l}{K_T} \right) \right]^{-1} + S^v \left[\frac{2}{3} + \frac{1}{3} \left(\frac{K_T^v}{K_T} \right) \right]^{-1} \right\} = 1.$$

The rock internal energy is assumed to be $U^r = c^r T$, where c^r is the specific heat capacity of the rock.

The relative permeabilities may be represented by the equations of Corey and others (1956):

$$k_r^l = \bar{S}^4 \quad \text{and} \quad k_r^v = (1 - \bar{S})^2 (1 - \bar{S}^2),$$

where the normalized saturation is

$$S = \frac{S^L - S_r^L}{1 - S_r^L - S_r^V}$$

with residual saturation S_r^L and S_r^V .

The permeability k as a function of porosity ϕ is approximated by the following relation:

$$k = k_o \left(\frac{\phi}{\phi_o} \right)^n \left(\frac{1 - \phi_o}{1 - \phi} \right)^m,$$

where n and m are empirical constants.

For the case when ϕ does not appreciably depend upon the shear stress, ϕ is expressed as a function of effective stress (confining pressure P_c minus fluid pressure P) and temperature T

$$\Delta\phi = \left(\frac{1}{K^r} - \frac{1 - \phi}{K} \right) \Delta(P_c - P) + 3(1 - \phi)(\eta - \eta^r) \Delta T,$$

where K , K^r are the bulk modulus of porous rock and of rock grain, respectively, and η , η^r are the coefficients of linear thermal expansion. In general, the bulk modulus K depends upon $P_c - P$, the loading direction, and the past stress history.

II. NUMERICAL SOLUTIONS

Finite Difference Method

The finite difference method is used. The advection terms are treated with upstream weighting technique.

Alternating Direction Implicit Method

For the solution of a multidimensional problem in a time step, the alternating-direction implicit (ADI) method is used. The two-or three dimensional problem is reduced to two or three one-dimensional problems. The series of one-dimensional implicit equations are solved iteratively until some preset convergence criterion is met.

Nonlinear Iteration

Within each one-dimensional problem, the coupled, nonlinear equations are solved by an iterative method. The Newton-Raphson procedure is employed to accommodate the nonlinearity, and the oscillations associated with crossing the steam-water saturation line are damped by requiring that the amplitude of each oscillation decreases by a specified amount (see Pinder 1979 for a communication with Pritchett).

III. COMPUTER CODE

Documentation

The code was developed by J. W. Pritchett and S. K. Garg of Systems, Science and Software for geothermal and geopressure simulations. The code characteristics deduced from the sample applications are listed below.

Spatial Grid

The model can be applied to one-dimensional (linear, radial, or spherical), two-dimensional (areal, vertical, or axisymmetric), and three-dimensional (rectangular) coordinate systems. For one- or two-dimensional modeling of an aquifer, the layer thickness and dip can be specified for each grid.

Material Properties

For each zone, the density, heat capacity, thermal conductivity, initial porosity, initial directional permeabilities, relative permeability curves, porosity-permeability relation, bulk moduli (loading, unloading), shear modulus, and thermal expansion coefficient can be independently specified.

Fluid Properties

The following constitutive packages are available: liquid water (one component, one phase), liquid water/steam (one component, two phases), liquid water/steam/dissolved NaCl/precipitated NaCl (two components, three phases), liquid water/dissolved methane/free methane gas (two components, two phases), and liquid water/dissolved NaCl/dissolved methane/free methane gas (three components, two phases).

Sources and Sinks

Several studies were made for the treatment of well blocks with dimensions much larger than the diameter of the well contained within the grid block. For single-phase flow, the dependence of the wellbore pressure on the shape of the grid block (radial or rectangular), the type of mesh (uniform or nonuniform) employed, and the character of the spatial discretization scheme were examined (Pritchett and Garg 1980). For two-phase flows, semianalytic equations were derived for ideal two-phase systems in terms of constitutive parameters at the boiling point (Pritchett 1979). An isothermal, two-phase wellbore model was used for the simulation of discharge of methane from geopressured fluids produced from multiple zones. The pressure distribution in each open interval were assumed to be hydrostatic (Pritchett and others 1979).

Initial Conditions

The temperature and pressure are specified in the sample problems.

Boundary Conditions

The boundary condition options are (i) impermeable and insulated (or prescribed heat flux or temperature), (ii) prescribed mass flux and insulated (or prescribed heat flux or temperature), and (iii) prescribed pressure/heat content. It is of interest to note the difference in specifying the production and the injection conditions. If the mass flow out of the system, the heat content (internal energy per unit mass) of the fluid being extracted is the same as that in the zone from which it is being removed. On the other hand, if fluid flows into the system, the heat content of the injected fluid must be supplied to complete the specification of the boundary condition.

Time Steps

The time steps can be automatically determined by the code.

Output

Results of computations are printed out at specified computational cycles.

IV. VALIDATIONS

Stanford Bench Experiments

Two experimental runs were simulated to test the calculated temperature profiles. These are (i) injection of cold water into a synthetic sandstone core containing hot water, and (ii) production of hot water and steam from a system containing pressurized water. To supplement the experimental data, empirical values of heat transfer coefficients through the boundaries and thermal properties of sandstone in the core were assumed (Garg and others 1975).

Grid Orientation Test

A 5 x 5 and a 7 x 7 areal grid with orientations differing by 45° were simulated for a five-spot injection into a producing hot-water field. The "five-spot" pattern is a checkerboard-like system with alternating injection and production wells. The simulated results indicate that the numerical scheme employed is free of grid orientation problems (Pritchett and others 1976b).

Pressure Drawdown Solution

The pressure drawdown from a two-phase reservoir were simulated with a 50-block radial grid. The values of mobility computed from the slope of the P-log(t) results agree with the actual values in the well blocks (Garg 1978).

V. APPLICATIONS

The code has been used in theoretical studies and in field simulations.

Reservoir Recharge by Deep Vertical Fault

A 20 (horizontal) by 6 (vertical) grid was used to simulate a shallow aquifer intersected by a vertical fault. The vertical boundary representing the fault face has specified temperature and hydrostatic pressure. The prominent feature of the flow field is the strong circulation of fluid entering the aquifer near its upper boundary, traveling downward, and then leaving near the bottom. Superimposed on the dominant feature is a weak net outward flow toward the outer boundary and a complicated array of weak eddies (Pritchett and Garg 1978).

Pressure Work and Viscous Dissipation

Numerical solutions of the steady radial temperature distributions indicate that the pressure work and viscous dissipation terms in the energy balance equation have negligible effects in single-phase liquid water and in two-phase liquid-vapor systems. For pure vapor systems, these two terms can produce significant variations in the computed reservoir response (Garg and Pritchett 1977).

Production/Reinjection

A hypothetical bounded hydrothermal reservoir was simulated for the gross thermal power output for different production and reinjection strategies. The production takes place from a central vertical crack and the fluid reinjection

is into two similar cracks located at the reservoir periphery. The results show that injection helps to maintain the reservoir pressure and increases the gross power output (Garg and others 1975b).

Well Testing Analyses

A one-dimensional cylindrical model and a two-dimensional axisymmetric model were used to simulate pressure drawdown and buildup well tests. The classical single-phase analytical models were shown to lead to large errors in the permeability values inferred for the producing formation (Pritchett and others 1976b).

Near-Wellbore Flashing

A one-dimensional cylindrical model was used to examine the severe reduction of well deliverability due to relative permeability effects associated with two-phase flow. If the ambient fluid is salt-saturated at reservoir conditions, the precipitation of salt during flashing of geothermal brine will plug the bores (Pritchett and others 1976b).

Subsidence Simulations

The reservoir model can be coupled to a rock stress/deformation program STAGR. The output tape from the finite-difference reservoir simulation calculations is used to derive the finite-element stress calculations. An axisymmetric model was used to study the dependences of stress distributions and surface horizontal and vertical displacements on the elastic properties of overburden and underburden (Pritchett 1978).

Wairakei Geothermal Reservoir

A one-dimensional vertical model with 22 blocks and a two-dimensional cross-section model with 162 blocks were used to match the production history of Wairakei, New Zealand, from 1953 to 1976. To account for the high compressibility and high discharge enthalpies at early production, the liquid-dominated reservoir is believed to have contained a steam cap prior to production. The simulations included the effects due to the recharge through the highly fractured interfaces between the reservoir and the underlying formation.

The permeability values used in the models to match the production history are much higher than those measured in the laboratory. The porosities reflected by the reservoir performance are lower than the measured values. The discrepancies are believed to be indicative that the system is largely controlled by the fracture network. The fractures or faults may also control the subsidence. The laboratory-determined formation compressibility is too small to account for the subsidence observed. The spatial distribution and temporal changes of the subsidence also suggest that the subsidence is controlled by a seismic slippage along preexisting buried faults.

Salton Sea Geothermal Reservoir

A 16 x 16 areal model was used to simulate the upper reservoir in the Salton Sea geothermal field, California. The simulations analyzed the effects of fluid reinjection and well patterns on reservoir performance (Riney and others 1977).

Geopressure Simulations

Sensitivity studies were made to assess the drive mechanisms (water compressibility, rock compaction, and methane evolution) for geopressured reservoirs. Axisymmetric calculations were performed for the long-term production behavior of the Austin Bayou Prospect (Pritchett and others 1979).

VI. SUMMARY

This is a two-phase model for steam production in hydrothermal reservoirs and for methane production in geopressured geothermal reservoirs. The reservoir model can accommodate different equation-of-state packages for multiphase, multicomponent simulations. A nonisothermal subsidence formulation is incorporated in the model to couple to a stress code. The basic governing equations of the reservoir model are formulated in terms of fluid density and internal energy. The numerical solutions are obtained by the alternating-direction implicit method.

The code has been extensively applied to theoretical studies and to field simulations. The various applications demonstrate the importance of the effects of fluid injection, reservoir recharge, steam flashing, methane evolution, and salt precipitation. The history match and the subsidence study for the Wairakei geothermal reservoir indicate that the coupling between nonisothermal fluid flow and nonlinear formation deformation may be important.

SHAFT79

SHAFT79 (Simultaneous Heat And Fluid Transport) is an integrated finite-difference program for computing three-dimensional, two-phase nonisothermal flow in porous media. The model is designed principally for geothermal reservoir simulation. It has been applied to history matching of the Serrazzano steam geothermal field in Italy and to simulations and well testings in other two-phase fields. The model is being used for generic studies of nuclear waste repositories, especially the pore-pressure buildup induced by a heat source. The various aspects of the model are discussed in Pruess and others (1979a-c), and Pruess and Schroeder (1979, 1980).

I. GOVERNING EQUATIONS

In this model, the governing equations are formulated in terms of fluid density ρ and internal energy U . The model solves coupled mass- and energy-balance equations of the following form:

$$\frac{\partial}{\partial t} (\phi \rho) = -\nabla \cdot \bar{F} + Q_F,$$

$$\frac{\partial}{\partial t} [\phi \rho U + (1-\phi) \rho^R c^R T] = -\nabla \cdot \bar{G} + Q_H.$$

The mass flux \bar{F} is given by Darcy's Law:

$$\bar{F} = \sum_{\alpha=l,v} \bar{F}^{\alpha} = - \sum_{\alpha} \frac{k k_r^{\alpha}}{\mu^{\alpha}} \rho^{\alpha} (\nabla P - \rho^{\alpha} g).$$

The energy flux contains conductive and convective terms

$$\bar{G} = -K_T \nabla T + \sum_{\alpha} H^{\alpha} \bar{F}^{\alpha}.$$

The governing equations describe the physical systems of porous rock saturated with one-component fluid in liquid and vapor form. The liquid l , vapor v , and rock matrix r , are assumed to be in local thermodynamic equilibrium with the same temperature and pressure at all times. The capillary pressure between liquid and vapor is neglected.

Equation-of-State and Constitutive Relationships

The description of the equilibrium thermodynamic properties of the fluid filling the void space is given by a fluid table inverted from the Steam Tables of the International Formulation Committee (see Meyer and others 1967). The fluid table gives all required quantities of the governing equations (temperature T , pressure P , vapor saturation S^v , heat conductivity K_T , liquid and vapor viscosities μ^l , μ^v , densities ρ^l , ρ^v , specific internal energies U^l , U^v) as functions of the two principal dependent variables (fluid density ρ and fluid specific internal energy U). The thermodynamic information, including all derivatives, is obtained by means of bivariate interpolation from the fluid table. The ρ, U grid is constructed in such a way that the intersections of the grid with the saturation line are tabulated (Pruess and others 1979b). This ensures that interpolation does not occur across the saturation line, where derivatives change discontinuously.

For the formation properties, the porosity ϕ can vary with pressure and temperature. All other rock properties (density ρ^r , specific heat c^r , thermal conductivity K_T , permeability k) are independent of temperature, pressure, or

vapor saturation. In most applications, relative permeabilities were obtained from a version of Corey's equation:

$$k_r^l = \bar{S}^4 = \frac{(r - s)^4}{r^4},$$

and

$$k_r^v = (1 - \bar{S})^2 (1 - \bar{S}^2) = \frac{(2r - S^v) S^{v3}}{r^4},$$

with the residual immobile steam saturation equal to zero and residual immobile water saturation $S_r^l = 1 - r$ varying between 0.4 and 0.7.

II. NUMERICAL SOLUTIONS

Implicit Integrated Finite-Difference Equations

Space discretization is achieved with the integrated finite-difference method. This method allows a very flexible geometric description because it does not distinguish between one-, two-, or three-dimensional regular or irregular geometries. Time is discretized fully implicitly as a first-order finite difference, resulting in the following finite-difference equations:

$$D_n(\bar{X}_{t+\Delta t}) \equiv (\psi_n \rho_n)_{t+\Delta t} - (\psi_n \rho_n)_t - \frac{\Delta t}{V_n} \left[\sum_m F_{nm} + V_n Q_{F,n} \right]_{t+\Delta t} = 0,$$

$$E_n(\bar{X}_{t+\Delta t}) \equiv (\psi_n \rho_n U_n)_{t+\Delta t} - (\psi_n \rho_n U_n)_t + (1 - \psi_n) \rho^{xx} (T_{n,t+\Delta t} - T_{n,t}) - \frac{\Delta t}{V_n} \left[\sum_m G_{nm} + V_n Q_{H,n} \right]_{t+\Delta t} = 0,$$

where n and m label the volume elements, and

$$\bar{X}_{t+\Delta t} = (\rho_1, \dots, \rho_N, U_1, \dots, U_N)_{t+\Delta t}$$

is the vector of the $2N$ unknowns for a system with N elements at time $t+\Delta t$,

Δt is the time step, V_n is the volume of element n , and

$$F_{nm} = A_{nm} \sum_{\alpha} k_{nm} \left(\frac{k_r^{\alpha}}{\mu^{\alpha}} \right)_{nm} \rho_{nm}^{\alpha} \left[\frac{P_m - P_n}{D_{nm}} - \rho_{nm}^{\alpha} g_{nm} \right],$$

$$G_{nm} = A_{nm} K_{T,nm} \left(\frac{T_m - T_n}{D_{nm}} \right) + \sum_{\alpha} H_{nm}^{\alpha} F_{nm}^{\alpha},$$

are the mass flow and the energy flow, respectively, from element m into element n with interface area A_{nm} over a distance D_{nm} . Whereas ϕ_n can vary with time, the apparent rock density $(1 - \phi_n)\rho^r$ is constant. Different weighting procedures can be selected for the various "interface quantities" labeled with subscript nm .

The permeability k and the thermal conductivity K_T are evaluated as harmonic means of the value in adjacent elements. The fluid density ρ is interpolated spatially from that of the adjacent elements (arithmetic mean weighted with differences from the block centers to the interface). The mobilities $kk_r^{\alpha}/\mu^{\alpha}$ and enthalpies H^{α} can be either interpolated spatially or weighted toward those of an upstream element.

Matrix Solver

The finite-difference equations above are solved with the Newton-Raphson method. The set of linear equations arising at each iteration step is solved with an efficient direct solver using sparse storage techniques (Duff 1977).

III. COMPUTER CODES

Documentation

SHAFT79 and a number of associated pre- and post-processor programs are written in FORTRAN IV. The code is presently being used on the CDC 7600 computers at Lawrence Berkeley Laboratory and at Sandia. Earlier versions have been installed on a UNIVAC 1108 and an IBM 370/168. Implementation on a Burroughs B-6800 is underway. The user's manuals for both the SHAFT78 version and the SHAFT79 version are available (Pruess and others 1979a; Pruess and Schroeder 1980). The input consists of several data blocks which are provided by the user either as disk files or as data cards. Some of the data blocks are optional.

Spatial Grid

To specify the grid for irregular geometries, the following data are required: element volume, distances from element centers to interfaces, interface areas, and cosine of the angle between the gravitational acceleration vector and the connecting lines between neighboring elements. The code can also generate internally simple regular grids in one, two, or three dimensions.

Material Properties

For each rock type, the rock density, permeabilities along the principal axes, rock heat conductivity, and rock specific heat are specified. The porosity can be evaluated as a constant or as a linear function of pressure and temperature by specifying the compressibility and expansivity.

Fluid Properties

The code requires an equation of state in tabular form to be provided through a disk file. The table can be generated by executing two programs: WATER for computing and tabulating the steam table equations (Meyer and others 1967) and PROPER for numerically inverting the tables into functions of (U, ρ) . For most geothermal problems within the $5^{\circ}\text{C} < T < 400^{\circ}\text{C}$ temperature range and $0.5 \text{ bar} < P < 220 \text{ bar}$ pressure range, one can use the fluid table called FLUTAB3 which is available as part of the SHAFT79 program package. The relative permeabilities can be determined: (i) in the equation of state table, (ii) from the Corey's equation, (iii) by interpolation from tabulated array, or (iv) as linear functions of vapor saturation between residual immobile value and perfectly mobile value.

Sources and Sinks

The mass and heat generation rates versus time can be tabulated. For mass injection, the value of specific enthalpy is required. The relative amounts of liquid and vapor of the produced fluid in the source element can be determined: (i) according to relative mobilities, (ii) with the same steam quality as the producing element, (iii) as pure vapor, or (iv) as pure liquid.

Initial Conditions

The initial conditions can be converted from the user-oriented variables (temperature-pressure or temperature-vapor saturation) to the internal program variables (energy-density). At the beginning of a simulation, volume-, mass-, and energy-balances and averages will be computed for the various reservoir domains.

Boundary Conditions

There is no special boundary blocks. The boundary conditions are specified through appropriately chosen elements, interfaces, initial conditions, and sources/sinks.

Time Steps and Solution Control

The array of the lengths of time steps are specified by the user. The user also specifies the convergence criteria for the energy equation and the density equations. If no convergence has been achieved yet, the linear equations for Newton-Raphson iteration will be solved. If there is a failure in solving the linear equations, in computing thermodynamic parameters, or in converging within a given number of iterations, the time step will be repeated with time increment cut in half. The simulation proceeds until it terminates for one of several criteria: (i) number of time steps, (ii) machine time, (iii) physical time.

Output

At the completion of a run, the results needed for a subsequent continuation of the problem are written onto a disk file. The amount of printout can be controlled. In addition to the dependent variables and parameters for each element at chosen time steps, one can specify additional printout for the fluxes, transductances, flow terms, accumulation terms, sinks/sources, equations of state, or linear equations. Two-dimensional contour plotting is available for the display of results.

IV. VALIDATIONS

SHAFT79 was validated against SHAFT78, which in turn was validated against a number of analytically solvable one-phase flow problems (Pruess and others 1978), as well as against published numerical results for two-phase flow problems (Pruess and others, 1979c).

Single-Phase Solutions

- (a) Linear Gas Flow: The computed pressure drops with a 30-element linear grid were compared with the analytic solutions of Kidder (1957).
- (b) Theis Problem: The type curves calculated with a 15-element radial grid were compared with the exponential integral solution.

Two-Phase Problems

- (a) Areal Saturation Distribution: The calculated liquid saturation values over a 6 x 6 grid were compared with the numerical results of Toronyi and Farouq Ali (1977) for a reservoir production problem in a vapor-dominated reservoir.
- (b) Pressure Drawdown: The pressure drawdown with boiling near the wellbore was compared with the results obtained by Garg (1978) with the same 50-block radial grid. The wellbore P versus $\log(t)$ plot is indeed a straight line with slope determined by the total kinematic mobility. The simulated results also show that P versus $\log(t/r^2)$ over all elements in the reservoir, not just the wellbore, is a straight line. This indicates that the mobilities could also be obtained from observation well data rather than just flowing wellbore data.

V. APPLICATIONS

The code has been applied to problems in geothermal reservoir simulation, well testing, and nuclear waste isolation.

Generic Studies

- (a) Reservoir Depletion: A vertical grid with 44 blocks was used to simulate the depletion of a reservoir with sharp steam/water interface. When steam is produced above the liquid water table, a two-phase layer is produced and the boiling front moves downward. The simulated results show that the top of the two-phase zone does not dry up until after the boiling point has reached the bottom of the reservoir (Pruess and Schroeder 1979).
- (b) Injection of cold water: The propagation of the hydrodynamic front and the temperature front were simulated with a 50-block radial grid for cold-water injection into a steam reservoir. It is shown that the fronts are propagated according to the parameter t/r^2 as is the case in pressure drawdown.
- (c) Fractured Reservoir: The double-porosity concept was generalized for numerically simulating two-phase flow in fractured porous media. A multiple-interacting continuum method was incorporated in SHAFT79 and was used in a radial grid simulation. With reservoir conditions representative of The Geysers, California, it was shown that for the cases with low matrix permeability, the mass flux of water from the matrix to the fractures could be continuously vaporized by heat transported by conduction (Pruess and Narasimhan 1981).

Geothermal Field Simulations

- (a) Serrazzano, Italy: A three-dimensional geologically accurate mesh with 234 irregular elements was used in the simulations that match the production history from 1959 to 1975 for the vapor-dominated geothermal reservoir at Serrazzano, Italy. The permeabilities and initial conditions were adjusted to reproduce the field observations. It is concluded that (i) the interface between overlying steam cap and deeper boiling aquifer remains stationary during exploitation, and (ii) the reservoir boils approximately uniformly throughout in response to production. The simulation also suggests that some steam flowing to the main well field originates from deep fractures rather than from boiling in the two-phase zones modeled. The reservoir model is used to forecast production rates on a well-by-well basis through 1990. Additional parametric studies were made with this geologically accurate model on the effects of cold water recharge, incomplete thermal equilibration between rock and fluid, and depth of steam/two-phase interface (Pruess and others 1980).
- (b) Krafla, Iceland: A 7 x 14 vertical grid was used to simulate production and injection at Krafla, Iceland. It is shown that deep injection is preferable to shallow injection in maintaining pressure and temperature and minimizing vapor saturation decrease (Jonsson 1978).

Repository Simulation

One- and two-dimensional models were used to simulate the pressure changes induced by spent fuel emplacement in argillite. The pore pressure is shown to be sensitive to the permeability and the porosity of the backfill

material in the repository draft and shaft. With perfect backfill, the pore pressure may exceed the local lithostatic pressure. With high-permeability, low-porosity backfill, overpressurization can be relieved (Eaton and others 1979).

VI. SUMMARY

This is a two-phase code for simulating reservoir models with an irregular mesh in multidimensional space. A multiple-interacting continua method has been developed recently to generalize the capabilities of this code to model fractured porous media. The numerical methodology incorporates the implicit treatment and iterative scheme to handle the nonlinear changes of fluid properties across the saturation line in the phase diagram.

The history match for the Serrazzano field demonstrates the use of a geologically accurate model for two-phase reservoirs. Generic studies were also made to gain better physical insights on the depletion of two-phase geothermal reservoirs and on the phase changes near the wellbores associated with fluid production and injection. The code has also been applied to simulate long-term pressure and temperature changes around a nuclear waste repository.

ACKNOWLEDGEMENTS

We are grateful to our colleagues in the Earth Sciences Division for their discussion and encouragement, especially Dr. P. A. Witherspoon and Dr. T. N. Narasimhan. Very helpful comments were made by Drs. J. O. Duguid, M. M. Lemcoe, and M. R. Wiggly of the Office of Nuclear Waste Isolation, Battelle, Columbus, and are also acknowledged.

The cooperation, comments, and suggestions from the model developers at the Workshop on Numerical Modeling of Thermohydrological Flow in Fractured Rock Masses, held in Berkeley, California, February 19-20, 1980, are appreciated. The proceedings of this workshop has been published as Lawrence Berkeley Laboratory report LBL-11566 (1981).

This work was supported by the Assistant Secretary for Nuclear Energy, Office of Waste Isolation of the U. S. Department of Energy under contract DE-AC03-76SF00098. Funding for this project is administered by the Office of Nuclear Waste Isolation at Battelle Memorial Institute.

NOMENCLATURE

A	surface area bounding a finite subdomain	$[L^2]$
$A_{m,n}$	area of interface between elements m and n	$[L^2]$
a	upstream weighting factor	
a_C	coefficient of concentration dependence of density, $\partial \rho^w / \partial C$	$[ML^{-3}]$
a_V	coefficient of compressibility, $a_V = -de/d\sigma'$	$[M^{-1}Lt^2]$
B	temperature coefficient	$[T]$
b	fracture aperture	$[L]$
$b_{1/2}$	half-aperture, $b/2$	$[L]$
C	concentration or mass fraction	
$\overset{\equiv}{C}$	elastic tensor of fourth rank	$[ML^{-1}t^{-2}]$
C_O	cohesion of fractures	$[L^2t^{-2}T^{-1}]$
C_C	compression index, slope of e versus $\log \sigma'$ for virgin loading curve	
C_H	heat capacity per unit volume, $C_H = \rho c$	$[ML^{-1}t^{-2}T^{-1}]$
C_k	slope of e versus $\log k$ straight line	
C_s	swelling index, slope of e versus $\log \sigma'$ in unloading or rebounding curve	
c	specific heat capacity, $c = C_H/\rho$	$[L^2t^{-2}T^{-1}]$
D	depth, $-z$	$[L]$
$D_{m,n}$	distance between node m and node n, $D_{mn} = d_{mn} + d_{nm}$	$[L]$
D_T	thermal dispersion coefficient	$[Mt^{-2}T^{-1}]$
D/Dt	material derivative in the coordinate system attached to the deforming rock solid	$[t^{-1}]$
$d_{m,n}$	perpendicular distance from node n to the interface between elements n and m	$[L]$
E	Young's modulus	$[ML^{-1}t^{-2}]$

e	void ratio V^p/V^r , $e = \phi/(1 - \phi)$	
\bar{f}	body force	$[Lt^{-2}]$
\bar{g}	gravitational acceleration, $\bar{g} = -g\hat{z}$ or $g\bar{V}D$	$[Lt^{-2}]$
H	enthalpy, $H = U + P/\rho^w$	$[L^2t^{-2}]$
h	hydraulic head, $h = P'/\rho_o^w g$	$[L]$
h_p	pressure head, $h_p = P/\rho_o^w g$	$[L]$
h^{fm}	fracture-rock matrix heat transfer coefficient	$[ML^{-1}t^{-3}T^{-1}]$
$h_{m,n}$	heat transfer coefficient between node m and n	$[ML^{-1}t^{-3}T^{-1}]$
\bar{I}	unit tensor	
K	modulus	$[M^{-1}Lt^2]$
\bar{K}_C	molecular diffusivity	$[L^2t^{-1}]$
\bar{K}_{CD}	solute dispersivity	$[L^2t^{-1}]$
\bar{K}_F	hydraulic conductivity tensor, $\bar{K}_F = \bar{k}\rho_o^w g/\mu_o$	$[Lt^{-1}]$
\bar{K}_H	thermal conductivity-dispersivity tensor, $\bar{K}_H = \bar{K}_T + \bar{K}_{TD}$	$[MLt^{-3}T^{-1}]$
K_N	normal stiffness of fracture	$[ML^{-1}t^{-2}]$
K_S	tangential stiffness of fracture	$[ML^{-1}t^{-2}]$
\bar{K}_T	thermal conductivity tensor	$[MLt^{-3}T^{-1}]$
\bar{K}_{TD}	thermal dispersivity tensor	$[MLt^{-3}T^{-1}]$
\bar{k}	permeability tensor	$[L^2]$
k_m	permeability of element m	$[L^2]$
$k_{m,n}$	harmonic mean of k evaluated at the interface between elements m and n	$[L^2]$
k_r	relative permeability	
L	length, half-dimension of porous medium block	$[L]$
M	Biot constant	$[ML^{-1}t^{-2}]$

M_C	fluid mass capacity of a finite subdomain	$[ML^{-1}]$
$M_{C,n}$	fluid mass capacity of element n	$[ML^{-1}]$
P	water pressure	$[ML^{-1}t^{-2}]$
P_C	capillary pressure, $P_C = P^v - P^l$	$[ML^{-1}t^{-2}]$
P_O	initial pressure, hydrostatic pressure	$[ML^{-1}t^{-2}]$
P'	incremental pressure, pressure above the hydrostatic pressure $P - P_O$	$[ML^{-1}t^{-2}]$
Q_F	fluid mass source	$[ML^{-3}t^{-1}]$
Q'_F	fluid mass withdrawal rate, $Q'_F = -Q_F$	$[ML^{-3}t^{-1}]$
Q_H	heat source	$[ML^{-1}t^{-3}]$
Q'_H	heat withdrawal rate, $Q'_H = -Q_H$	$[ML^{-1}t^{-3}]$
Q'_L	heat loss to surrounding strata	$[ML^{-1}t^{-3}]$
\bar{q}	Darcy's velocity	$[Lt^{-1}]$
q_F	strength of fluid source	$[t^{-1}]$
q'_F	strength of fluid withdrawal rate, $q'_F = -q_F$	$[t^{-1}]$
r	radial coordinate in cylindrical or spherical coordinate system	$[L]$
\bar{r}	position vector	$[L]$
S	saturation	
S_r	irreducible saturation	
S_s	coefficient of specific storage	$[L^{-1}]$
s	acceleration factor	
T	temperature	$[T]$
t	time	$[t]$
Δt	time interval	$[t]$

Δt_n^C	stability limit of time constant of element n	[t]
U	internal energy, $U = H - P/\rho$	$[L^2 t^{-2}]$
$U_{i+1/2,j,k}$	interface transmissibility between nodes $i+1,j,k$ and i,j,k	[Lt]
$U_{m,n}$	interface conductance between elements m and n	$[ML^{-1} t^{-1}]$
\bar{u}	solid displacement vector	[L]
\bar{v}	fluid velocity within fractures or pores	$[Lt^{-1}]$
V	volume of a finite subdomain or element	$[L^3]$
x	horizontal coordinate	[L]
y	horizontal coordinate	[L]
z	vertical coordinate, with $z = 0$ at the ground surface or water table	[L]
z_m	z of element m	[L]
α_l	longitudinal dispersivity	[L]
α_t	transverse dispersivity	[L]
α^f	Biot's coupling constant for fractures	
α^m	Biot's coupling constant for rock medium	
α^{fm}	fracture-porous matrix fluid mass transfer coefficient	$[ML^{-3}]$
β_h^W	compressibility of water to head change, $\beta_h^W = (1/\rho^W)(\partial\rho^W/\partial h_p)$	$[L^{-1}]$
β_P^W	compressibility of water to pressure change, $\beta_P^W = (1/\rho^W)/(\partial\rho/\partial P)$	$[M^{-1} Lt^2]$
β_h^P	compressibility of pores to head change, $\beta_h^P = \partial\phi/\partial h_p$	$[L^{-1}]$
β_P^P	compressibility of pores to pressure change $\beta_P^P = \partial\phi/\partial P$	$[M^{-1} Lt^2]$
β_T^W	expansivity of water to temperature change, $\beta_T^W = (-1/\rho)(\partial\rho^W/\partial T)$	$[T^{-1}]$

Δ	fracture spacing	[L]
ϵ	volumetric strain of the solid skeleton	
$\bar{\epsilon}$	strain tensor	
η	linear thermal expansivity	[T ⁻¹]
θ	angle of friction of fractures	
λ	time differencing interpolation factor	
λ'	parameter for compensating entry and exit effects at tubule intersection	
μ	coefficient of dynamic viscosity of water	[ML ⁻¹ t ⁻¹]
μ_0	constant viscosity	[ML ⁻¹ t ⁻¹]
ν	Poisson's ratio	
ξ	seating stress	[ML ⁻¹ t ⁻²]
ρ^w	mass density of water	[ML ⁻³]
ρ_0^w	reference mass density of water (at P ₀ and T ₀)	[ML ⁻³]
ρ^r	mass density of rock	[ML ⁻³]
$\rho_{m,n}$	harmonic mean of ρ evaluated at the interface between element m and n	[ML ⁻³]
$\bar{\sigma}$	total stress tensor	[ML ⁻¹ t ⁻²]
σ_N	normal stress (overburden)	[ML ⁻¹ t ⁻²]
σ'	effective stress, $\sigma' = \sigma_N - P$	[ML ⁻¹ t ⁻²]
ϕ	porosity of pores or fractures	
λ	boundary porosity or Bishop's coefficient, relating effective stress and water pressure in unsaturated zone	
λ'	$\lambda + h_p d\lambda/dh_p$ parameter correlating changes in effective stress and water pressure	
Γ	transient mass flux	[ML ⁻³ t ⁻¹]

$\hat{\Omega}$	unit vector along the direction of a tubule	
∇	spatial gradient differential operator	$[L^{-1}]$

Superscripts

b	boundary
d	discrete fracture
f	fractures
fm	fracture-porous medium interface
i, j	phase index, i, j = f or m
k	iteration
l	liquid water
m	porous medium blocks, including the rock matrix and the pore water
p	pores in the porous medium block
r	solid rock
v	water vapor
w	water
α	fluid phase index, $\alpha = w, l, \text{ or } v$

Subscripts

D	dispersion
F	fluid
H	heat
m	node index
n	node index
o	reference value at P_0 and T_0
P	pressure
S	saturation
T	temperature

ABBREVIATIONS

ADI	Alternating direction implicit method
AECL	Atomic Energy of Canada, Limited
CRRE	Army Cold Regional Research Engineering Laboratory, Hanover, New Hampshire
D&M	Dames and Moore, Los Angeles, California
FD	Finite-difference method
FE	Finite-element method
IFD	Integrated finite-difference method
KBS	Swedish Nuclear Fuel Safety Project, Karnbranslesakerhet
LBL	Lawrence Berkeley Laboratory, Berkeley, California
NRC	Nuclear Regulatory Commission
ONWI	Office of Nuclear Waste Isolation, Department of Energy, Columbus, Ohio
SOR	Successive-overrelaxation method
S ³	System, Science and Software, La Jolla, California
UCB	University of California, Berkeley, California
WIPP	Waste Isolation Pilot Plant

REFERENCES CITED

- Aifantis, E. C., 1979, On the response of fissured rocks: Proceedings, 16th Midwestern Mechanics Conference, Manhattan, Kansas, September.
- Avdonin, N. A., 1964, Some formulas for calculating the temperature field of a stratum subjected to thermal injection: *Neft 'i Gaz*, v. 3, p. 37-41.
- Ayatollahi, M. S., 1978, Stress and flow in fractured porous media: Ph.D. thesis, Department of Material Science and Mineral Engineering, University of California, Berkeley, California, 154 p.
- Ayatollahi, M. S., J. Noorishad, and P. A. Witherspoon, 1980, A finite element method for stress and flow analysis in fractured rocks: Lawrence Berkeley Laboratory Report LBL-11430, Berkeley, California.
- Aydelotte, S. R., 1980, Transient well testing in two-phase geothermal reservoirs: Lawrence Berkeley Laboratory Report LBL-10562, GREMP-8, 139p.
- Barenblatt, G. I., I. P. Zheltov, and I. N. Kochina, 1960, Basic concepts in the theory of seepage of homogeneous liquids in fissured rocks (strata): *PMM* v. 24, no. 5, p. 852-864, English translation: *Applied Mathematics and Mechanics*, v. 24, p. 1286-1303, 1960).
- Berman, A. S., 1953, Laminar flow in channels with porous walls: *J. Appl. Phys.*, v. 24, no. 9, p. 1232-1235.
- Biot, M. A., 1941, General theory of three-dimensional consolidation: *J. Appl. Phys.*, v. 12, p. 155-164.
- Biot, M. A., 1955, Theory of elasticity and consolidation for a porous anisotropic solid: *J. Appl. Phys.*, v. 26, no. 2, p. 182-185.
- Biot, M. A., 1956, Theory of deformation of a porous viscoelastic anisotropic solid: *J. Appl. Phys.*, v. 27, no. 5, p. 459-467.
- Biot, M. A., 1961, Mechanics of deformation and acoustic propagation in porous media: *J. Appl. Phys.*, v. 34-A, p. 1483-1498.
- Bodvarsson, G. S., and M. J. Lippmann, 1980, Numerical Model CCC: Proceedings, Workshop on Numerical Modeling of Thermohydrological Flow in Fractured Rock Masses, Lawrence Berkeley Laboratory Report LBL-11566, Berkeley, California.
- Bodvarsson, G. S., M. J. Lippmann, and T. N. Narasimhan, 1979, Recent modifications of the numerical code "CCC": Earth Sciences Division Annual Report 1979, Lawrence Berkeley Laboratory Report LBL-10686, Berkeley, California.

- Brace, W. F., 1980, Permeability of crystalline and argillaceous rocks: Status and problems: *Int. J. Rock Mech. Min. Sci.*, v. 17, p. 241-251.
- Bredehoeft, J. D., and G. F. Pinder, 1970, Digital analysis of areal flow in multiaquifer groundwater systems: A quasi three-dimensional model: *Water Resources Research*, v. 6, no. 3, p. 883-888.
- Brownell, D. H., Jr., S. K. Garg, and J. W. Pritchett, 1977, Governing equations for geothermal reservoirs: *Water Resources Research*, v. 13, no. 6, p. 929-934.
- Budiansky, B., 1970, Thermal and thermoelastic properties of isotropic composites: *J. Compos. Mater.*, v. 4, p. 286.
- Burgess, A., 1977, Groundwater movements around a repository, regional groundwater flow analyses, part 1: Initial conditions, part 2: Long term residual conditions: *KBS teknisk rapport 54:03*, Hagconsult AB, Karnbransslesakerhet, Stockholm, Sweden.
- Burgess, A. S., R. G. Charlwood, E. L. Skiba, J. L. Ratigan, P. F. Gnirk, H. Stille, and U. E. Lindblom, 1979, Analyses of groundwater flow around a high-level waste repository in crystalline rock: *OECD Nuclear Energy Agency Workshop on Low-Flow, Low-Permeability Measurements in Largely Impermeable Rocks*, Paris, France, March.
- Carslaw, H. W., and J. C. Jaeger, 1959, *Conduction of heat in solids*. 2nd edition: Oxford Univ. Press, Oxford, England.
- Carter, R. D., and G. W. Tracy, 1960, An improved method for calculating water in flux: *Trans. AIME*, p. 415.
- Chan, T., N. G. W. Cook, and C. F. Tsang, 1978, Theoretical temperature fields for the Stripa Heater Project. 2 volumes: *Technical Project Report no. 9*, Swedish-American Cooperative Program on Radioactive Waste Storage in Mined Caverns in Crystalline Rock, Lawrence Berkeley Laboratory Report LBL-7082, Berkeley, California.
- Cinco-Ley, H., and F. Samaniego V., 1978, Transient pressure analysis for fractured wells: 53rd Annual Fall Technical Conference and Exhibition of the Society of Petroleum Engineers of AIME, Houston, Texas, SPE-7490, 12p.
- Cinco-Ley, H., F. Samaniego V., and N. Dominguez A., 1978, Transient pressure behavior for a well with a finite-conductivity vertical fracture: *Soc. Pet. Eng. J.*, v. 18, no. 4, p. 253-264.
- Coats, K. H., 1977, Geothermal reservoir modeling: 52nd Annual Fall Technical Conference and Exhibition of the Society of Petroleum Engineers of AIME, Denver, Colorado, October 1977, SPE-6892, 33p.

- Coats, K. H., W. D. George, C. Chu, and B. E. Marcum, 1974, Three-dimensional simulation of steamflooding: Soc. Pet. Eng. J., p. 573-592.
- Coats, K. H., A. B. Ramesh, and A. G. Winestock, 1977, Numerical modeling of thermal reservoir behavior: Oil Sands, p. 399-410.
- Cole, C. R., and S. K. Gupta, 1979, A brief description of the three-dimensional finite element ground-water flow model adapted for waste isolation safety assessment: Battelle Pacific Northwest Laboratory Report PNL-2652, Richland, Washington.
- Corey, A. T., C. H. Rathjens, J. H. Henderson, and R. J. Wyllie, 1956, Three-phase relative permeability: Trans. AIME, v. 207, 349p.
- Dahlquist, G., and A. Bjorck, 1974, Numerical methods: Prentice-Hall, Englewood Cliffs, New Jersey.
- Dames and Moore, 1977, Heat transfer calculations with special reference to the nuclear waste disposal problem: Dames and Moore Report TN-LN-3, London, England.
- Dames and Moore, 1978, Groundwater movement and nuclide transport: Office of Waste Isolation Report Y/OWI/TM-36/21, Oak Ridge, Tennessee.
- Dillon, R. T., R. B. Lantz, and S. B. Pahwa., 1978, Risk methodology for geologic disposal of radioactive waste: The Sandia waste isolation flow and transport (SWIFT) model: Sandia Laboratories Report SAND78-1267, NUREG/CR-0424, Albuquerque, New Mexico.
- Duff, I. S., 1977, MA28--A set of Fortran subroutines for sparse unsymmetric linear equations: Harwell Report AERE - R 8730, Oxfordshire, Great Britain.
- Duguid, J. O., Jr., 1973, Flow in fractured porous media: Ph.D. thesis, Department of Civil and Geological Engineering, Princeton University, Princeton, New Jersey.
- Duguid, J. O., and J. F. Abel, 1974, Finite element Galerkin method for analysis of flow in fractured porous media, in: Finite element methods in flow problems, ed. by J. T. Oden, O. C. Zienkiewicz, R. H. Gallagher, and C. Taylor, University of Alabama, UAH Press, Huntsville, Alabama, p. 599-615.
- Duguid, J. O., and P. C. Y. Lee, 1973, Flow in fractured porous media: Research report 73-WR-1, Dept. Civil and Geological Engineering, Princeton University, Princeton, New Jersey, 101 p.
- Duguid, J. O., and P. C. Y. Lee, 1977, Flow in fractured porous media: Water Resources Research, v. 13, no. 3, p. 558-566.

- Earlougher, R. C., Jr., 1977, Advances in well test analysis: Henry L. Doherty series monograph, v. 5, Soc. Pet. Eng., AIME, Dallas, Texas, 264 p.
- Eaton, R. R., W. D. Sundberg, D. E. Larson, and M. P. Sherman, 1979, Status of SHAFT78 with respect to modeling radioactive waste burial in Eleana argillite including calculations to date: Sandia Laboratories Report SAND 79-1484, Albuquerque, New Mexico.
- Edwards, A.L., 1972, TRUMP: A computer program for transient and steady-state temperature distributions in multidimensional systems: Lawrence Livermore Laboratory Report UCRL-14754, Livermore, California.
- Eisenstat, S. C., and A. H. Sherman, 1974, Subroutines for envelope solution of sparse linear systems: Research report 35, Yale University, New Haven, Connecticut.
- Evans, G. W., R. J. Brousseau, and R. Keirstead, 1954, Instability considerations for various difference equations derived from the diffusion equation: Lawrence Livermore Laboratory Report UCRL-4476, Livermore, California.
- Faust, C. R., 1976, Numerical simulation of fluid flow and energy transport in liquid- and vapor-dominated hydrothermal systems: Ph.D. thesis, Department of Geosciences, Pennsylvania State University, University Park, Pennsylvania.
- Faust, C. R., and J. W. Mercer, 1975, Mathematical modeling of geothermal systems: Proceedings, 2nd U.N. Symposium on the Development and Use of Geothermal Resources, San Francisco, California, May, v. 3, p. 1635-1641.
- Faust, C. R., and J. W. Mercer, 1976, An analysis of finite-difference and finite-element techniques for geothermal reservoir simulation: Proceedings, 4th Symposium on the Numerical Simulation of Reservoir Performance of the Society of Petroleum Engineers of AIME, Los Angeles, California, p. 337-354, SPE-5742.
- Faust, C. R., and J. W. Mercer, 1977a, Theoretical analysis of fluid flow and energy transport in hydrothermal systems: U.S. Geological Survey Open-file report 77-60, Reston, Virginia, 85 p.
- Faust, C. R., and J. W. Mercer, 1977b, Finite-difference model of two-dimensional, single-, and two-phase heat transport in a porous medium--version I: U. S. Geological Survey Open-file report 77-234, Reston, Virginia, 84 p.
- Faust, C. R., and J. W. Mercer, 1979a, Geothermal reservoir simulation: 1. Mathematical models for liquid- and vapor-dominated hydrothermal systems: Water Resources Research, v. 15, no. 1, p. 23-30.

- Faust, C. R., and J. W. Mercer, 1979b, Geothermal reservoir simulation: 2. Numerical solution techniques for liquid- and vapor-dominated hydrothermal systems. *Water Resources Research*, v. 15, no. 1, p. 31-46.
- Gale, J. E., 1975, A numerical, field and laboratory study of flow in rocks with deformable fractures: Ph.D. thesis, Department of Civil Engineering, Geotechnical Engineering Group, University of California, Berkeley, California, 255 p.
- Garg, S. K., 1978, Pressure transient analysis for two-phase (liquid water/steam) geothermal reservoirs: 53rd Annual Fall Technical Conference and Exhibition of the Society of Petroleum Engineers of AIME, Houston, Texas, SPE-7479, 12 p.
- Garg, S. K., T. R. Blake, D. H. Brownell, Jr., A. H. Nayfeh, and J. W. Pritchett, 1975a, Simulation of fluid-rock interactions in a geothermal basin: System, Science and Software Report SSS-R-76-2734, La Jolla, California, 63 p.
- Garg, S. K., D. H. Brownell, Jr., and J. W. Pritchett, 1977a, Dilatancy-induced fluid migration and the velocity anomaly. *J. Geophys. Research*, v. 82, no. 5, p. 855-864.
- Garg, S. K. and J. W. Pritchett, 1977, On pressure-work, viscous dissipation and the energy balance relation for geothermal reservoirs: *Adv. Water Resources*, v. 1, no. 1, p. 41-47.
- Garg, S. K., and J. W. Pritchett, 1978, Two-phase flow in geopressured geothermal wells: *Energy Conversion*, v. 18, p. 45-51.
- Garg, S. K., J. W. Pritchett, and D. H. Brownell, Jr., 1975b, Transport of mass and energy in porous media: *Proceedings, 2nd U. N. Symposium on the Development and Use of Geothermal Resources*, San Francisco, California, May, v. 3, p. 1651-1656.
- Garg, S. K., J. W. Pritchett, D. H. Brownell, Jr., and T. D. Riney, 1978, Geopressured geothermal reservoir and wellbore simulation. *Systems, Science and Software report SSS-R-78-3639*, La Jolla, California, 151 p.
- Garg, S. K., J. W. Pritchett, D. H. Brownell, Jr., and J. Sweet, 1975c, Multiphase fluid flow in geologic media and land surface subsidence: *Proceedings, 12th Annual Meeting of the Society of Engineering Science*, University of Texas, Austin, Texas, October, 1975, p. 691-693.
- Garg, S. K., J. W. Pritchett, M. H. Rice, and T. D. Riney, 1977b, U.S. Gulf Coast geopressured geothermal reservoir simulation: *Systems, Science and Software Report SSS-R-77-3147*, La Jolla, California, 116 p.

- Goodman, R. E., 1976, *Methods of geological engineering in discontinuous rocks*: West Publishing Co., Mineola, New York.
- Goodman, R. E., R. L. Taylor, and T. L. Brekke, 1968, A model for the mechanics of jointed rock: *J. Soil Mech. Found. Div., ASCE*, v. 94, p. 637.
- Gringarten, A. C., 1971, Unsteady-state pressure distributions created by a well with a single horizontal fracture, partial penetration, or restricted entry: Ph.D. thesis, Department of Petroleum Engineering, Stanford University, Stanford, California.
- Gringarten, A. C., and H. J. Ramey, Jr., 1974, Unsteady-state pressure distributions created by a well with a single horizontal fracture, partial penetration, or restricted entry: *Soc. Pet. Eng. J.*, v. 14, no. 4, p. 413-426.
- Gringarten, A. C., and J. P. Sauty, 1975, A theoretical study of heat extraction from aquifers with uniform regional flow: *J. Geophys. Research*, v. 80, no. 35, p. 4956-4962.
- Gupta, S. K., C. R. Cole, and F. W. Bond, 1979, Finite-element three-dimensional groundwater (FE3DGW) flow model--formulation, program listings, and users' manual: Pacific Northwest Laboratory Report PNL-2939, Richland, Washington.
- Gupta, S. K., C. R. Cole, C. P. Kincaid, and F. E. Kaszeta, 1980, Description and application of the FE3DGW and CFEST, Proceedings, Workshop on Numerical Modeling of Thermohydrological Flow in Fractured Rock Masses, Lawrence Berkeley Laboratory Report LBL-11566, Berkeley, California.
- Gupta, S. K., and K. K. Tanji, 1976, A three-dimensional Galerkin finite-element solution of flow through multiaquifers in Sutter Basin, California: *Water Resources Research*, v. 12, no. 2, p. 155-162.
- Gupta, S. K., and K. K. Tanji, 1977, Computer program for solution of large, sparse, unsymmetric systems of linear equations: *Internat. J. Numer. Methods Eng.*, v. 11, p. 1251-1259.
- Gupta, S. K., K. K. Tanji, and J. N. Luthin, 1975, A three-dimensional finite element ground water model: California Water Resources Center Contribution No. 152, University of California, Davis, California.
- Hardy, M. P., and G. Hocking, 1978, Numerical modeling of rock stresses within a basaltic nuclear waste repository. Phase II--Parametric design studies: Rockwell Hanford Operations Report RHO-BWI-C-23, Hanford, Washington.
- Hardy, M. P., C. M. St. John, and G. Hocking, 1979, Numerical modeling of the geomechanical response of a rock mass to a radioactive waste repository: Presented at the 40th International Congress on Rock Mechanics, September.

- Helm, D. C., 1975, One-dimensional simulation of aquifer system compaction near Pixley, California. I. Constant parameters: Water Resources Research, v. 11, no. 3, p. 465-478.
- Hellstrom, G., C. F. Tsang, and J. Claesson 1979, Heat storage in aquifers. Buoyancy flow and thermal stratification problems: Department of mathematical Physics, Lund Institute of Technology, Lund, Sweden.
- Iwai, K., 1976, Fundamental studies in fluid flow through a single fracture: Ph.D. thesis, Department of Civil Engineering, University of California, Berkeley, California, 208 p.
- Jonsson, V., 1978, Simulation of the Krafla geothermal field: Lawrence Berkeley Laboratory Report LBL 7076, Berkeley, California.
- Keenan, J. H., F. G. Keyes, P. G. Hill, and J. G. Moore, 1969, Steam Tables: John Wiley and Sons, New York.
- Kidder, R. E., 1957, Unsteady flow of gas through a semi-infinite porous medium: J. Appl. Mech., p. 329-332.
- Kruger, P., and H. J. Ramey, Jr., 1974, Stimulation and reservoir engineering of geothermal resources: Stanford Geothermal Program Report SGP-TR-1, Stanford University, Stanford, California.
- Lantz, R. B., 1971, Quantitative evaluation of numerical diffusion (truncation error): Soc. Pet. Eng. J., p. 315-320.
- Lawrence Berkeley Laboratory, 1980, Proceedings, Workshop on Numerical Modeling of Thermohydrological Flow in Fractured Rock Masses. Lawrence Berkeley Laboratory Report LBL-11566, Berkeley, California.
- Lew, H. S., and Y. C. Fung, 1970, Formulation of a statistical equation of motion of a viscous fluid in an anisotropic non-rigid porous solid: Internat. J. Solids Struct. v. 6, p. 1323-1340.
- Lindblom, U., and others, 1977, Groundwater movements around a repository, final report: KBS teknisk rapport 54:06, Hagconsult AB, Karnbranslesakerhet, Stockholm, Sweden.
- Lippmann, M. J., G. S. Bodvarsson, P. A. Witherspoon, and J. Rivera R., 1978, Preliminary simulation studies related to the Cerro Prieto Field: Proceedings, 1st Symposium on the Cerro Prieto Geothermal Field, San Diego, California, Lawrence Berkeley Laboratory Report LBL 7098, Berkeley, California, p. 375-383.
- Lippmann, M. J., and K. P. Goyal, 1979, Numerical modeling studies of the Cerro Prieto Reservoir--A progress report: Proceedings, 2nd Symposium on the Cerro Prieto Geothermal Field, Mexicali, Mexico, October.

- Lippmann, M. J., T. N. Narasimhan, and P. A. Witherspoon, 1976, Numerical simulation of reservoir compaction in liquid dominated geothermal systems: Presented at 2nd International Symposium on Land Subsidence, Anaheim, California, December. Lawrence Berkeley Laboratory Report LBL-4462, Berkeley, California, 11 p.
- Lippmann, M. J., T. N. Narasimhan, and P. A. Witherspoon, 1977a, Modeling subsidence due to geothermal fluid production: Presented at ASCE Fall Convention and Exhibit, San Francisco, California, October, 24 p.
- Lippmann, M. J., C. F. Tsang, and P. A. Witherspoon, 1977b, Analysis of the response of geothermal reservoirs under injection and production procedures: 47th Annual California Regional Meeting of the Society of Petroleum Engineers of AIME, Bakersfield, April, SPE-6537, 15 p.
- Mangold, D. C., M. J. Lippmann, and G. S. Bodvarsson, 1980, CCC user's manual, Version II: Lawrence Berkeley Laboratory Report LBL-10909, Berkeley, California.
- Mangold, D. C., C. F. Tsang, M. J. Lippmann, and P. A. Witherspoon, 1979, A study of thermal effects in well test analysis: 54th Annual Fall Technical Conference SPE-AIME, Las Vegas, Nevada, Lawrence Berkeley Laboratory Report LBL-9769 (SPE-8232), Berkeley, California.
- Mangold, D. C., H. Wollenberg, and C. F. Tsang, 1978, Thermal effects in overlying sedimentary rock from in situ combustion of a coal seam: Lawrence Berkeley Laboratory Report LBL 8172, Berkeley, California.
- Mercer, J. W., and C. R. Faust, 1979, Geothermal Reservoir Simulation: 3. Application of liquid- and vapor-dominated hydrothermal modeling techniques to Wairakei, New Zealand: Water Resources Research, v. 15, no. 3, p. 653-671.
- Mercer, J. W., G. F. Pinder, and I. G. Donaldson, 1975, A Galerkin-finite element analysis of the hydrothermal system at Wairakei, New Zealand: J. Geophys. Research, v. 80, no. 17, p. 2608-2620.
- Meyer, C. A., R. B. McClintock, G. J. Silvestri, and R. C. Spencer, Jr., 1967, ASME Steam Tables: The American Society of Mechanical Engineers, New York, New York.
- Mueller, T. D., and P. A. Witherspoon, 1965, Pressure interference effects within reservoirs and aquifers: J. Pet. Tech., April, p. 471-474.
- Narasimhan, T. N., 1975, A unified numerical model for saturated-unsaturated groundwater flow: Ph.D. thesis, Department of Civil Engineering, University of California, Berkeley, California, 244 p.

- Narasimhan, T. N., 1980a, Program TERZAGI user's manual: Lawrence Berkeley Laboratory Report LBL-10908, Berkeley, California.
- Narasimhan, T. N., 1980b, Multidimensional numerical simulation of fluid flow in fractured porous media: Proceedings, Workshop on Numerical Modeling of Thermohydrological Flow in Fractured Rock Masses. Lawrence Berkeley Laboratory Report LBL-11566, Berkeley, California.
- Narasimhan, T. N., and W. A. Palen, 1979, A purely numerical approach for analyzing flow to a well intercepting a vertical fracture: Society of Petroleum Engineers California Regional Meeting, Ventura, California, April 1979, Lawrence Berkeley Laboratory Report LBL-8816, Berkeley, California.
- Narasimhan, T. N., and P. A. Witherspoon, 1976, An integrated finite difference method for analyzing fluid flow in porous media: Water Resources Research, v. 12, no. 1, p. 57-64.
- Narasimhan, T. N., and P. A. Witherspoon, 1977, Numerical model for saturated-unsaturated flow in deformable porous media. 1. Theory: Water Resources Research, v. 13, no. 3, p. 657-664.
- Narasimhan, T. N., and P. A. Witherspoon, 1978, Numerical model for saturated-unsaturated flow in deformable porous media. 3. Applications: Water Resources Research, v. 14, no. 6, p. 1017-1034.
- Narasimhan, T. N., P. A. Witherspoon, and A. L. Edwards, 1978, Numerical model for saturated-unsaturated flow in deformable porous media. 2. The algorithm: Water Resources Research, v. 14, no. 2, p. 255-261.
- Noorishad, J., 1971, Finite element analysis of rock mass behavior under coupled actions of body forces, flow forces and external loads: Ph.D. thesis, Department of Civil Engineering, University of California, Berkeley, California.
- Noorishad, J. and M. S. Ayatollahi, 1980, Program ROCMAS; introduction and user's guide: Lawrence Berkeley Laboratory Report LBL-12987, Berkeley, California.
- Noorishad, J., M. S. Ayatollahi, and P.A. Witherspoon, 1980, A finite-element method for stress and flow analysis in fractured rock masses: Lawrence Berkeley Laboratory Report LBL-12730, Berkeley, California.
- Noorishad, J., P. A. Witherspoon, and T. L. Brekke, 1971, A method for coupled stress and flow analysis of fractured rock masses: Geotechnical Engineering Publication No. 71-6, University of California, Berkeley, California.

- Norton, D., and R. Knapp, 1979, Transport phenomena in hydrothermal systems: The nature of porosity. *Amer. J. Science*, v. 277, p. 913-936, October.
- Ogata, A., and R. B. Banks, 1961, A solution of the differential equation of longitudinal dispersion in porous media: U. S. Geological Survey Professional Paper 411-A, Washington, D. C.
- O'Neill, K., 1977, Calculation of the flow of liquid and heat in fractured porous media (computer code documentation): Water Resource Program Report 77-WR-15, Princeton University, Princeton, New Jersey.
- O'Neill, K., 1978, The transient three-dimensional transport of liquid and heat in fractured porous media: Ph.D. thesis, Department of Civil Engineering, Princeton University, Princeton, New Jersey.
- Pahwa, S. B., and J. R. Wayland, 1978, Far field thermal calculations for the WIPP site in southeastern New Mexico: Proceedings, Scientific Basis for Nuclear Waste Management, Plenum Press, New York, v. 2, p. 817-824.
- Philip, J. R., 1969, Theory of infiltration: *Adv. Hydroscience*, v. 5, p. 215-296.
- Pinder, G. F., 1979, State-of-the-art review of geothermal reservoir modeling: Lawrence Berkeley Laboratory Report LBL-9093, GSRMP-5, Berkeley, California, 144 p.
- Pinder, G. F., and W. G. Gray, 1977, Finite element simulation in surface and subsurface hydrology. Academic Press, New York.
- Price, H. S., and K. H. Coats, 1974, Direct methods in reservoir simulation. *Soc. Pet. Eng. J.*, v. 14, no. 3, p. 295-308.
- Pritchett, J. W., 1975, Numerical calculation of multiphase fluid and heat flow in hydrothermal reservoirs: Proceedings, Workshop on Geothermal Reservoir Engineering, Stanford University Report SGP-TR-12, Stanford, California, p. 201-205.
- Pritchett, J. W., 1978, Geohydrological environmental effects of geothermal power production--phase IIb. Systems, Science and Software Report SSS-R-78-3631, La Jolla, California, 127 p.
- Pritchett, J. W., 1979, A semi-analytic description of two-phase flow near production wells in hydrothermal and geopressured reservoirs: Proceedings, Stanford Geothermal Reservoir Engineering Meeting, December, Stanford, California.
- Pritchett, J. W., and S. K. Garg, 1978, Flow in an aquifer charged with hot water from a fault zone: *Pageoph.*, v. 117, p. 309-320.

- Pritchett, J. W., and S. K. Garg, 1980, Determination of effective well-bore radii for numerical reservoir simulations: *Water Resource Research*, v. 16, p. 665-674.
- Pritchett, J. W., S. K. Garg, and D. H. Brownell, Jr., 1976a, Numerical simulation of production and subsidene at Wairakei, New Zealand: *Proceedings, 2nd Workshop on Geothermal Reservoir Engineering*, Stanford University Report SGP-TR-20, Stanford, California, p. 310-323.
- Pritchett, J. W., S. K. Garg, D. H. Brownell, Jr., and H. B. Levine, 1975, Geohydrological environmental effects of geothermal power production, phase I: *Systems, Science and Software Report SSS-R-75-2733*, La Jolla, California, 90 p.
- Pritchett, J. W., S. K. Garg, D. H. Brownell, Jr., L. F. Rice, M. H. Rice, T. D. Riney, and R. R. Hendrickson, 1976b, Geohydrological environmental effects of geothermal power production, phase IIa: *Systems, Science and Software Report SSS-R-77-2998*, La Jolla, California, 186 p.
- Pritchett, J. W., S. K. Garg, M. H. Rice, and T. D. Riney, 1979, Geopressured reservoir simulation: *Systems, Science, and Software Report SSS-R-79-4022*, La Jolla, California, 127 p.
- Pritchett, J. W., L. F. Rice, and S. K. Garg, 1980, Reservoir simulation studies: Wairakei geothermal field, New Zealand: *Lawrence Berkeley Laboratory Report LBL-11497, GREMP-11*, Berkeley, California, 103 p.
- Pruess, K., G. Bodvarsson, R. C. Schroeder, P. A. Witherspoon, R. Marconcini, G. Neri, and C. Ruffilli, 1979a, Simulation of the depletion of two-phase geothermal reservoirs: *54th Annual Fall Technical Conference and Exhibition of the Society of Petroleum Engineers*, Las Vegas, Nevada, SPE-8266.
- Pruess, K., and T. N. Narasimhan, 1981, On fluid reserves and the production of superheated steam from fractured, vapor-dominated geothermal reservoirs: *Lawrence Berkeley Laboratory Report LBL-12921*, Berkeley, California, 35 p.
- Pruess, K., and R. C. Schroeder, 1979, Geothermal reservoir simulation with SHAFT79: Presented at the 5th Geothermal Reservoir Engineering Workshop, Stanford, California, 1979. *Lawrence Berkeley Laboratory Report LBL-10066*, Berkeley, California.
- Pruess, K., and Schroeder, R. C., 1980, SHAFT79 user's manual: *Lawrence Berkeley Laboratory Report LBL-10861*, Berkeley, California.
- Pruess, K., R. C. Schroeder, P. A. Witherspoon, and J. M. Zerzan, 1979b, SHAFT78, a two-phase multidimensional computer program for geothermal reservoir simulation: *Lawrence Berkeley Laboratory Report LBL-8264*, Berkeley, California.

- Pruess, K., R. C. Schroeder, and J. M. Zerzan, 1978, Studies of flow problems with simulator SHAFT78. Proceedings, 4th Workshop on Geothermal Reservoir Engineering, Stanford University Report SGP-TR-30, Stanford, California, p. 308-321.
- Pruess, K., O. Weres, R. Schroeder, R. Marconcini, and G. Neri, 1980, Performance matching and prediction for Serrazzano geothermal reservoir by means of numerical simulation: Lawrence Berkeley Laboratory Report LBL-12174, Berkeley, California, 47 p.
- Pruess, K., J. M. Zerzan, R. C. Schroeder, and P. A. Witherspoon, 1979c, Description of the three-dimensional two-phase simulator SHAFT78 for use in geothermal reservoir studies: Proceedings, 5th Symposium on Reservoir Simulation of the Society of Petroleum Engineers of AIME, Denver, Colorado, February, p. 253-268, SPE-7699.
- Raghavan, R., 1977, Pressure behavior of wells intercepting fractures: Proceedings, Invitational Well Testing Symposium, Lawrence Berkeley Laboratory Report LBL-7027, Berkeley, California, p. 117-160.
- Raghavan, R., A. Uraiet, and G. W. Thomas, 1978, Vertical fracture height: Effect on transient flow behavior: Soc. Pet. Eng. J., v. 18, no. 4, p. 265-277.
- Ratigan, J. L., 1977a, Groundwater movements around a repository thermal analyses, part 1 conduction heat transfer, part 2 advective heat transfer: KBS teknisk rapport 54:02, Hagconsult AB, Karnbranslesakerhet, Stockholm, Sweden.
- Ratigan, J. L., 1977b, Groundwater movements around a repository, rock mechanics analyses: KBS teknisk rapport 54:04, Hagconsult AB, Karnbranslesakerhet, Stockholm, Sweden.
- Ratigan, J. L., A. S. Burgess, E. L. Skiba, and R. Charlwood, 1977, Groundwater movements around a repository, repository domain groundwater flow analyses, part 1 permeability perturbations, part 2 inflow to repository, part 3 thermally induced flow: KBS teknisk rapport 54:05, Hagconsult AB, Karnbranslesakerhet, Stockholm, Sweden.
- Riney, T. D., J. W. Pritchett, and S. K. Garg, 1977, Salton Sea geothermal reservoir simulations: Proceedings, 3rd Workshop on Geothermal Reservoir Engineering, Stanford University, Stanford, California.
- Rubin, J. and R. Steinhardt, 1963, Soil-water relations during rain infiltration, I, theory: Soil Sci. Soc. Amer. Proc. v. 27, p. 246-251.
- Runchal, A., and T. Maini, 1980, The impact of a high level radioactive waste repository on the regional groundwater flow: Int. J. Rock Mech. Min. Sci., v. 17, p. 253-264.

- Runchal, A., J. Treger, and G. Segal, 1979, Program EP21 (GWTHERM): Two-dimensional fluid flow, heat, and mass transport in porous media: Advanced Technology Group, Dames and Moore Technical note TN-LA-34, Los Angeles, California.
- Schiffman, R. L., and R. E. Gibson, 1964, Consolidation of non-homogeneous clay layers: J. Soil Mech. Ground Eng., ASCE, v. 90 (SM5), p. 1-30.
- Science Applications, Inc., 1978, Technical Support for GEIS: Radioactive waste isolation in geologic formations. Office of Waste Isolation Report Y/OWI/TM-36/19, Oak Ridge, Tennessee, April.
- Skiba, E. L., 1977, FINI 520, 2-D planar and axisymmetric hydrothermal flow: Acres Consulting Services Limited, Niagara Falls, New York.
- Skiba, E. L., R. B. Allen, and R. G. Charlwood, 1977, FINI 500, 2-D planar and axisymmetric groundwater flow: Acres Consulting Services Limited, Niagara Falls, New York.
- Sorey, M. L., 1975, Numerical modeling of liquid geothermal systems: Ph.D. thesis, Department of Geological Engineering, University of California, Berkeley, California, 66 p.
- Stille, H., A. Burgess, and U. E. Lindblom, 1977, Groundwater movements around a repository, geological and geotechnical conditions: KBS teknisk rapport 54:01, Hagconsult AB, Karnbranslesakerhet, Stockholm, Sweden.
- Streltsova-Adams, T. D., 1978a, Fluid flow in naturally fractured reservoirs: Proceedings, 2nd Invitational Well Testing Symposium, Lawrence Berkeley Laboratory Report LBL-8883, Berkeley, California, p. 71-77.
- Streltsova-Adams, T. D., 1978b, Well hydraulics in heterogeneous aquifer formations: Adv. Hydroscience, v. 11, p. 357-423.
- Taylor, R. L., 1974, Analysis of flow of compressible or incompressible fluids in porous elastic solids: Consulting report to the Naval Civil Engineering Lab., Port Hueneme, California.
- Theis, C. V., 1935, The relation between the lowering of the piezometric surface and the rate and duration of discharge of a well using ground-water storage: Trans. Am. Geophys. Union, p. 619-624.
- Thomas, L. K., and R. G. Pierson, 1978, Three-dimensional geothermal reservoir simulation: Soc. Pet. Eng. J., p. 151-161.
- Toronyi, R. M., and S. M. Farouq Ali, 1977, Two-phase, two-dimensional simulation of a geothermal reservoir: Soc. Pet. Eng. J., p. 171-183.

- Tsang, C. F., T. Buscheck, and C. Doughty, 1979a, Aquifer thermal energy storage--a numerical simulation of Auburn University field experiments: Lawrence Berkeley Laboratory Report LBL 10210, Berkeley, California.
- Tsang, C. F., T. Buscheck, D. C. Mangold, and M. J. Lippmann, 1978a, Mathematical modeling of thermal energy storage in aquifers. Presented at the Thermal Energy Storage in Aquifers Workshop, Lawrence Berkeley Laboratory, Berkeley, California, May 1978. Lawrence Berkeley Laboratory Report LBL-9970, Berkeley, California.
- Tsang, C. F., C. B. Goranson, M. J. Lippmann, and P. A. Witherspoon, 1977, Modeling underground storage in aquifers of hot water from solar power systems: Presented at "Solar World" meeting at Orlando, Florida, June 6-9, 1977, Lawrence Berkeley Laboratory Report LBL-6327, Berkeley, California.
- Tsang, C. F., M. J. Lippmann, C. B. Goranson, and P. A. Witherspoon, 1976, Numerical modeling of cyclic storage of hot water in aquifers: Presented at the Symposium on Use of Aquifer Systems for Cyclic Storage of Water, San Francisco, December, Lawrence Berkeley Laboratory Report LBL-5929, Berkeley, California, 29p.
- Tsang, C. F., M. J. Lippmann, and P. A. Witherspoon, 1978b, Underground aquifer storage of hot water from solar energy collectors: Presented at the International Solar Energy Congress, New Delhi, India, January, Lawrence Berkeley Laboratory Report LBL-7034, Berkeley, California.
- Tsang, C. F., D. C. Mangold, and M. J. Lippmann, 1979b, Simulation of reinjection at Cerro Prieto using an idealized two-layer geologic model: Proceedings, 2nd Symposium on the Cerro Prieto Geothermal Field, Mexicali, Mexico, October.
- Tsang, C. F., M. Zerzan, and others, 1978c, Numerical modeling studies in well test analysis. Proceedings, 2nd Invitational Well Testing Symposium, Lawrence Berkeley Laboratory, Berkeley, California, Lawrence Berkeley Laboratory Report LBL-8883, Berkeley, California.
- U. S. Department of Energy, 1979, Draft Environmental Impact Statement, Waste Isolation Pilot Plant: U. S. Department of Energy Report DOE/EIS-0026-D, Volume 1, Washington, D.C.
- U. S. Geological Survey, 1976, A model for calculating effects of liquid waste disposal in deep saline aquifer, Part I--development, Part II--documentation: U. S. Geological Survey Water-Resources Investigations Report 76-61, Reston, Virginia.
- van Everdingen, A. F., and W. Hurst, 1949, The application of the Laplace transformation to flow problems in reservoirs: Petroleum Transactions, AIME, p. 305-324.

- Verruijt, A., 1969, Elastic storage of aquifers, in: Flow through porous media, ed. by R. J. M. De Wiest, Academic Press, New York, Chapter 8, p. 331-376.
- Wang, J. S. Y., T. N. Narasimhan, C. F. Tsang, and P. A. Witherspoon, 1977, Transient flow in tight fractures: Proceedings, Invitational Well-testing Symposium, Lawrence Berkeley Laboratory, Berkeley, California, October, Lawrence Berkeley Laboratory Report LBL-7027, Berkeley, California, p. 103-116.
- Wang, J. S. Y., and C. F. Tsang, 1980, Buoyancy flow in fractures intersecting a nuclear waste repository: Symposium Proceedings, Heat Transfer in Nuclear Waste Disposal: edited by F. A. Kulucki and R. W. Lyczkowski, Winter Annual Meeting of ASME, Chicago, Illinois, November, HTD-Vol. 11, p. 105-112 (LBL-11112).
- Wang, J. S. Y., C. F. Tsang, N. G. W. Cook, and P. A. Witherspoon, 1980, Long-term thermohydrologic behavior of nuclear-waste repositories: Symposium on Predictive Geology, 26th International Geological Congress, France, July.
- Warren, J. E., and P. J. Root, 1963, The behavior of naturally fractured reservoirs: Soc. Pet. Eng. J., p. 245-255.
- Weeks, E. P., 1977, Aquifer tests--the state of the art in hydrology: Proceedings, Invitational Well-Testing Symposium, Lawrence Berkeley Laboratory Report LBL-7027, Berkeley, California, p. 14-26.
- Williams, J. R., R. W. Lewis, and K. Morgan, 1979, An elasto-viscoplastic thermal stress model with application to the continuous casting of metals. Internat. J. Numer. Methods Eng., v. 14, p. 1-9.
- Wilson, C. R., and P. A. Witherspoon, 1974, Steady state flow in rigid networks of fractures. Water Resources Research, v. 10, no. 2, p. 328-335.
- Witherspoon, P. A., J. E. Gale, and N. G. W. Cook, 1979a, Investigations in granite at Stripa, Sweden, for nuclear waste storage: Lawrence Berkeley Laboratory Report LBL-8801, Berkeley, California.
- Witherspoon, P. A., J. S. Y. Wang, K. Iwai, and J. E. Gale, 1980, Validity of cubic law for fluid flow in a deformable rock fracture: Water Resources Research, v. 16, p. 1016-1024.
- Witherspoon, P. A., C. R. Wilson, J. C. S. Long, A. O. DuBois, J. E. Gale, and M. McPherson, 1979b, The role of large-scale permeability measurements in fractured rock and their application at Stripa: Lawrence Berkeley Laboratory Report LBL-9903, Berkeley, California.

Yuan, S. and A. Finkelstein, 1956, Laminar pipe flow with injection and suction through a porous wall, Trans. AIME, v. 78, p. 719-724.

Zienkiewicz, O. C., 1977, The finite element method: McGraw-Hill, London, England.

